A REDUCTIONIST STUDY INTO THE PHYSIOLOGY, PATHOLOGY, AND PHARMACOLOGY OF THE MITOTIC SPINDLE

By

Emma Gray Sturgill

Dissertation

Submitted to the Faculty of the

Graduate School of Vanderbilt University

in partial fulfillment of the requirements

for the degree of

DOCTOR OF PHILOSOPHY

in

Cell and Developmental Biology

December 2014

Nashville, Tennessee

Approved:

Matthew J. Tyska, Ph.D.

Irina Kaverina, Ph.D.

Ethan Lee, M.D., Ph.D.

Alissa M. Weaver, M.D., Ph.D.

For Mom and Beattie

ACKNOWLEDGEMENTS

First and foremost, I thank my mentor and friend, Dr. Ryoma “Puck” Ohi, for supporting my pursuit of biological discovery. Puck provided me with dream-space, ensuring that resources were never limiting to my graduate studies. If I could imagine it, I could test it. For that I am truly grateful. I also thank the members of my thesis committee, Drs. Matthew J. Tyska, Irina Kaverina, Ethan Lee, and Alissa M. Weaver, for their dedication to my professional development. And I am grateful to Drs. Melanie D. Ohi and Matthew J. Lang for their unparalleled knowledge and expertise. Finally, I owe a debt of gratitude to my lab mates, Dr. Yaqing Du, Sophia Gayek, Jen Landino, and Megan Dumas, for their stimulating discussions and camaraderie.

The unwavering support of my family and friends deserves more thanks than I can give. My mom, Laura, and brother, Beattie, are my stronghold. Without them I would be lost. The unconditional love from my grandparents, Jackson “Hadad” and Rosamond “Hama” McCarty, has never failed. For this and their timeless guidance, I am immensely grateful. I am also thankful for the companionship and solace found in the McCarty and Snider families. And for the faithful devotion of my stepdad, Chris, and sister-in-law, Ali, I am forever beholden. Last but not least, I have my friends to thank. They are my joy, inspiration, and sanity.

TABLE OF CONTENTS

Page

LIST OF FIGURES

LIST OF ABBREVIATIONS

ADP	Adenosine diphosphate
AMPPNP	Adenylyl imidodiphosphate
ATP	Adenosine triphosphate
β-ME	β-mercaptoethanol
BSA	Bovine serum albumin
CAFE	Computer-aided feature extraction
CCD	Charge-coupled device
CFEOM1	Congenital Fibrosis of the Extraocular Muscles Type 1
CIN	Chromosomal instability
DIC	Differential interference microscopy
DMSO	Dimethyl sulfoxide
DTT	Dithiothreitol
EDTA	Ethylenediaminetetraacetic acid
EIC	Eg5-indpendent cell
EM	Electron microscopy
EGTA	Ethylene glycol tetraacetic acid
FCS	Fetal calf serum
GTP	Guanosine triphosphate
GFP	Green fluorescent protein
K-fiber	Kinetochore fiber
K-MT	Kinetochore microtubule

K5I	Kinesin-5 inhibitor
NEB	Nuclear envelope breakdown
MAP	Microtubule-associated protein
MI	Mitotic index
MPI	Monopolar index
MT	Microtubule
MTOC	Microtubule organizing center
MW	Molecular weight
NA	Numerical aperature
ORF	Open reading frame
P_i	Inorganic phosphate
PAGE	Polyacrylamide gel electrophoresis
PBS	Phostphate buffered saline
r.m.s.d	Root mean square deviation
S	Sedimentation coefficient
SAC	Spindle assembly checkpoint
SD	Standard deviation
SDS	Sodium dodecyl sulfate
STLC	S-trityl-L-cysteine
SVAU	Sedimentation velocity analytical ultracentrifugation
TIRF	Total internal reflection fluorescence

CHAPTER I

INTRODUCTION

The Cell: a Macromolecular Factory

As the fundamental compartment of life, the cell houses all of the components necessary for survival. The cell and its molecular constituents are subjected to the same natural laws that govern all matter, including the tendency toward disorder. Yet the cell behaves as a well-orchestrated factory with its components masterfully ordered in space and time. A central aim of cell biology is to understand how the cell avoids succumbing to a state of randomness, as this ability distinguishes the cell from nonliving matter.

Thermodynamic Movement

To understand how the molecules within a cell are so elegantly arranged, one must study how the cellular constituents move through space over time. Here, the focus will be on proteins, the molecular workhorses of the cell. Proteins experience the same forces that influence materials on the macroscopic scale. However, the relevancy of these forces differs at the single molecule level. This is owed to the exceptionally small mass of proteins and the relatively high viscosity of the intracellular fluid.

Proteins can be likened to hard plastics in terms of their material properties, but their mass averages a mere ~1.7 x 10^{-22} kg (Howard 2001). Inertial forces therefore have negligible effects on protein movement. Frictional forces, on the other hand,

impart highly relevant forces on proteins. Being ~1 x 10^6 -times more viscous than water, the cytosol dampens protein movement by frictional drag (Howard 2001). At the single molecule level inside cells, frictional drag exceeds gravitational pull by ~1 x 10^{10} -fold (Howard 2001). As a result, proteins remain suspended in the cytosol instead of falling to the bottom of the cell.

Soluble proteins do not remain stationary in the cytosol; rather, they undergo highly agitated movement. This *Brownian motion* results from collisions with solvent molecules. Collision frequency depends on temperature and molecular crowding, but on average a 100 kD protein will strike a solvent molecule every ~24 pm (Howard 2001). Therefore, a protein is likely to change direction before moving as far as it is wide. And as collision angles vary, directional changes are random. Collectively, this behavior is termed *diffusion*.

The diffusive nature of the cytoplasm causes proteins to collide with neighboring macromolecules. These collisions create opportunity for repulsive or attractive interactions, depending on the chemical and structural makeup of the molecules involved. Attractive electrostatic interactions, or non-covalent bonds, cooperate to hold two complementary molecules together (Alberts et al.). In this manner, soluble proteins spontaneously assemble into higher order structures. Such *self-assembly* capitalizes on thermodynamics to organize the intracellular space (Fletcher and Mullins 2010).

Catalytic Movement

Self-assembly is the fundamental mechanism by which disordered molecules become spatially arranged within the cell (S. Zhang 2002). However, the resulting

structures are at equilibrium, maintaining a relatively constant size and shape (Kirschner 1986). Catalytic reactions free self-assembled structures from the constraints of thermodynamic equilibrium, enabling them to change over time (Nicolis and Prigogine 1977). Such dynamicity converts protein *assemblies* into *machines* capable of generating force and performing essential functions (Mitchison 1992).

Consider a microtubule (MT), a type of cytoskeletal filament, as a self-assembled proteinaceous machine. Lateral and longitudinal non-covalent bonds polymerize αβ-tubulin subunits into hollow tubes of ~13 protofilaments (Amos and Klug 1974; Evans, Mitchison, and Kirschner 1985; Nogales et al. 1999). Given no other chemical changes, MTs will polymerize to thermodynamic equilibrium (Oosawa et al. 1975). However, tubulin polymerization is coupled with the catalytic hydrolysis of guanosine triphosphate (GTP, (Weisenberg, Deery, and Dickinson 1976; David-Pfeuty, Erickson, and Pantaloni 1977)). Energy released from this high-energy nucleotide provides a means for MT disassembly (Caplow, Ruhlen, and Shanks 1994). Therefore, MTs are not simple equilibrium polymers, but rather coexist as polymerizing and depolymerizing populations at steady-state (Figure 1.1, (Mitchison and Kirschner 1984)).

The textbook model for dynamic instability incorporates MT assembly as a thermodynamics-governed reaction and MT disassembly as a catalyzed reaction (Figure 1.1). The probability of tubulin subunits colliding with MT ends depends on the concentration of free tubulin; therefore, the MT polymerization rate scales with tubulin concentration (Walker et al. 1988). In contrast, GTP hydrolysis occurs with fixed probability (David-Pfeuty, Erickson, and Pantaloni 1977). So at relatively high tubulin concentrations, the polymerization rate exceeds that of GTP-hydrolysis and the MT

gains a protective GTP-tubulin cap (Mandelkow, Mandelkow, and Milligan 1991). As MTs polymerize, the pool of free tubulin dissipates and the polymerization rate slows. Eventually, the rate of GTP-hydrolysis supersedes that of polymerization, resulting in the exposure of GDP-tubulin at the MT ends (Mitchison and Kirschner 1984; Carlier, Hill, and Chen 1984). Curved GDP-tubulin protofilaments lose stabilizing lateral interactions and thereby prompt MT depolymerization. As MTs disassemble, the pool of free tubulin is restored and the cycle continues (note: MT nucleation will be discussed on page 8, (Desai and Mitchison 1997)).

This historical description of MT dynamic instability is admittedly oversimplified (Anderson et al. 2013). For example, polymerizing MTs age as evidenced by a non-exponential distribution of MT lengths at steady state (Odde, Cassimeris, and Buettner 1995; Gardner et al. 2011). This challenges previous single-filament models (Hill 1984; Verde et al. 1992), indicating that the multi-protofilament composition of a MT makes its catastrophe a multi-step process (Odde, Cassimeris, and Buettner 1995; Gardner et al. 2011). Other unknowns include the size of the GTP-cap and the coupling of GTP-hydrolysis among neighboring subunits (VanBuren, Odde, and Cassimeris 2002; Gardner et al. 2011). But regardless of the mechanism, it remains well appreciated MTs capitalize on GTP-hydrolysis in order to remodel (Desai and Mitchison 1997).

A final point of consideration regarding MTs is their inherent polarity. α- and β-tubulin differ chemically and structurally. As $\alpha\beta$-tubulin heterodimers polymerize end-on-end, the resulting MT has directionality along its lattice and distinct ends wherein the faces of α-tubulin (minus-end) or β-tubulin (plus-end) subunits are exposed (Jiang and Akhmanova 2011). As a result, the two MT ends differ in their dynamic behavior (Allen

and Borisy 1974). For example, MT minus-ends polymerize more slowly *in vitro* and are often capped in cells (Jiang and Akhmanova 2011). While recent efforts have championed a functional significance of minus-end dynamics in cells, MT plus-ends are generally regarded as the more relevant end for force generation (Lecland and Lüders 2014).

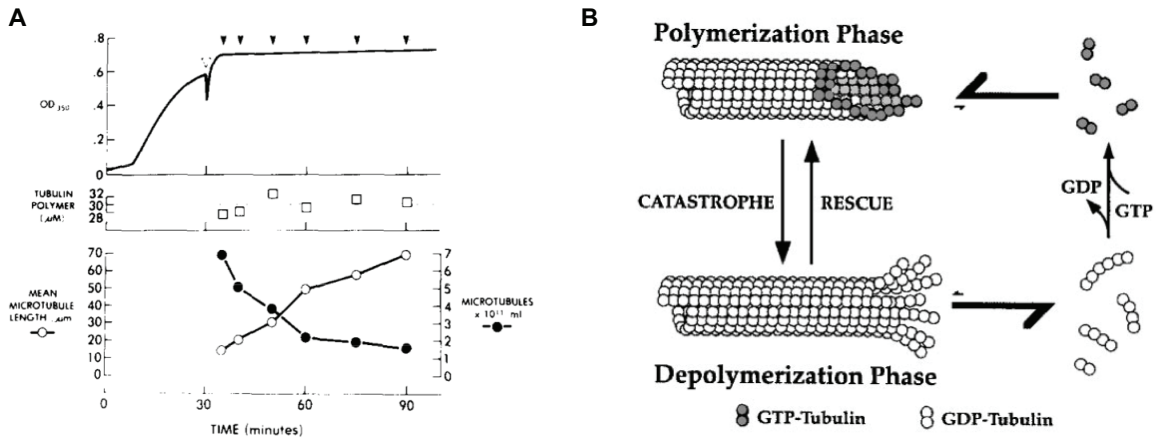

Figure 1.1: MT dynamic instability. A) Length distributions of MTs at steady-state. Top, MTs assemble to steady-sate. MT polymerization off of preassembled seeds was measured by turbidity. MTs were sheared at the time indicated by the open triangle. MT lengths were determined by fix-and-stain methodology at the times indicated by the closed arrows and analyzed in the middle and bottom pannels. Middle, the bulk MT mass remains relatively constant at steady-state. The concentration of polymerized tubulin was measured at indicated times by multiplying the average MT length by the average MT number. Bottom, MT length and number inversely redistribute while the population is at steady-state. Shown are the average MT length (open circles) and number (closed circles) at indicated times. Adapted from Mitchison and Kirshner (1984). B) Model of MT dynamic instability. GTP-tubulin is incorporated at polymerizing MT ends, the bound GTP is hydrolyzed soon after polymerization, and Pi is subsequently released. Thus the MT lattice is predominantly composed of GDP-tubulin. Polymerizing MTs infrequently transit, or catastrophe, to the depolymerization phase. Depolymerization is characterized by the very rapid loss of GDP-tubulin subunits and oligomers from the MT end. Depolymerizing MTs can also infrequently transit back, or rescue, to the polymerization phase. This model incorporates the notions of a stabilizing GTP-tubulin cap and bent GDP-tubulin protofilament ends. Adapted from Desai and Mitchison (1997).

Like MTs, kinesins catalyze a chemical reaction in order to generate force (Vale, Reese, and Sheetz 1985). The kinesin motor head contains both a MT-binding site and nucleotide-binding pocket. In this manner, kinesins are equipped to simultaneously bind MTs and hydrolyze the high-energy nucleotide adenosine triphosphate (ATP, (Sablin et al. 1996; Kull et al. 1996)). Directly adjacent to the motor head is the neck linker, a short peptide that serves as a lever arm (Morii et al. 1997; Tripet, Vale, and Hodges 1997; Vale et al. 2000). Together, the motor head and neck linker couple the chemistry of ATP hydrolysis to mechanical force-generation (Vale and Fletterick 1997).

The canonical kinesin *mechanochemical* cycle begins with the motor head devoid of nucleotide and only weakly attracted to MTs. Kinesins diffuse along MTs in this basal state and lock onto MTs upon entry of ATP into the nucleotide-binding pocket. The motor head subsequently hydrolyzes ATP, which triggers the force-generating motion of neck-linker docking. Upon release of P_i from the motor head, kinesins dissociate from MTs and reset the neck-linker in preparation for another round of the cycle (Gilbert et al. 1995; Howard 1996; Cross and McAinsh 2014).

Most kinesins homo-oligomerize by coiled-coil stalk interactions (Yang, Laymon, and Goldstein 1989; de Cuevas, Tao, and Goldstein 1992). These self-assembled multimers harness the energy from ATP hydrolysis to walk hand-over-hand along a MT (Asbury, Fehr, and Block 2003; Yildiz et al. 2004). Such directed motility enables kinesins to overcome the limitations of Brownian motion. And by attaching cargos with their globular tail domains, kinesins extend tight spatiotemporal control to other cellular components (Seiler et al. 2000; Vale 2003).

MTs and kinesins exemplify ways in which additional energy-dissipating steps convert self-assembled *structures* into self-organized *machines*. Other self-organizing machines include the cytoskeletal filament actin and its associated myosin motor proteins (Engelhardt and LJUBIMOWA 1939; Pollard and Weeds 1984; Lauffenburger and Horwitz 1996; Loisel et al. 1999). And the proteasome and ribosome represent non-cytoskeletal machines that impart further spatiotemporal control over proteins by governing their intracellular concentrations (Voges, Zwickl, and Baumeister 1999; Steitz 2008). By coordinating the efforts of autonomous self-organizing machines, the cell behaves as a macromolecular factory.

The Spindle: a Case Study in Self-Organizing Cellular Machines

While machines in their own right, cytoskeletal filaments assemble into higher-order arrays. Add to this the layered complexity of factors that dynamically associate with and influence cytoskeletal filaments, and self-organizing *systems* emerge. Some examples of actin-based self-organizing systems include the lamellipodium involved in cell locomotion and the contractile ring responsible for cytokinesis (Pollard and Borisy 2003; Mendes Pinto, Rubinstein, and Li 2013). Here, the MT-based mitotic spindle responsible for chromosome segregation will be examined as a case study in essential self-organizing systems.

Spindle Assembly in Brief

The spindle is a bipolar array of highly dynamic MTs (Wittmann, Hyman, and Desai 2001). This contrasts the configuration of interphase cells, wherein the MT

cytoskeleton is aster-like and relatively stable. Therefore, the MT cytoskeleton must undergo a massive rearrangement at mitotic onset. This is a complex process involving the concerted efforts of numerous dynamic counterparts; however, the individual force-generating components are relatively simple (Cross and McAinsh 2014). Therefore, spindle assembly is often studied as a collection of subsystems.

MTs are inherently capable of reorganizing based on their structural features and enzymatic activity. But the cell imparts additional levels of spatiotemporal control through the action of proteins that dynamically associate with and influence MTs. In human cells, the spindle consists of two *MT-organizing centers* (MTOCs), 16 *kinesin* subtypes, cytoplasmic *dynein*, and an assortment of *MT-associated proteins* (MAPs, (Walczak and Heald 2008)). Below, these components are introduced in brief followed by a more detailed examination of their contribution to spindle assembly.

MTOCs impart tight control over the number of cellular MTs by dominating over spontaneous MT nucleation (De Brabander et al. 1981; Euteneuer and McIntosh 1981; Tucker 1984). Spontaneous MT nucleation is unlikely in cells, as it requires the aggregation of ~9 $\alpha\beta$-tubulin subunits (Voter and Erickson 1984). MTOCs alleviate this kinetic burden by providing preassembled seeds from which MTs can polymerize (Mitchison and Kirschner 1983). In this manner, MTOCs generate a stable array of dynamic MTs.

Kinesins are conventionally viewed as molecular freight trains that transport cargos by motoring along a MT track (Verhey and Hammond 2009). However, the function of some kinesins relates more to track maintenance than transportation. For example, *organizational* kinesins sort MTs within a complex array by transporting them

as cargos (Welburn 2013). Meanwhile, *regulatory* kinesins modulate the dynamics of MT ends instead of walking along MT lattices. Although the exact mechanisms remain elusive, regulatory kinesins are thought to recognize and modify the structural features of MT ends (Walczak, Gayek, and Ohi 2013). Altogether, kinesins both configure the MT cytoskeleton and capitalize on its layout to organize intracellular components.

To date, 16 mitotic kinesins have been identified in humans (Rath and Kozielski 2012). While kinesins share a conserved motor head, functional diversity arises from subtle modulations in the mechanochemical cycle and variable non-motor domains. The motility parameters of each kinesin, including speed, processivity, and duty ratio, are fine-tuned for its specific function. And the kinesin stalk and tail domains specify its oligomerization state, binding partners, and post-translational modifications. Furthermore, positioning of the motor head relative to the non-motor domains correlates with directionality: Kinesins-1 through -12 posses N-terminal motor heads and are plus-end directed while Kinesin-14 has a C-terminal motor head and is minus-end directed. Kinesin-13s, on the other hand, have an internal motor head and function as MT depolymerases (Vale and Fletterick 1997; Welburn 2013). Such molecular diversity enables kinesins to fulfill a variety of specialized functions within the cell.

Lastly, *dynein* and *MAPs* influence the distribution of spindle MTs. Cytoplasmic dynein, a minus-end directed MT motor, functions in both transport and MT organization by associating with a cohort of various factors (Kardon and Vale 2009). And MAPs influence the overall MT mass by either directly or indirectly affecting MT dynamics (Andersen 2000). The concerted efforts of these multifaceted components allow spindle assembly to be a tunable and robust process.

Spindle Assembly I: MT Distribution

The redistribution of MTs at mitotic onset demonstrates the ability of the cell to use genetically identical tubulin to perform highly divergent tasks (Figure 1.2). During interphase, stable MTs integrate cellular behavior by spanning vast distances in the cytoplasm. In contrast, more dynamic MTs segregate the duplicated genome during mitosis (Salmon et al. 1984; Saxton, Stemple, and Leslie 1984). And as if the extent of MT remodeling at mitotic onset were not impressive enough, spindle assembly occurs on a timescale of minutes. This reflects the remarkable design of MTs in that they serve as stable tracks while being at-the-ready to reconfigure (Kirschner 1986).

Key to remodeling the MT cytoskeleton at mitotic onset is an increase in both nucleation and catastrophe frequency (Figure 1.2). MTs are nucleated at the spindle poles and chromatin, as well as on the lattices of preexisting MTs. Centrosomes, the primary MTOCs in animal cells, serve as the spindle poles during mitosis. Centrosomes duplicate and recruit γ-tubulin in a cell-cycle dependent manner, increasing their nucleation capacity ~5-fold at mitotic onset (Khodjakov and Rieder 1999; Piehl et al. 2004). Augmin, a hetero-octomeric protein complex, also recruits γ-tubulin to the spindle (Lawo et al. 2009). But instead of localizing to the spindle poles, augmin disperses along spindle MT lattices to mediate branched MT-nucleation (Goshima et al. 2008; Uehara et al. 2009; Petry et al. 2013). Finally, the MAP TPX2 contributes to the increase in MT number during mitosis by mediating their nucleation at chromatin (Schatz et al. 2003; Brunet et al. 2004).

The mechanism by which TPX2 promotes MT nucleation remains unknown, but its exquisite regulation demonstrates the recycling of cellular components to fulfill highly

divergent tasks. Importin-α, a nuclear import factor, blocks TPX2 MT-nucleation activity during mitosis. The small GTPase Ran dissociates TPX2 from importin-α. Since Ran is activated near chromatin, the nuclear transport machinery restricts TPX2-mediated MT nucleation to chromosomes during mitosis (Gruss et al. 2001). It is unclear how chromatin-nucleated MTs integrate with centrosome-nucleated MTs during spindle assembly. But together, centrosomes, augmin, and TPX2 increase the number of MTs in mitotic cells.

In addition to increased nucleation, MTs experience ~10-fold increase in catastrophe frequency coincident with mitotic onset (Belmont et al. 1990; Verde et al. 1992). The MT depolymerase kinesin-13 MCAK is primarily responsible, as it reaches a maximum intracellular concentration at the G2/M transition (Figure 1.3, (Wordeman and Mitchison 1995; Walczak, Mitchison, and Desai 1996; Ganguly, Bhattacharya, and Cabral 2008)). The proteasome rapidly degrades MCAK during the later stages of mitosis, thereby reestablishing the relatively stable MT configuration in interphase cells (Ganguly, Bhattacharya, and Cabral 2008). Such cell-cycle dependent expression and degradation exemplifies ways in which the cell imparts exquisite spatiotemporal control over its molecular constituents.

The mechanism by which MCAK induces MT catastrophe has been intensively studied. Its mechanochemical cycle is limited by ATP hydrolysis rather than adenosine diphosphate (ADP) release, as is the case for conventional kinesin (Friel and Howard 2011). MCAK therefore diffuses along MT lattices instead of taking gated steps. Diffusional motility enables MCAK to reach the MT ends, where it exchanges nucleotide and transits into a tightly bound state (Helenius et al. 2006; Friel and Howard 2011).

These unique features enable MCAK to depolymerize MTs by recognizing and stabilizing curved protofilaments (Su, Ohi, and Pellman 2012). It remains to be seen whether this kinesin-13 paradigm is universal, or if other regulatory kinesins capitalize on unique biochemistries to modulate MT dynamics.

To prevent total MT disappearance during this sudden tendency toward catastrophe, the cell recruits a cohort of MAPs to protect MTs (Andersen 2000). MAP4, XMAP215, XMAP230, and XMAP310 all promote an increase in MT mass in mitotic human cells, albeit by different mechanisms. MAP4 and XMAP310 both increase the rescue frequency (Ookata, Hisanaga, and Bulinski 1995; Andersen and Karsenti 1997). Meanwhile, XMAP215 accelerates the polymerization rate and XMAP230 slows the depolymerization rate (Vasquez, Gard, and Cassimeris 1994; Andersen et al. 1994). Altogether, the factors described here promote the accumulation of highly dynamic MTs within mitotic cells (Andersen 2000).

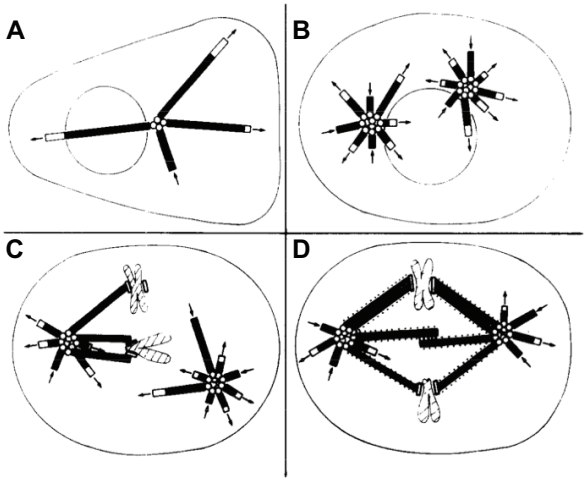

Figure 1.2: Simplified model of spindle assembly, incorporating features of MT dynamic instability. A) During interphase, cells have long MTs with large GTP caps and a small centrosome. B) During prophase, the duplicated centrosomes increase in size, producing a larger number of shorter and more dynamic MTs. C) During prometaphase, a subpopulation of MTs are captured and selectively stabilized by kinetochores. Improper attachments, such as the binding of both sister kinetochores to MTs emanating from the same pole, are corrected by MT depolymerization. D) During metaphase, MTs are further stabilized by molecular motors and MAPs, generally represented here as dots. Adapted from Kirshner and Mitchison (1986).

Spindle Assembly II: MT Layout

MTOCs both focus and cap MT minus-ends, thereby uniformly orienting MTs with their dynamic plus-ends radiating away from the central pole toward the cell periphery (Brinkley 1985). This monopolar array is the MT layout of most animal cells during interphase, and is critical for proper intracellular organization (Kelly 1990). During late G2, the duplicated centrosomes begin to separate by the MT-sliding action of the organizational kinesin-5 Eg5 (Figure 1.3, (Kapitein et al. 2005; Ferenz, Gable, and Wadsworth 2010)). The resulting bipolar geometry is key for proper spindle function, as it enables sister chromosomes to associate with and separate to opposite spindle poles (Figure 1.2, (Tanenbaum and Medema 2010)).

The kinesin-12 Kif15 appears functionally redundant to Eg5, as its overexpression can rescue spindle assembly in cells with inhibited Eg5 activity (Figure 1.3, (Tanenbaum et al. 2009)). However, the biochemical activities of Eg5 and Kif15 seem to be distinct. Eg5 operates as homotetramers in order to crosslink and slide antiparallel MTs (Kapitein et al. 2005). Kif15, on the other hand, is suspected to function as a homodimer complexed with TPX2 (Wittmann et al. 2000; Tanenbaum et al. 2009; Vanneste et al. 2009). Cytoplasmic dynein also generates centrosome-separation forces, but works by sitting on the nuclear envelope and sliding MTs overhead with minus-end directed motility (Raaijmakers and van Heesbeen 2012). This functional redundancy of biochemically distinct molecules imparts robustness to the essential process of spindle assembly.

The kinesin-14 HSET also behaves as an organizational motor (Figure 1.3). But in contrast to Eg5, its second MT-binding site is non-motile and its motor heads are

minus-end directed (Kuriyama et al. 1995). With these distinct biochemical properties, HSET focuses MTs at the spindle poles (Goshima and Vale 2003; Goshima, Nédélec, and Vale 2005). The opposing directionalities of Eg5 and HSET generate antagonistic forces on spindle MTs, exemplifying the emergence of a balanced system from the integration of individual force-generating components (Mountain et al. 1999).

Transport motors capitalize on the layout of spindle MTs to carry macromolecular cargos to specific locations within mitotic cells (Verhey and Hammond 2009). For example, dynein transports kinetochores, the proteinaceous interface between chromosomes and MTs, toward the spindle poles by walking toward MT minus-ends (Howell et al. 2001; Cleveland, Mao, and Sullivan 2003). As MT density is highest at the spindle poles, this dynein-driven transport promotes kinetochore-MT capture.

The transportational kinesin-7 CENP-E also moves kinetochores, but in the opposite direction as dynein (Figure 1.3). By binding to kinetochores and walking processively toward MT plus-ends, CENP-E promotes chromosome alignment and biorientation (Wood et al. 1997). Similarly, kinesin-10 Kid moves chromosomes toward the spindle equator (Figure 1.3, (Funabiki and Murray 2000; Antonio et al. 2000)). But in contrast to CENP-E, Kid binds the chromosome arms directly and walks non-processively (Yajima et al. 2003). Kid must act in ensembles of non-processive motors as to not rip the chromosome arms, while CENP-E acts as individual processive motors since its cargo can withstand persistent forces (Brouhard and Hunt 2005; Wood et al. 1997). A comparision of dynein, CENP-E, and Kid demonstrates that the biochemistry of each motor is fine-tuned to match its specific cellular function.

Spindle Assembly III: MT Dynamics

Spindle MTs can broadly be categorized into two populations, *non-kinetochore-MTs* (non-K-MTs) and *kinetochore-MTs* (K-MTs). Non-K-MTs experience robust plus-end dynamics, as evidenced by their short half-life of ~10 seconds (Zhai, Kronebusch, and Borisy 1995). Non-K-MTs capitalize on this property to search for kinetochores upon NEB at mitotic onset (Kirschner 1986; G. K. Chan, Liu, and Yen 2005). The task of attaching all 92 kinetochores in human cells in non-trivial, considering their small surface area and the relatively vast space of the cytoplasm. But given the increase in MT number and dynamicity at mitotic onset, non-K-MTs find all of the kinetochores in a timely manner (Figure 1.2, (Hayden, Bowser, and Rieder 1990; Holy and Leibler 1994)).

MTs attached end-on to a kinetochore are termed K-MTs. ~25 K-MTs can bind to a single kinetochore, resulting in their incorporation into kinetochore-fibers (K-fibers, (McDonald, O'Toole, and Mastronarde 1992; McEwen, Heagle, and Cassels 1997)). Molecular crosslinks, such as the MAPs TPX2 and HURP, help maintain the integrity of K-fibers by binding along the length of K-MT lattices (Bird and Hyman 2008; Silljé et al. 2006; Wong and Fang 2006). K-MTs are stabilized by both their end-on attachments and incorporation into bundles, as evidenced by their relatively slow turnover of ~7 minutes (Zhai, Kronebusch, and Borisy 1995).

By maintaining long-lived attachments with kinetochores while simultaneously experiencing dynamic instability, K-MTs communicate to both the error correction machinery and spindle assembly checkpoint (SAC, (Pinsky and Biggins 2005; Inoué and Salmon 1995)). Improperly attached MTs generate low tension across the kinetochore and are subsequently depolymerized by MCAK (Andrews et al. 2004; Kline-

Smith et al. 2004). Properly attached MTs generate high tension on the kinetochore interface, which both stabilizes the K-MTs through a catch-bond-type mechanism and fulfills the SAC to prompt anaphase onset (Kotwaliwale and Biggins 2006; Powers et al. 2009; Akiyoshi et al. 2010). MT dynamics therefore confer proofreading capabilities to the kinetochore in order to bias the spindle toward forming proper kinetochore-MT attachments (Figure 1.2, (Pinsky and Biggins 2005)).

At anaphase, depolymerizing K-MTs segregate sister chromosomes to opposing spindle poles (Khodjakov and Rieder 1996). The force required to drag a single chromosome through the cytoplasm is estimated as ~700 pN (Nicklas 1983). This is non-trivial, as molecular motors generate forces on the order of ~5 pN (Svoboda and Block 1994). Similarly, a single depolymerizing protofilament generates ~5 pN of force (Grishchuk et al. 2005). But considering the number of protofilaments within a K-MT and the number of K-MTs within a K-fiber, force from K-fiber depolymerization can theoretically approach ~1.6 nN (Cassimeris 2006). The ability of K-fibers to move chromosomes through the cytosol exemplifies their power, and demonstrates their function as force-generating machines during essential processes.

Regulatory kinesins fine-tune K-MT dynamics for optimized performance. For example, the kinesin-8 Kif18A dampens K-MT dynamics to prevent excessive chromosome movement (Figure 1.3, (Du, English, and Ohi 2010)). Kif18A exhibits remarkable ultra-processivity, enabling it to accumulate at K-MT plus-ends as a function of K-fiber length (Stumpff et al. 2011; Su et al. 2011; L. N. Weaver et al. 2011). By measuring MT length, Kif18A coordinates the action of autonomous K-fibers (Stumpff et al. 2011).

K-fibers demonstrate an unusual property in that they continuously translocate poleward while maintaining a constant length. Termed *flux*, this process is attributed to balanced K-MT plus-end polymerization and minus-end depolymerization (Mitchison 1989; Sawin and Mitchison 1991; Cameron et al. 2006). Flux is thought to exert tension on the kinetochore-MT interface to both stabilize K-MTs and segregate chromosomes during anaphase (G. C. Rogers, Rogers, and Sharp 2005). However, flux remains a largely unexplained phenomenon, both mechanistically and functionally.

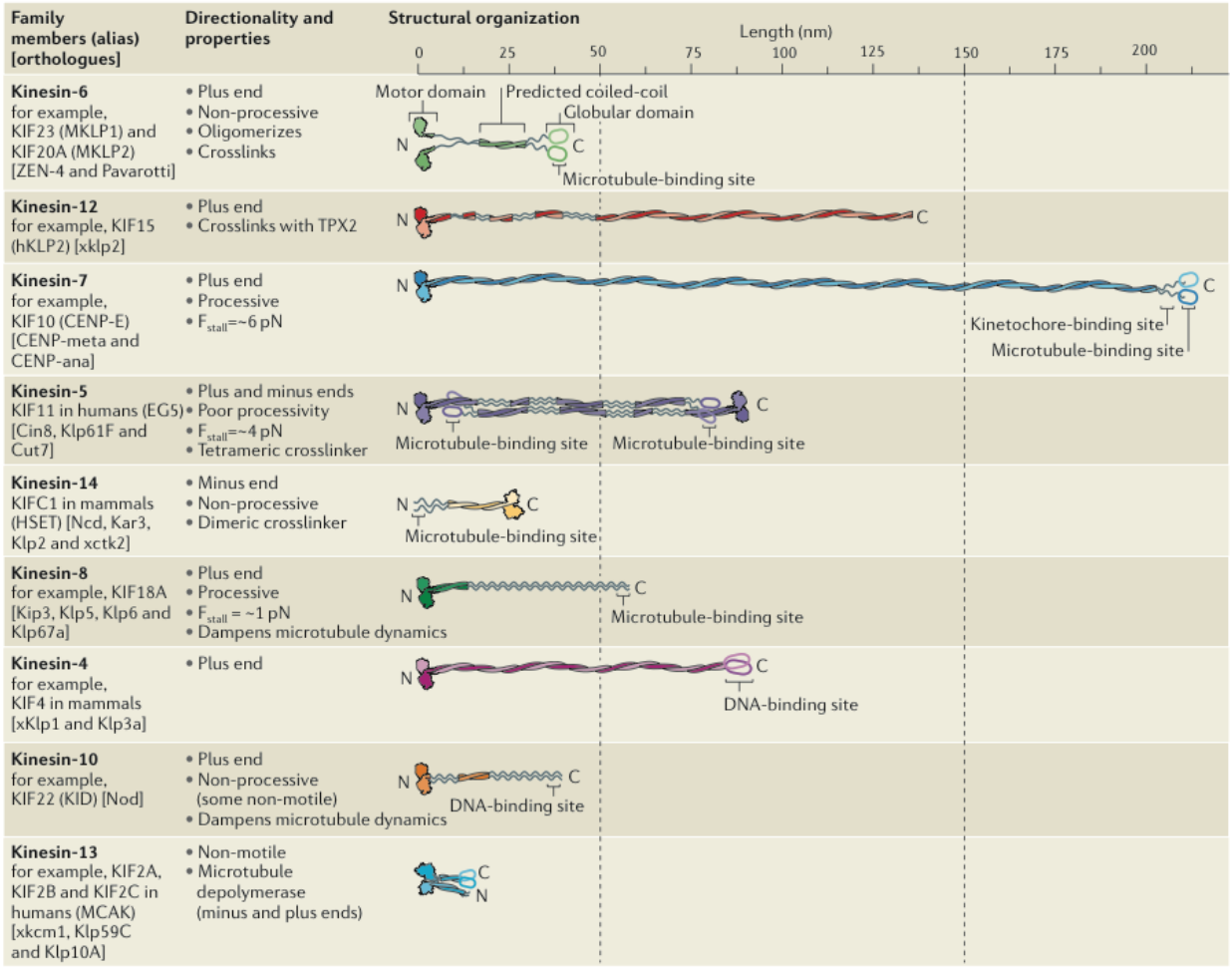

Figure 1.3: Topology of mitotic kinesins. Homologous motor heads are coupled to subfamily-specific stalks and tails in order to acquire functional specificity. Adapted from Cross and McAinsh (2014).

Spindle Adaptability and Robustness

As a self-organized macromolecular machine, the spindle explores different configurations before arriving at a stable steady state. But what it lacks in efficiency, the spindle makes up for in adaptability. Continuous MT turnover enables the spindle to constantly rebuild itself. Flux alone can turn over the entire spindle in ~10 minutes. In this way, spindles can rapidly recover from damage and adapt to changing conditions (Kirschner 1986).

This concept has been shown experimentally by completely dismembering spindles with MT poisons. Upon removal of the drug, spindles successfully reassemble on the order of minutes (Brinkley, Stubblefield, and Hsu 1967; De Brabander et al. 1981). The weight of these results are made greater in that the damaging agents are synthetic, emphasizing the ability of the spindle to manage unpredictable disturbances.

In addition to chemical perturbations, the spindle responds to physical disruption. Spindles elongate upon cellular compression and shorten upon an increase in hydrostatic pressure or decrease in temperature (S. Dumont and Mitchison 2009). Spindles also remodel in response to compressive forces by microneedles (Itabashi et al. 2009). In the early divisions of Xenopus embryos, spindle length decreases proportionately with cell length (Wühr et al. 2008). Therefore, spindle remodeling in response to physical stimuli is likely important for proper function in cells of varying morphologies.

In addition to adaptability, the spindle is quite robust. This is owed largely to molecular redundancy, as spindle constituents often have overlapping functions but act through distinct biochemical mechanisms (Welburn 2013). For example, both

centrosomes and chromatin nucleate MTs during mitosis. Centrosomes serve as the dominant source for MT nucleation in vertebrate somatic cells; however, the chromatin-mediated pathway is sufficient to drive spindle assembly upon centrosome destruction (Khodjakov et al. 2000; Megraw, Kao, and Kaufman 2001). Similarly, Eg5 and Kif15 have overlapping functions during spindle assembly in human cells (Tanenbaum et al. 2009).

Diversity in spindle assembly strategies among eukaryotes also denotes robustness. Proteins considered key for spindle function in some organisms are dispensable in others. For example, mitosis in plant cells and meiosis in animal cells occur without centrosomes by utilizing the chromatin-mediated nucleation pathway (H. Zhang and Dawe 2011; J. Dumont and Desai 2012). Similarly, the Eg5 homolog in *C. elegans*, BMK-1, is dispensable for spindle assembly, while the Kif15 homolog, KLP18, is essential (Saunders et al. 2007; Segbert et al. 2003; Wignall and Villeneuve 2009). By employing multiple mechanisms to assemble, the spindle avoids catastrophe upon failure of one component. Self-organization, while complicated and elusive, is key for macromolecular machines to maintain structural integrity while performing essential functions.

Pharmacological Poisoning of the Mitotic Spindle

Mitosis serves as a powerful point for therapeutic intervention in the treatment of neoplastic diseases like cancer (K. S. Chan, Koh, and Li 2012). Anti-mitotic pharmacological agents tame the proliferative capacity of human tumor cells by poisoning the mitotic spindle (Marzo and Naval 2013). Classically, spindle poisons

target tubulin (Wall 1998). For example, vinca alkaloids prevent MT polymerization and are commonly administered for the treatment of lymphomas, myelomas, breast, and lung cancers. Meanwhile, taxanes stabilize MTs and are given to patients suffering from lung, breast, ovarian, and prostate cancers (Jordan and Wilson 2004). Tubulin poisons have long been assumed to induce a lethal mitotic arrest; however, recent experimental evidence suggests that they instead generate lethal doses of chromosomal instability (CIN, (Orth et al. 2011; Zasadil et al. 2014; McClelland, Burrell, and Swanton 2009)). Regardless of their mechanism of action, tubulin poisons remain the most clinically effective of any anti-mitotic drug.

Despite the powerful anti-proliferative potential of tubulin poisons, a major challenge to their clinical success stems from their harsh side effects (Schmidt and Bastians 2007). The functional diversity of tubulin, while highly intriguing from a biological perspective, causes tubulin poisons to also target non-mitotic cells. Post-mitotic neuronal cells are particularly reliant upon MTs for axonal transport, so dose-limiting toxicities of tubulin poisons mostly arise from neurotoxicity. Therefore, recent efforts have focused on the identification of MT-independent spindle poisons whose effects are confined to mitotic cells (Schmidt and Bastians 2007).

The next generation of spindle poisons target mitotic kinesins (Rath and Kozielski 2012). As described above, ~16 kinesins subtypes are involved in various aspects of spindle assembly and function. Kinesins are considered highly druggable because they contain catalytic binding pockets (Wood, Cornwell, and Jackson 2001). While kinesins generally share a common catalytic domain, unique features have been identified that create opportunity for drug specificity (Vale and Fletterick 1997; Welburn 2013). For

example, the kinesin-5 Eg5 has an unusually long loop-5 in its catalytic domain (Yan et al. 2004). A number of pharmacological agents recognize this unique feature to efficiently inhibit Eg5 activity with no known off-target effects.

Eg5 inhibitors (K5Is) have been developed over the past decade by researchers and pharmaceutical companies alike (Mayer et al. 1999; Jackson et al. 2007). The primacy of Eg5 during spindle assembly has made it an attractive target for anti-mitotic chemotherapies. Indeed, K5Is induce a potent and lethal mitotic arrest in cell culture and murine xenografts (Kapoor et al. 2000; Purcell et al. 2010). This preclinical success spurred the enthusiastic entry of K5Is into clinical trials.

K5Is have been administered in over 38 clinical trials (Rath and Kozielski 2012). As anticipated, K5Is gave no neurotoxic side effects in Phase I clinical trials. However, K5Is failed to induce even partial tumor regression during Phase II trials. This devastating clinical performance has halted any further development of K5I monotherapies (K. S. Chan, Koh, and Li 2012; Rath and Kozielski 2012; Marzo and Naval 2013).

A number of theories exist as to why K5Is failed in the clinic. One hypothesis suggests that an overexpression of efflux pumps prevents adequate drug accumulation in cells (Longley and Johnston 2005). However, K5Is do not appear to be substrates of P-glycoprotein, the prominent efflux pump responsible for conferring multi-drug resistance to cancer cells (K. S. Chan, Koh, and Li 2012). Another theory postulates that mitotic slippage uncouples mitotic arrest from cell death. In this scenario, cells exit mitosis prematurely and become highly aneuploid (Brito and Rieder 2006). This haunting possibility infers that K5Is may actually accelerate aggressive tumor

phenotypes by producing chronic low-grade CIN (Kuukasjärvi et al. 1997; Kops, Weaver, and Cleveland 2005). A final theory holds that tumor cells actually proliferate slowly *in vivo*, thereby questioning the strategy of anti-mitotics altogether (Komlodi-Pasztor, Sackett, and Fojo 2012; Mitchison 2012).

One way to reconcile both mitotic slippage and a slow proliferation rate is with combinatorial therapies. Mitotic slippage occurs by untimely proteasome activation (Brito and Rieder 2006). So K5Is are being paired with the proteasome inhibitors bortezomib and cafilzomib in an effort to strengthen the mitotic arrest (Marzo and Naval 2013). K5Is are also being administered in combination with S-phase inhibitors (Jones, Plummer, and Burris 2006; Rath and Kozielski 2012). This multiphase combinatorial strategy aims to increase the odds of killing tumor cells in slowly proliferating tumor cells.

Perhaps the most compelling explanation for the clinical shortcomings of K5Is stems from the functional redundancy of distinct molecules. While advantageous from an evolutionary standpoint, molecular redundancy complicates the pharmacological inhibition of cellular machines (Stelling et al. 2004). Compensatory changes of parallel pathways could confer drug resistance to cells, thereby enabling disease progression. In this scenario, a combination of drugs that inhibit the same process but target different molecular players would eradicate tumor cells (Welburn 2013).

In addition to the design of intelligent combinatorial strategies, investigators are on the hunt for novel molecular targets in the development of anti-mitotic chemotherapies. CENP-E represents one such emerging target, as the CENP-E inhibitor GSK-923295 has just entered Phase I clinical trials (K. S. Chan, Koh, and Li

2012; Rath and Kozielski 2012). Preclinical studies of GSK-923295 in cell culture and mouse models have produced promising results (Schafer-Hales et al. 2007; Wood et al. 2010). And preliminary results from Phase I trials are indicative of a high dose-limiting toxicity (Chung et al. 2012). But the true clinical benefit of CENP-E inhibition has yet to be tested.

In addition to the spindle, other cytoskeletal-based cellular machines may serve as attractive targets for chemotherapies. For example, the actin-based machines of the lamellipodium and invadapodium are key for tumor cell invasion and metastasis (Martin et al. 2000; A. M. Weaver 2006). Understanding how such cellular machines assemble and operate will provide insight into cancer progression and elucidate more powerful methods of treatment.

CHAPTER II

MATERIALS AND METHODS

Cell Culture, Transfections, and Drug Treatments

HeLa "Kyoto" cells were cultured in DMEM containing 10% fetal calf serum (FCS) and antibiotics. Culturing medium for HeLa cells stably expressing GFP-Tubulin and mCherry-H2B (a gift from Dr. Dan Gerlich) additionally contained 500 μg/ml G418. Eg5-independent cell lines were generated by continuously incubating HeLa cells in 10 μM STLC. Individual clonal lines were isolated ~4 weeks following the initiation of selection, and cultured in the presence of 10 μM STLC.

siRNA transfections were performed using HiPerfect (Qiagen) or Oligofectamine (Invitrogen) according to the manufacturers' recommendations. The following siRNAs were used in this study: Kif15 GGACAUAAAUUGCAAAUAC (Dharmacon), Nuf2 AAGCATGCCGTGAAACGTATA (Qiagen), and Eg5 CUGAAGACCUGAAGACAAUdTdT (Qiagen, (Tanenbaum et al. 2009; DeLuca et al. 2002; Weil et al. 2002)). For control depletions, cells were transfected with 40 nM All Stars siRNA (Qiagen). All depletions were subjected to immunofluorescence or live cell imaging ~48 hours post-transfection. Plasmid transfections were performed using Lipofectamine 2000 (Invitrogen) according to the manufacturer's recommendations and subjected to immunofluorescence ~24 hours post-transfection.

For drug treatments, Monastrol (Sigma-Aldrich) was used at 100 μM, GSK-923295 (MedChem Express) at 50 nM or 100 nM as indicated, Taxol (Sigma-Aldrich) at

2 nM, and dimethyl sulfoxide (DMSO) at 0.3%. After ~24 hours, treated cells were subjected to imaging with transmitted light. FCPT (a gift from Drs. Aaron Groen and Tim Mitchison) was used at 200 μM and DMSO at 0.1%. After ~30 minutes, treated cells were subjected to immunofluorescence.

For adenylyl imidodiphosphate (AMPPNP) infusion, cells were pretreated with 4 μM Taxol in OptiMem containing 10% FCS for 15 minutes. Cells were then washed twice with permeabilization buffer (PB; phosphate buffered saline (PBS), 1 mg/ml bovine serum albumin (BSA), 4 μM Taxol) and permeabilized with digitonin at 0.006% in PB for 30 seconds. Cells were again washed twice with PB and treated with AMPPNP diluted to 1 mM in treatment buffer (TB; 25 mM HEPES, pH = 7.4, 115 mM potassium acetate, 5 mM sodium acetate, 5 mM $MgCl_2$, 0.5 mM ethylene glycol tetraacetic acid (EGTA), 10 mg/ml BSA, 4 μM Taxol) for 10 minutes. This protocol was adapted from Cai *et al*. and Hammond *et al.* (Cai et al. 2007; Hammond et al. 2009).

To cold treat cells, culturing medium was exchanged for fresh medium cooled to 0°C. Cells were then placed on ice for 10 minutes. To synchronize cells at metaphase prior to cold-treatment, cells were incubated in 9 μM RO3306 (Axxora) overnight to induce a G2 arrest (Vassilev et al. 2006). The drug was removed by washing 3 times with fresh media. Cells were then incubated 40 minutes at 37°C prior to exposure to cold temperatures. To generate monoasters, cells were incubated in 100 μM Monastrol overnight (Mayer et al. 1999).

Generation of Kif15 Antibodies

The C-terminal 427 amino acids of Kif15 were fused to GST as an *EcoRI/XhoI* fragment in pGEX6P-1 and used to immunize rabbits (Cocalico). Kif15 antibodies (αC2) were affinity-purified by passing anti-GST-depleted serum over Affi-Gel 10 coupled to GST-Kif15^{CT}. Antibodies were dialyzed into PBS and frozen in liquid N_2.

Immunoblotting

Immunoblots were blocked with 5% w/v milk in PBS-T and then probed with 1 μg/ml αC2, 1 μg/ml anti-*Xenopus laevis* Eg5 (a gift from Tim Mitchison; (Miyamoto et al. 2004)), 1 μg/ml anti-His (Sigma), or anti-Hec1 (Abcam) at 1:1000, followed by fluorescently tagged anti-rabbit secondary antibodies (Invitrogen) according to the manufacturer's recommendations. Tubulin was used as a loading control and detected with DM1α antibodies (Sigma) followed by fluorescently tagged anti-mouse secondary antibodies (Invitrogen) according to the manufacturer's recommendations. Bound antibodies were detected using an Odyssey fluorescence detection system (Mandel Scientific) and quantified using ImageJ.

To measure Kif15 and Eg5 protein levels in EIC^{HeLa} cells, cultures of a 6-well tissue culture plate (Corning) were trypsinized, washed with PBS, and resuspended in NP40 buffer (10 mM sodium phosphate, pH = 7.2, 150 mM NaCl, 2 mM ethylenediaminetetraacetic acid (EDTA), 1% NP-40) containing protease inhibitors. After 15 minutes on ice, extracts were clarified at 4°C for 15 minutes and mixed with Laemmli buffer. Equivalent amounts of protein were resolved by SDS-PAGE (sodium dodecyl sulfate-polyacrylamide gel electrophoresis) and analyzed by immunoblotting.

Immunostaining and Fixed Cell Imaging

HeLa and EIC^{HeLa} cells were fixed with methanol at -20°C for 10 minutes. Where indicated, cells were pre-extracted with 100 mM PIPES, pH = 6.8, 1 mM $MgCl_2$, and 1% TX-100 for 30 seconds prior to methanol fixation. The following primary antibodies were used in this study: αC2 and anti-*Xenopus laevis* Eg5 at 1 µg/ml, and anti-Hec1 (Abcam) and CREST (Immunovision) at 1:1000. Cells were incubated with primary antibodies for 1 hour. Tubulin was labeled with DM1α at 1:500 for 30 minutes. Secondary antibodies conjugated to Alexa 488 or Alexa 594 (Invitrogen) were used at 1:1000 for 45 minutes. DNA was counterstained with 5 µg/ml Hoechst-33342. Stained cells were mounted in Prolong (Invitrogen). Images were acquired at 37°C with a DeltaVision Elite image restoration system (GE Healthcare) equipped with a 60X 1.4 numerical aperature (NA) lens (Olympus) and a Cool SnapHQ2 charge-coupled device (CCD) camera (Photometrics). Either single optical slices or z-sections spaced 200 nm apart were acquired with SoftWorx (GE Healthcare). Images were subsequently processed with ImageJ (adjusting levels, rotating, and cropping).

Live Cell Imaging

For live imaging of spindle assembly, HeLa cells stably expressing GFP-Tubulin and mCherry-H2B were plated onto glass-bottomed dishes (MatTek Corporation) ~16 hours prior to siRNA transfection. ~30 hours post transfection, an equal volume of media containing 200 µM Monastrol was added to each dish yielding a final concentration of 100 µM and incubated overnight. Prior to imaging, cells were washed 3 times with 2 mls of CO_2-independent media (Life Technologies). Z-sections spaced 2

μm apart were acquired in both GFP and mCherry channels every 90 seconds using a DeltaVision Core system (Applied Precision) equipped with an environmental chamber (Applied Precision), 60X 1.4 NA lens (Olympus), and a CCD camera.

For live imaging of spindle assembly in EIC^{HeLa} cells, cells were plated onto glass-bottomed dishes (MatTek Corporation) ~16 hours prior to being transfected with mCherry-Tubulin. ~24 hours post transfection, cells were imaged in the presence of CO_2 at 37°C in L-15 medium without phenol red supplemented with 10% FCS, 10 μM STLC, antibiotics, and 7 mM K-HEPES, pH = 7.7. Z-sections spaced 2 μm apart were acquired with the DeltaVision Core system described above using a 40X 1.4 NA lens (Olympus).

For live imaging of GFP-EB3 in EIC^{HeLa} cells, cells were plated on glass-bottomed dishes (MatTek Corporation) ~24 hours prior to being transfected with Nuf2-targeting siRNAs. Cells were transfected with GFP-N1-EB3 ~48 hours following plating. Cells were imaged ~72 hours following plating using a Nikon TE2000-E system equipped with a 1.4 NA 60X objective (Nikon), a CSU-10 spinning disk confocal head (Yokogawa), and a Cascade 512B EM CCD camera (Princeton Instruments).

Molecular Biology and Baculovirus Construction

A full-length human Kif15 cDNA (Source BioScience, GenBank accession number BC143752) was modified by site-directed mutagenesis (Stratagene) to remove two frame shift mutations within the open reading frame (ORF). Specifically, a “C” was inserted following nucleotide 64, and a “G” was removed at nucleotide 1048. The resulting ORF is identical in sequence to the cDNA reported by Vanneste *et al.* except

that it lacks the codons for amino acid residues 8-21 (ELRSVTNGQSNQPS) (Vanneste et al. 2009).

pEGFP-C1-Kif15-FL, pEGFP-C1-Kif15-N700, pET15-Kif15-N700, and pET15-Kif15-Coil-1 were constructed by isothermal assembly (Gibson et al. 2009). PCR fragments encompassing Kif15 amino acids 1-1374 (pEGFP-C1-Kif15-FL), 1-700 (pEGFP-C1-Kif15-N700, pET15-Kif15-N700), and 365-700 (pET15-Kif15-Coil-1) were generated with Phusion DNA polymerase (Thermo) and assembled into pEGFP-C1 (Clontech) or pET15 (Novagen) with *EcoR*I and *Kpn*I or *Nde*I and *Xho*I, respectively. GFP-Kif15-FL is functional, as it rescues spindle assembly in cells treated with Monastrol (data not shown; (Vanneste et al. 2009; Tanenbaum et al. 2009)). pFASTBAC-HTa-GFP-Kif15 was constructed by amplifying the GFP-Kif15 coding region from pEGFP-C1-Kif15-FL, and assembling this fragment into *EcoR*I/*Xho*I-restricted pFASTBAC-HTa (Life Technologies) by isothermal assembly. pFASTBAC-HTa-GFP-Kif15 was used with the Bac-to-Bac system (Invitrogen) to create a baculovirus that expresses His_6-GFP-Kif15-FL.

pEGFP-C1-HSET was constructed by isothermal assembly. A PCR fragment encompassing amino acids 1-673 (GenBank accession number BC121041) was generated with Phusion DNA polymerase and assembled into pEGFP-C1 restricted with *EcoR*I and *Kpn*I. pFASTBAC-HTa-GFP-HSET was constructed by amplifying the GFP-HSET coding region from pEGFP-C1-HSET, and assembling this fragment into *EcoR*I/*Xho*I-restricted pFASTBAC-HTa by isothermal assembly. pFASTBAC-HTa-GFP-HSET was used with the Bac-to-Bac system (Invitrogen) to create a baculovirus that expresses His_6-GFP-HSET.

pET15b-mCherry-TPX2 was constructed by three-part isothermal assembly. PCR fragments encompassing mCherry and amino acids 1-747 of human TPX2 (GenBank accession number AK312549) were generated by Phusion DNA polymerase and assembled into pET15b restricted with *Nde*I and *Xho*I.

Protein Expression and Purification

His_6-GFP-Kif15-FL was expressed in *Sf*9 cells for 72 hours and purified using methods described previously except that it was subjected to size exclusion chromatography on a Hiload 16/60 Superdex 200 preparatory grade column (GE Healthcare, (Du, English, and Ohi 2010)). The bed volume for this column is 120 mls, and the void volume is 56 mls. "High salt" gel filtration buffer (10 mM K-HEPES, pH = 7.7, 1 mM dithiothreitol (DTT), 0.1 mM MgATP) contained 300 mM KCl, whereas "low salt" gel filtration buffer contained 50 mM KCl. 2 ml peak fractions were combined and concentrated using Amicon centrifugal filter units (Millipore). Protein concentrations were determined using Bradford assays, taking into account that Kif15 exists as a dimer in solution. Powdered sucrose was added to 20% w/v. Protein was aliquoted, frozen in liquid N_2, and stored at -80°C. His_6-GFP-HSET was similarly expressed and purified.

His_6-Kif15-N700 was expressed in BL21DE3 cells with 0.4 mM IPTG for 4 hours. For purification, cells were pelleted and resuspended in lysis buffer (PNI [50 mM sodium phosphate, 500 mM NaCl, 20 mM imidazole], 5 mM β-mercaptoethanol (β-ME), and 1% NP40, and protease inhibitors [1 mM phenylmethylsulfonyl fluoride, 1 mM benzamidine, and 10 µg/ml each of leupeptin, pepstatin, and chymostatin]). Lysate was incubated with 1 mg/ml lysozyme for 30 minutes, sonicated, and clarified by centrifugation at

35,000 rpm for 1 hour in a Ti 45 rotor (Beckman). ~3 ml of Ni^{++}-NTA agarose (Qiagen) was incubated with the supernatant for 1 hour at 4°C, and then washed extensively with wash buffer (PNI, 5 mM β-ME, and 50 μM MgATP). Protein was eluted with PNI, 5 mM β-ME, 0.1 mM MgATP, and 180 mM imidazole, and peak fractions subjected to size exclusion chromatography on a Superdex 200 column (GE Healthcare) equilibrated in 10 mM K-HEPES, pH = 7.7, 300 mM KCl, 1 mM DTT, 0.1 mM MgATP. Protein concentrations were determined using Bradford assays, taking into account that Kif15 exists as a dimer in solution. Powdered sucrose was added to 20% w/v. Protein was aliquoted, frozen in liquid N_2, and stored at -80°C.

His_6-Kif15-Coil-1 was similarly expressed and purified in BL21DE3 cells, except wash and elution buffers were devoid of MgATP and included 10% glycerol. Instead of size exclusion chromatography, protein was desalted with a PD10 column (GE Healthcare) equilibrated in 10 mM K-HEPES, pH = 7.7, 100 mM KCl, 1 mM DTT, and 20% sucrose.

GST-Kif15-Coil-2 was expressed in BL21DE3 cells using pGEX6P-1-$Kif15^{CT}$ (described under generation of Kif15 antibodies) with 0.4 mM IPTG for 4 hours. To purify, cells were pelleted and resuspended in lysis buffer (PBS, 500 mM NaCl, 5 mM β-ME, and 1% NP40, and protease inhibitors [1 mM phenylmethylsulfonyl fluoride, 1 mM benzamidine, and 10 μg/ml each of leupeptin, pepstatin, and chymostatin]). Lysate was incubated with 1 mg/ml lysozyme for 30 minutes, sonicated, and clarified by centrifugation at 35,000 rpm for 1 hour in a Ti 45 rotor (Beckman). ~3 ml of glutathione agarose (Sigma) was incubated with the supernatant for 1 hour at 4°C, and then washed extensively with wash buffer (PBS, 500 mM NaCl, and 5 mM β-ME). Protein

was eluted with 50 mM Tris, pH = 8.0, 500 mM KCl, and 5 mM reduced glutathione. Peak fractions were combined and dialyzed against 1 L of 10 mM K-HEPES, pH = 7.8, 500 mM KCl, 1 mM DTT, and 10% glycerol in 12kD-14kD molecular weight cut off dialysis tubing (Fisherbrand). Protein concentrations were determined using Bradford assays, taking into account that Kif15 exists as a dimer in solution. Protein was aliquoted, frozen in liquid N_2, and stored at -80°C.

His_6-PRC1 was expressed in and purified from BL21DE3 cells using pET-Duet1-His6-TEV-PRC1 (a gift from Drs. Subramanian and Kapoor, Rockefeller University) as previously described (Subramanian et al. 2010). PRC1 was labeled with Alexa 647 using a protein labeling kit (Life Technologies). Labeling conditions were as recommended with the exception that the protein was incubated with the dye for 1 minute at 4°C prior to desalting.

His_6-mCherry-TPX2 was expressed and purified in BL21DE3 cells as described for His_6-Kif15-Coil-1, with the exception that the protein was subjected to size exclusion chromatography on a Superdex 200 column.

MT Assays

For gliding assays with Kif15-N700, flow cells were constructed with double-stick tape and infused with Kif15-N700 at 1.9 μM for 3 minutes, 1% Pluronic F-127 in BRB80 for 1 minute, and uniformly Alexa 488-labeled GMPCPP MTs (488-MTs, 1:9 labeled:unlabeled) at 1 μM tubulin in BRB80 for 3 minutes. For gliding assays with GFP-Kif15-FL, flow cells were infused with GFP-Kif15-FL at 0.7 μM for 3 minutes, 1% Pluronic F-127 for 1 minute, and X-rhodamine-labeled GMPCPP MTs (XR-MTs, 1:9

labeled:unlabeled) at 62 nM tubulin in BRB80 for 3 minutes or αC2 at 1 mg/ml in BRB80 for 3 minutes, 1% Pluronic F-127 for 1 minute, 0.7 μM motor for 3 minutes, and 62 nM XR-MTs for 3 minutes. For all, flow cells were washed between each infusion with 3 volumes wash buffer (WB; BRB80, 1 mM MgATP, 500 μg/ml casein). After the final infusion, the flow cells were washed with 3 volumes flow cell buffer (FCB; BRB80, 1 mM MgATP, 500 μg/ml casein, oxygen scavenging mix [200 μg/ml glucose oxidase, 35 μg/ml catalase, 25 mM glucose, 70 mM β-ME]). MT motility was recorded at 2-second intervals by time-lapse microscopy. For polarity-marked MT gliding by Kif15-N700, bright/dim polarity marked GMPCPP MTs were assembled as previously described and used in place of 488-MTs (Hyman 1991).

For sliding assays, flow cells were infused with biotinylated BSA at 2 mg/ml for 10 minutes, streptavidin at 10 mg/ml for 10 minutes, 1% Pluronic F-127 for 1 minute, biotin/rhodamine-labeled GMPCPP MTs (0.18:1:9 biotinylated:rhodamine:unlabeled) at 1 μM tubulin in 20 μl BRB80 for 20 minutes, Kif15-N700 at 1.9 μM for 2 minutes, and 0.5 μM 488-MTs for 3 minutes. Between each infusion, the chamber was washed with 3 volumes WB devoid of MgATP. After the final infusion, the chamber was washed with 3 volumes FCB devoid of MgATP. After starting image acquisition, flow cells were infused with FCB containing 750 μM MgATP. Images were acquired every 2 seconds by time-lapse microscopy.

For bundling assays, 488-MTs at 0.5 μM tubulin were combined with 45 nM Kif15-N700 in 20 μl BRB80 for 10 minutes. 1 μl reaction volumes were sandwiched between a coverslip and slide for imaging. For two-color bundling assays, 488-MTs and XR-MTs were mixed 1:1 and diluted to 0.2 μM tubulin in 20 μl BRB80. Kif15-N700 was

added to 83 nM. 1 mM MgATP was included where indicated. Mixes were incubated for 5 minutes followed by preparation of a 1 µl squash for imaging.

To localize GFP-Kif15-FL on MTs bundled by PRC1, GMPCPP XR-MTs were diluted to 1 µM in BRB80 supplemented with 1 mM MgATP and 1 mM DTT. PRC1 and GFP-Kif15-FL were included at 100 nM where indicated. After a 15 minute incubation at room temperature, 1 µl reaction volumes were sandwiched between a coverslip and slide for imaging.

For all, images were acquired at ambient temperatures by widefield fluorescence microscopy on an Eclipse 90i (Nikon) equipped with a 100X 1.4 NA (Nikon) objective and a Cool SnapHQ2 CCD camera (Photometrics). Nikon Elements was used for acquisition and ImageJ for subsequent image processing (adjusting levels, rotating, and cropping).

MT-co-pelleting was performed with Coil-1 or Coil-2 at 1 µM in 100 µl reaction buffer (RB; 10 mM HEPES, pH = 7.7, 50 mM KCl, 1mM DTT) with tubulin or taxol-stabilized MTs at 1 µM. Reactions were incubated for 15 minutes at room temperature and spun over a 150 µl sucrose cushion (10 mM HEPES, pH = 7.7, 50 mM KCl, 40% sucrose w/v) at 60k rpm for 20 minutes. 1 µM Taxol was included in the RB and sucrose cushion for MT-containing reactions. 50 µl of the supernatants were collected and mixed 1:1 with 2X sample buffer (2X SB; 100 mM Tris-Cl, pH = 6.8, 4% SDS, 20% glycerol, 200 mM DTT, and 200 µg/ml bromophenol blue). The supernatant/cushion interfaces were washed twice with RB, followed by complete removal of the cushions. Pellets were resuspended in 100 µl 2X SB. 20 µl of each fraction was boiled, separated on a 10% SDS-PAGE gel, and transferred to nitrocellulose for immunoblotting.

Analysis of MT Gliding

Images of MT gliding were taken every 2 seconds. Computer-aided feature extraction (CAFE) was applied to each frame (1392x1040 pixels at 0.07 μm/pixel) to identify individual MTs. Technical details of the CAFE algorithm will be published elsewhere. But in brief, the identification procedure involved assigning `beads' to high pixel intensity-regions whose sizes are comparable to the diameter of a MT. `Bonds' were then assigned between beads based on their proximity, which singles out isolated beads that are not part of a MT. Among connected beads, MTs were identified based on the orientational persistence of bonds. Additional steps were taken to deal with cases such as multiple filaments crossing each other or two nearly parallel filaments being connected by bonds. Individual MTs were traced across frames by examining their axial displacement, *i.e.*, when two identified filaments in consecutive frames nearly overlap and are displaced mainly in the axial direction, they were considered to be the trace of a single MT. Due to the pixel intensity fluctuation and various noises, the number and location of MTs varied across frames. Stringent criteria were imposed for fault-tolerance, where only clearly resolved and isolated MTs were used. As a result, tracing of a single MT may be broken into multiple trajectories since certain frames in the middle may be discarded by this criteria. Thus, the number of trajectories exceeds the total number of MTs identified in a set of experiments for a given Kif15 construct. In total, the number of independent movies analyzed was: 9 (GFP-Kif15-FL with αC2), 9 (GFP-Kif15-FL), and 3 (Kif15-N700).

Single Molecule Imaging and Analysis

GFP-Kif15-FL molecules were imaged at 1 nM on individual Taxol-stabilized, rhodamine MTs (1:20 labeled:unlabeled) in an imaging assay buffer (IAB; 80 mM PIPES, pH = 6.9, 1 mM EGTA, 4 mM $MgCl_2$, 1 mM DTT, 20 μM Taxol, 1 mg/ml Casein, 1 mM ATP, and anti-fade reagents 5 mg/ml β-D-glucose, 250 μg/ml glucose oxidase, and 30 μg/ml catalase). Where indicated, GFP-Kif15-FL was mixed with αC2 (1:20) for 15 minutes and diluted to 1 nM prior to imaging. For photobleaching experiments, GFP-Kif15-FL and GFP-Kif15-FL-αC2 were nonspecifically adsorbed to etched coverslips at 5 nM in IAB. Imaging of GFP-Kif15-FL in MT bundles was performed by first creating MT bundles with 10 nM PRC1, followed by introducing GFP-Kif15-FL at 1 nM in IAB. Images were acquired every 0.12 seconds using TIRF microscopy equipped with an EMCCD Camera with a brief exposure of green light to image MTs followed by excitation at 488 nm for imaging GFP-Kif15-FL.

Locating and tracking of individual fluorescent GFP-Kif15-FL molecules was performed from analysis of video frames similar to previously described using custom software written in Matlab (Mathworks, (Shin et al. 2009)). Dwell times for single MT-associated GFP-Kif15-FL molecules were determined by multiplying the number of frames the spot remained bright by the acquisition interval. Speeds were measured by calculating the slope of a straight line fit to a plot of distance traveled *versus* time. Analysis and fitting of the dwell time histograms, run length distributions and speed distributions were all calculated in Matlab. Kymographs for individual GFP-Kif15-FL trajectories were created using ImageJ.

SVAU

Purified GFP-Kif15-FL was run in an Optima XLI ultracentrifuge (Beckman Coulter, Brea, CA) equipped with a four-hole An-60 Ti rotor at 42,000 rpm at 4°C. Samples were loaded into double-sector cells (path length of 1.2 cm) with charcoal-filled Epon centerpieces and sapphire windows. Sedfit (version 12.0) was used to analyze velocity scans using every scan from 1-50 (Schuck 2000). Approximate size distributions were determined for a confidence level of p = 0.95, a resolution of n = 300, and sedimentation coefficients (S) between 0 and 15.

EM

Uranyl-formate stained samples were prepared for electron microscopy (EM) as previously described (M. Ohi et al. 2004). In brief, 3 µl of sample was absorbed to a glow discharged 400-mesh copper grid covered with carbon-coated film. The grid was washed in two drops of water and then stained with two drops of 0.75% uranyl formate. Samples were imaged on a F20 electron microscope (FEI, Hillsboro, OR) operated at an acceleration voltage of 200 kV and equipped with 4kx4k Ultrascan CCD (Gatan, Pleasanton, CA). Images were recorded at a magnification of 100,000X and a defocus value of -1.5 mm.

Statistical Analysis

Statistically relevant differences in experimental data were determined using the T.TEST function in Excel (Microsoft). In all cases, P-values report the two-tailed distribution of a two-sample Student's t-Test assuming unequal variance.

CHAPTER III

A TRANSIENT MONOPOLAR SPINDLE SERVES AS AN ACHILLES' HEEL OF K5I-RESISTANT CELLS

Emma G. Sturgill and Ryoma Ohi

Department of Cell and Developmental Biology, Vanderbilt University Medical Center, Nashville, TN

Previously published in part as:

Sturgill EG and Ohi R. (2013). Kinesin-12 differentially affects spindle assembly depending on its microtubule substrate. *Current Biology* 23, 1280-1290.

Abstract

Documented here is the generation and characterization of a cell-culture model system with which to study kinesin-5 Eg5-inhibitor (K5I) resistance. Human tumor cells that survived chronic K5I treatment were clonally isolated and cultured into cell lines. A novel spindle assembly pathway circumvents the requirement for Eg5 in these cells, offering a potential explanation for why K5Is fail in the clinic. This "reverse jackknifing" pathway is mechanically distinct from Eg5-dependent spindle assembly, rendering K5I-resistant cells susceptible to perturbations that do not affect normal cells. For example, depletion of the kinesin-12 Kif15 induces a lethal mitotic arrest from failed spindle assembly in K5I-resistant cells, but has no noticeable affect on Eg5-competent cells. This work provides the first example of cancer cells naturally acquiring K5I-resistance through the action of Kif15, indicating that a combination of Eg5- and Kif15-inhibitors would serve as a powerful strategy in the treatment of neoplastic diseases.

Introduction

At the onset of mitosis, the cell orchestrates a rearrangement of the microtubule (MT) cytoskeleton into a dynamic bipolar array termed the mitotic spindle (Hyman and Karsenti 1996). Key to spindle assembly are cell-cycle-dependent changes in MT dynamics and motor proteins that recognize MT polarity (Belmont et al. 1990; Verde et al. 1992; Tanenbaum and Medema 2010). Both produce molecular forces that separate the duplicated centrosomes to opposite poles of the cell (Walczak and Heald 2008). As centrosomes mature into the spindle poles, their separation establishes the essential

bipolar geometry required for proper segregation of the duplicated genome (Rieder, Ault, and Eichenlaub-Ritter 1993).

The timing of centrosome separation proves critical in establishing proper kinetochore-MT attachments (Silkworth et al. 2012). Centrosome separation prior to nuclear envelope breakdown (NEB) encourages the generation of proper kinetochore-MT attachments because of the bioriented geometry of initial capture events. However, delayed centrosome separation increases the risk for erroneous kinetochore-MT attachments as MTs initially emanate from a single pole. Cells make every effort to correct these aberrant attachments, but if gone unnoticed faulty cell divisions may ensue (Cimini et al. 2002; Lampson et al. 2004; Silkworth et al. 2012).

In mammalian somatic cells, the kinesin-5 Eg5 begins sliding antiparallel MTs during late G2 in order to separate the centrosomes prior to NEB (Kapitein et al. 2005; Ferenz, Gable, and Wadsworth 2010). The primacy of Eg5 during mitosis and its susceptibility to small molecule inhibitors has made it an attractive target for novel chemotherapies (Rath and Kozielski 2012; K. S. Chan, Koh, and Li 2012; Marzo and Naval 2013). Eg5-inhibitors, or K5Is, efficiently kill tumor cells in culture and murine xenografts by blocking spindle assembly (Gascoigne and Taylor 2008; Purcell et al. 2010). However, K5Is lack therapeutic efficacy, suggesting that human cells evade death by assembling spindles through an Eg5-independent means (Rath and Kozielski 2012; K. S. Chan, Koh, and Li 2012; Marzo and Naval 2013).

Several lines of evidence support the existence of Eg5-independent centrosome separation pathways. For example, reduced dynein activity negates the requirement for Eg5 during spindle assembly (Mitchison et al. 2005; Tanenbaum, Macůrek, and Galjart

2008; Goshima et al. 2005). Perhaps more compellingly, kinesin-5s are nonessential in *Dictyostelium* and *C. elegans* (Tikhonenko et al. 2008; Saunders et al. 2007). In the latter, the kinesin-12 KLP-18 drives spindle assembly (Segbert et al. 2003; Wignall and Villeneuve 2009). Similarly, overexpression of the human kinesin-12 Kif15 can rescue spindle assembly in Eg5-inhibted cells despite being non-essential (Tanenbaum et al. 2009; Vanneste et al. 2009). Such molecular redundancy may compensate for a loss of Eg5 activity in cancer cells, rendering K5Is ineffective *in vivo*.

Results

Generation of EIC Lines

To develop a cell-culture model with which to study K5I resistance, HeLa cells were cultured in saturating doses of the Eg5 inhibitor S-trityl-L-cysteine (STLC, (DeBonis et al. 2004)). As expected, STLC induces a potent and lethal mitotic arrest (Figure 3.1A). However, roughly 1 in 16.7 x 10^6 cells survive chronic STLC treatment. 5 of these resilient cells were clonally isolated and cultured into *Eg5-independent cell* (EIC) lines that grow in the continuous presence of STLC (Figure 3.1A). All 5 EIC lines exhibit an abnormally high mitotic index (MI, percentage of cells in mitosis, n ≥ 905, Figure 3.1B). Consistent with Eg5-indpendence, a K5I structurally unrelated to STLC, Monsastrol (Mayer et al. 1999), does not dramatically alter the MI of the EIC lines (n ≥ 649, Figure 3.1C). However, endogenous Eg5 localizes to spindles in EIC-2, -4, and -5 cells, suggestive of residual albeit crippled Eg5 activity (Figure 3.1D). Eg5 fails to colocalize with spindle MTs in EIC-1 and -3 cells despite normal expression levels, indicating these EIC lines are truly Eg5-independent (Figures 3.1D and E).

EIC-1 Cells Assemble Spindles through a Monopolar Intermediate

To study Eg5-indpendent cell division, mitotic EIC-1 cells were imaged by time-lapse differential interference contrast (DIC) microscopy. Cells were blocked in late G2 with the CDK-1 inhibitor RO-3306 (Vassilev et al. 2006), and mitotic duration was measured as the time from RO-3306 release to initiation of furrow ingression. Mitosis lasts 195 ± 218 minutes in EIC-1 cells and only 105 ± 60 minutes in HeLa cells, likely accounting for the ~2-fold difference in MI between these cell types (median ± range, n ≥ 24, Figures 3.2A and B). These data show that Eg5-independent cell division is relatively inefficient and stochastic.

By fix-and-stain methodology, EIC-1 cells exhibit a significantly higher monopolar index (MPI, percentage of pre-anaphase cells containing monopolar spindles) than HeLa cells, averaging 75.3 ± 2.7 *versus* 10.6 ± 0.9 (average ± standard deviation (SD), $p \leq 0.0002$, $n \geq 1400$, Figure 3.2C). As centrosomes appear abutted in 88% of EIC-1 cells in late G2, monopolar spindles may arise from delayed centrosome separation ($n \geq 48$, Figure 3.2D). Live imaging of EIC-1 cells expressing mCherry-tubulin confirmed this notion, as centrosomes remain juxtaposed throughout mitotic entry (Figure 3.2E). Normally, centrosomes begin separating prior to NEB in HeLa cells (Figure 3.2D and E). Since monopolar spindles increase the occurrence of kinetochore-MT attachment errors and necessitate non-canonical forces to bipolarize (Silkworth et al. 2012), this discrepancy has momentous implications for the “Achilles’ heel” of K5I-resistant cells.

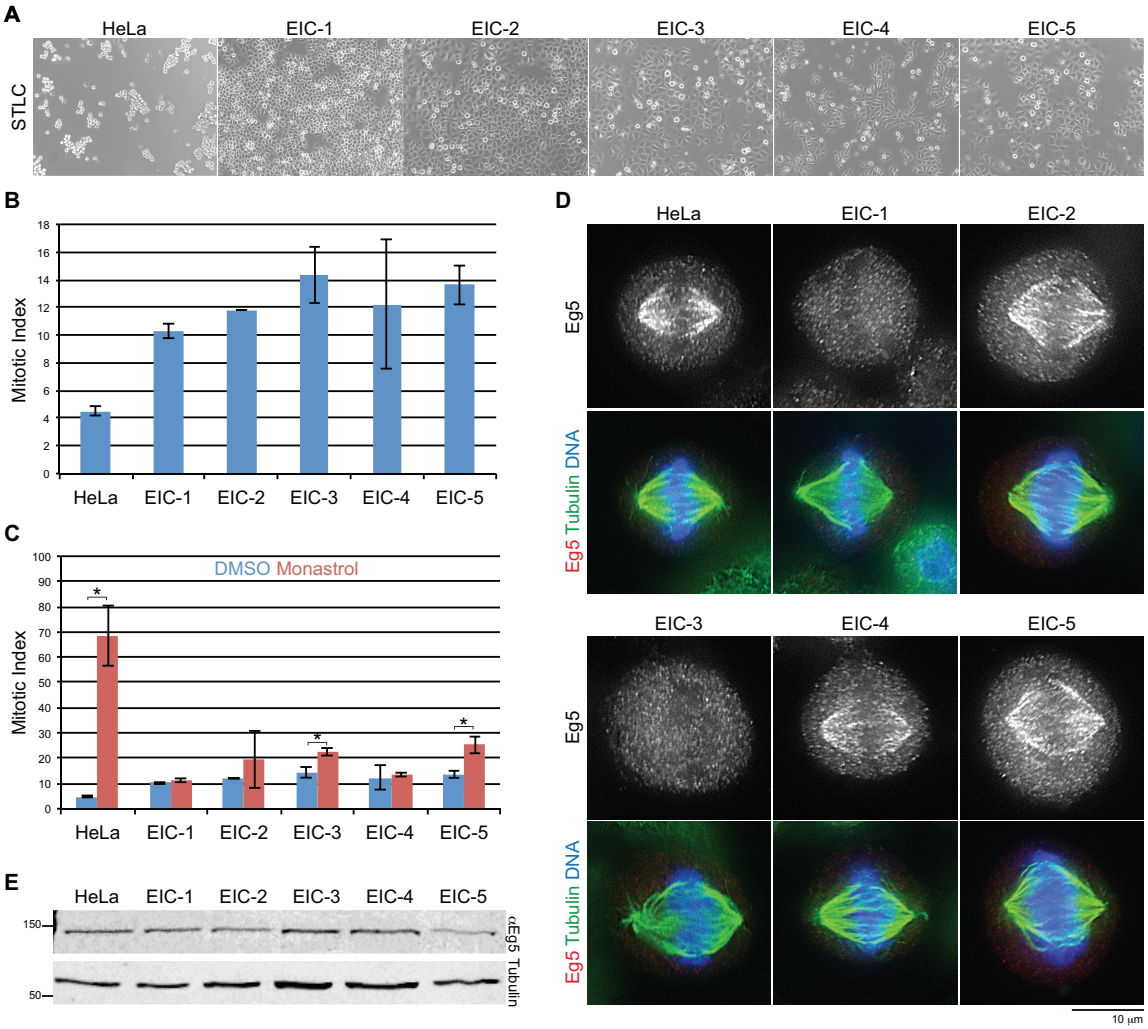

Figure 3.1: Generation of EIC lines. A) EIC-1 through -5 cells are resistant to STLC. Representative fields of indicated cell types cultured in 10 μM STLC for ~20 hours prior to imaging by DIC microscopy. B) EIC-1 through -5 cells exhibit a preponderance of mitotic cells. Quantitation of the MI in indicated cell types cultured in 0.3% DMSO for ~20 hours. Mitotic cells were identified as having a round cellular morphology. Columns and error bars represent the average ± 1 SD. HeLa, 4.5 ± 0.3; EIC-1, 10.3 ± 0.5; EIC-2, 11.8 ± 0.0; EIC-3, 14.3 ± 2.0; EIC-4, 12.2 ± 4.7; EIC-5, 13.6 ± 1.4. n ≥ 905. C) EIC-1 through -5 cells are resistant to Monastrol. Quantitation of the MI in indicated cell types cultured in 0.3% DMSO or 100 μM Monastrol for ~20 hours. Mitotic cells were identified as having a round cellular morphology. Columns and error bars represent the average ± 1 SD. DMSO data set is the same as in (B). Monastrol: HeLa, 68.5 ± 11.9; EIC-1, 10.9 ± 0.8; EIC-2, 19.3 ± 11.3; EIC-3, 22.5 ± 1.5; EIC-4, 13.4 ± 0.7; EIC-5, 25.2 ± 3.3. *, $p \leq 0.1$. n ≥ 649. D) Eg5 is displaced from spindle MTs in EIC-1 and EIC-3 cells. Images of representative mitotic cells in indicated cell types fixed and stained with antibodies targeting Eg5 (red) and tubulin (green). DNA (blue) was detected with Hoechst-33342. LUTs were scaled identically for Eg5 channel. Scale bar, 10 μm. E) Eg5 protein levels are equivalent across the HeLa and EIC cell lines. Representative immunoblot of whole cell lysate from indicated cell lines probed with antibodies against Eg5 (top) and tubulin (bottom). Molecular weight indicated in kD.

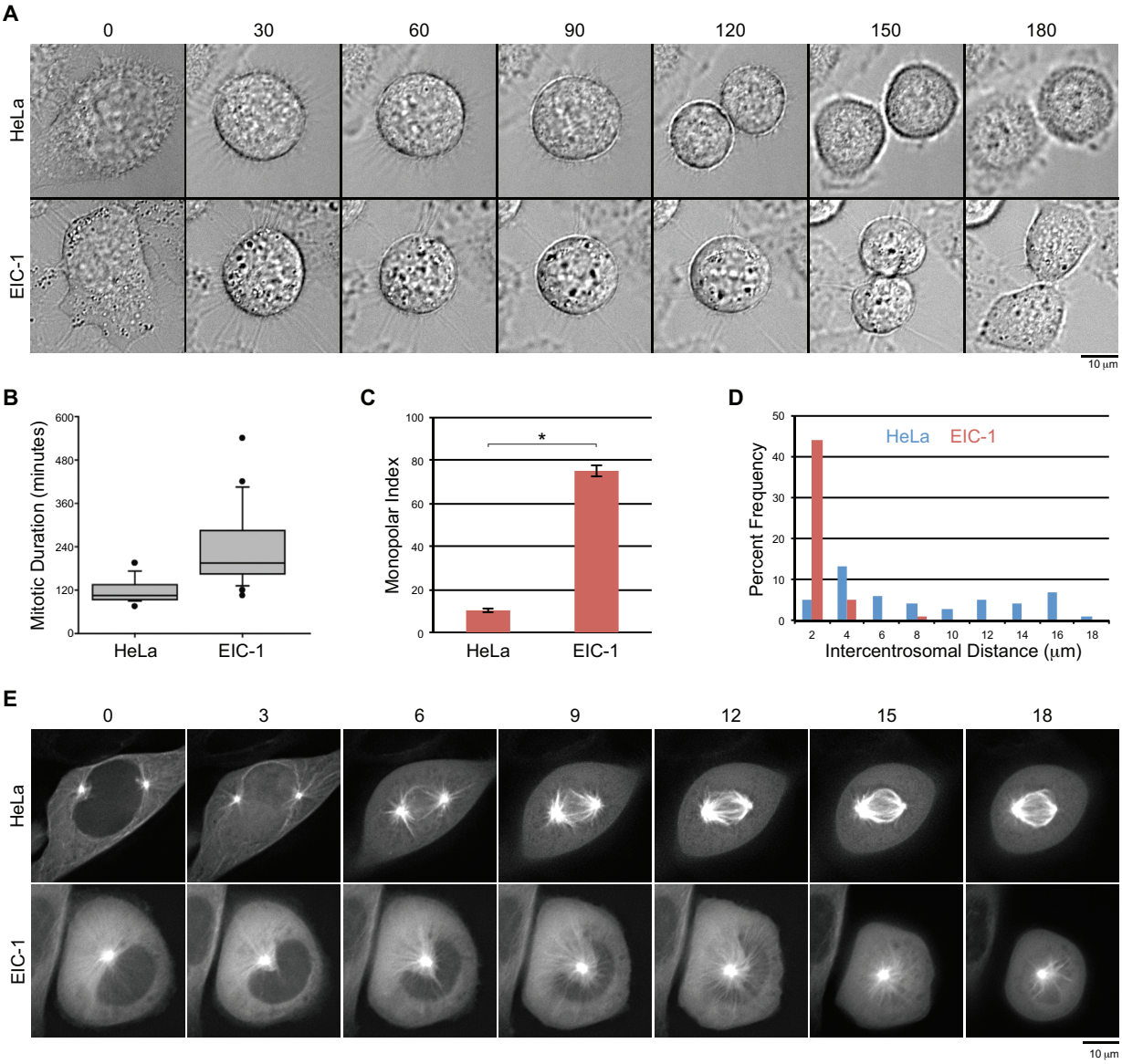

Figure 3.2: EIC-1 cells assemble spindles through a monopolar intermediate. A) EIC-1 cells experience a prolonged mitosis. Still frames from time-lapse movies of a representative HeLa (top) and EIC-1 (bottom) cell released from a RO-3306-induced G2 block and imaged by DIC microscopy. Time relative to the initial frame is indicated in minutes. Scale bar, 10 μm. B) Quantitation of experiment described in (A). Mitotic duration was measured as time in minutes from initial frame to furrow-ingression. Box-and-whisker plots represent the median,10th-, 25th-, 75th-, and 90th-percentiles. Median: Hela, 105; EIC-1, 195. $n \geq 24$. C) EIC-1 cells exhibit a preponderance of monopolar spindles. Quantitation of monopolar index in indicated cell lines. Spindle geometry was assessed by tubulin immunostaining. Columns and error bars represent the average ± 1 SD. HeLa, 10.6 ± 0.9; EIC-1, 75.3 ± 2.7. *, $p \leq 0.0002$. $n \geq 1400$. D) Centrosomes are atypically juxtaposed during late G2 in EIC-1 cells . Histogram of the intercentrosomal distance in μm during late G2 in indicated cell types. Distance between centrosomes was assessed by tubulin immunostaining in cells with condensed chromatin and an intact nuclear envelope. $n \geq 48$. E) Centrosomes fail to separate in EIC-1 cells during mitotic entry. Still frames from time-lapse movies of a representative HeLa (top) and EIC-1 (bottom) cell expressing fluorescent tubulin. Centrosomes are observed as bright tubulin foci. Time after initial frame is indicated in minutes. Scale bar, 10 μm.

EIC-1 Cells Are Hypersensitive to CENP-E Inhibition

Consistent with a preponderance of kinetochore-MT attachment errors, EIC-1 cells take an abnormally long time to divide (Figure 3.2B). Furthermore, roughly half of the mitotic events in EIC-1 cells culminate in cell death (Figure 3.3A). Indeed, lateral kinetochore-MT attachments abound in pre-metaphase EIC-1 cells, suggesting that EIC-1 cells may rely heavily upon the error-correction machinery (Figure 3.3B).

The kinesin-10 CENP-E is specifically involved in the conversion of lateral kinetochore-MT attachments to end-on attachments (Wood et al. 1997; Schaar et al. 1997). To test whether CENP-E endures a heavier work load in EIC cells, the CENP-E-inhibitor GSK-923295 was used (Qian et al. 2010). Strikingly, low doses of GSK-923295 that have little effect on HeLa cells induce massive chromosome alignment defects and dramatically increase the MI in EIC-1 cells (Figures 3.3C and D).

Hypersensitivity to CENP-E inhibition is not generalizable to all EIC lines, as EIC-2 through -5 cells are non-responsive to low doses of GSK-923295 ($n \geq 859$, Figure 3.3D). Endogenous CENP-E displays an unusual localization pattern in EIC-1 cells, distributing along spindle MTs instead of concentrating at the kinetochores as in HeLa cells (Figure 3.3E). This fundamental difference may account for the hypersensitivity of EIC-1 cells to CENP-E inhibition, as low doses of GSK-923295 completely displace CENP-E from kinetochores in EIC-1 cells but not in HeLa cells (Figure 3.3E). These data suggest that CENP-E variants exist in human cells, having important implications for the clinical administration of CENP-E inhibitors.

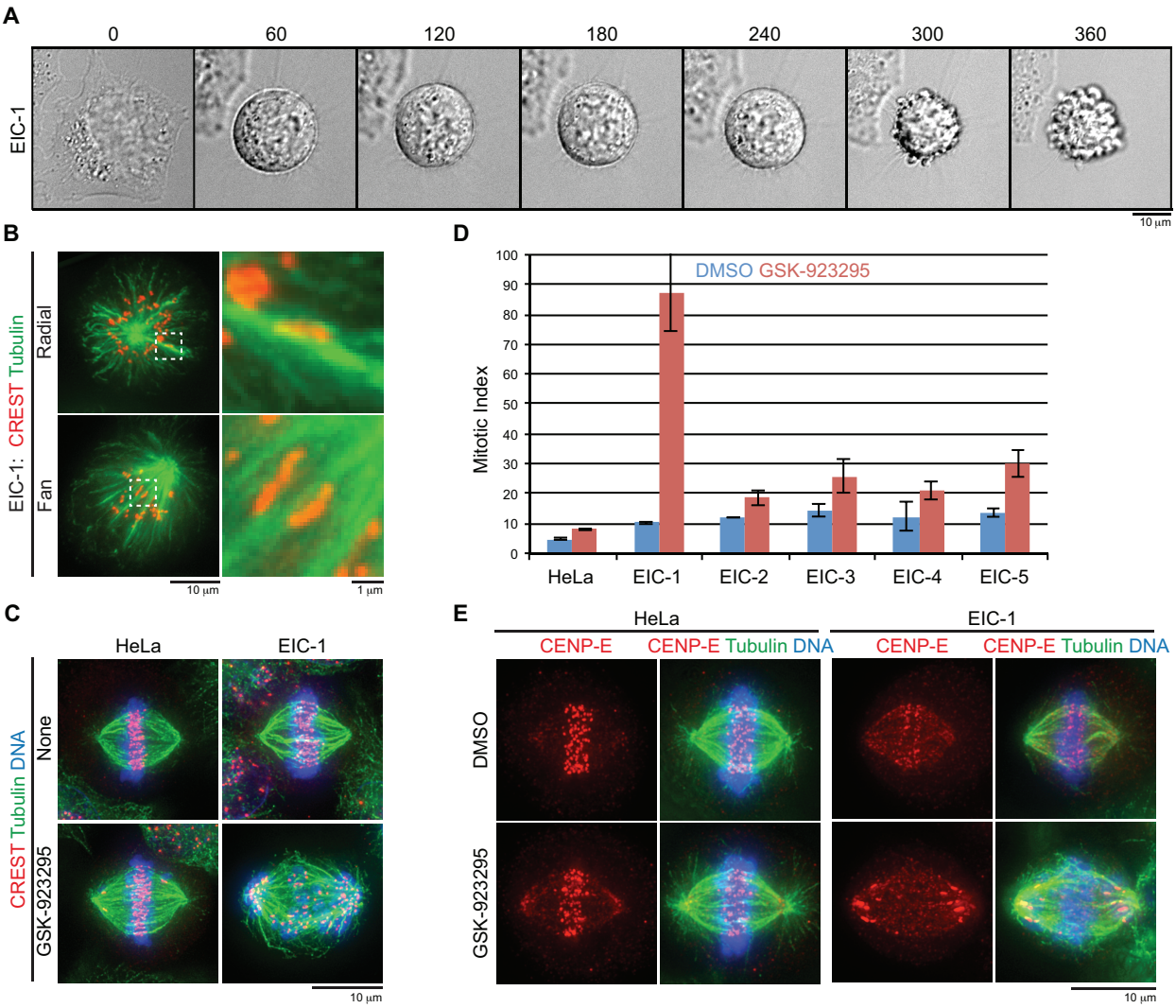

Figure 3.3: EIC-1 cells are hypersensitive to CENP-E inhibition. A) EIC-1 cells often die during mitosis. Still frames from a time-lapse movie of a representative EIC-1 cell released from a RO-3306-induced G2 block imaged by DIC microscopy. Time relative to the initial frame is indicated in minutes. Scale bar, 10 μm. B) Maximum z-projections of representative EIC-1 cells containing a radial (top) or fan-shaped (bottom) monopolar spindle. Cells were fixed and stained with CREST (red) and antibodies targeting tubulin (green). Enlarged images of boxed sections are shown (right) to emphasize lateral kinetochore-MT attachments. Scale bars, 10 μm and 1 μm. C) Low doses of GSK-923295 cause massive chromosome alignment defects in EIC-1 cells. Maximum z-projections of representative mitotic cells in indicated cell types that were either unperturbed (top) or treated with 100 nM GSK-923295 (bottom) for ~20 hours prior to being fixed and stained with CREST (red) and antibodies targeting tubulin (green). DNA (blue) was detected with Hoechst-33342. Scale bar, 10 μm. D) Quantitation of the MI in indicated cell types cultured in 0.3% DMSO or 50 nM GSK-923295 for ~20 hours. Mitotic cells were identified as having a round cellular morphology. Columns and error bars represent the average ± 1 SD. DMSO data set is the same as in Figure 3.1. GSK-923295: HeLa, 8.1 ± 0.4; EIC-1, 87.4 ± 13.0; EIC-2, 18.7 ± 2.6; EIC-3, 25.7 ± 5.5; EIC-4, 21.1 ± 3.4; EIC-5, 30.0 ± 4.4. n ≥ 859. E) CENP-E has an unusual localization pattern in EIC-1 cells. Maximum z-projections of representative mitotic cells in indicated cell types treated with 0.3% DMSO (top) or 50 nM GSK-923295 (bottom). Cells were fixed and stained with antibodies targeting CENP-E (red) and tubulin (green). DNA (blue) was detected with Hoechst-33342. LUTs were scaled identically for CENP-E channel. Scale bar, 10 μm.

EIC Cells Are Hypersensitive to MT Stabilization

Monopolar spindles necessitate non-canonical forces in order to bipolarize (Rosenblatt et al. 2004; Toso et al. 2009). This becomes evident upon watching spindle assembly in EIC-1 cells expressing mCherry-tubulin by time-lapse fluorescence microscopy. First, radial monopolar spindles (monoasters) break symmetry to produce fan-shaped monoasters (Figure 3.4A). Fan-shaped monoasters subsequently bipolarize by ‘‘reverse jackknifing,’’ wherein one spindle half rotates in three-dimensions to essentially unfold the spindle (Figure 3.4A). A majority of monoasters in EIC-1 cells are radially-symmetric as opposed to fan-shaped, indicating that monoaster symmetry breaking is rate-limiting to Eg5-independent spindle assembly (Figure 3.4B).

Unique to fan-shaped monoasters is the presence of stable MT bundles. MT stability was assessed with cold temperatures, a condition that prompts MT depolymerization (Brinkley and Cartwright 1975). In contrast to radial monasters, fan-shaped monoasters consistently retained MT polymer during cold treatment (Figure 3.4C). These data suggest that MT stabilization may be involved in the rate-limiting step of monoaster symmetry breaking

Notably, many of the cold-stable MTs in fan-shaped monoasters do not terminate at a kinetochore. This unusual property indicates that non-kinetochore-MTs are atypically stable in EIC-1 cells (Figure 3.4C). Concomitant with this result, low doses of a MT-stabilizing agent, Taxol (Wall 1998), significantly increase the MI of EIC-1, -2, -3, and -5 cells without altering the MI of HeLa cells ($p \leq 0.01$, $n \geq 825$, Figure 3.4D). While the mechanistic details are not yet clear, these data demonstrate that some K5I-resitant cells cannot tolerate further MT stabilization.

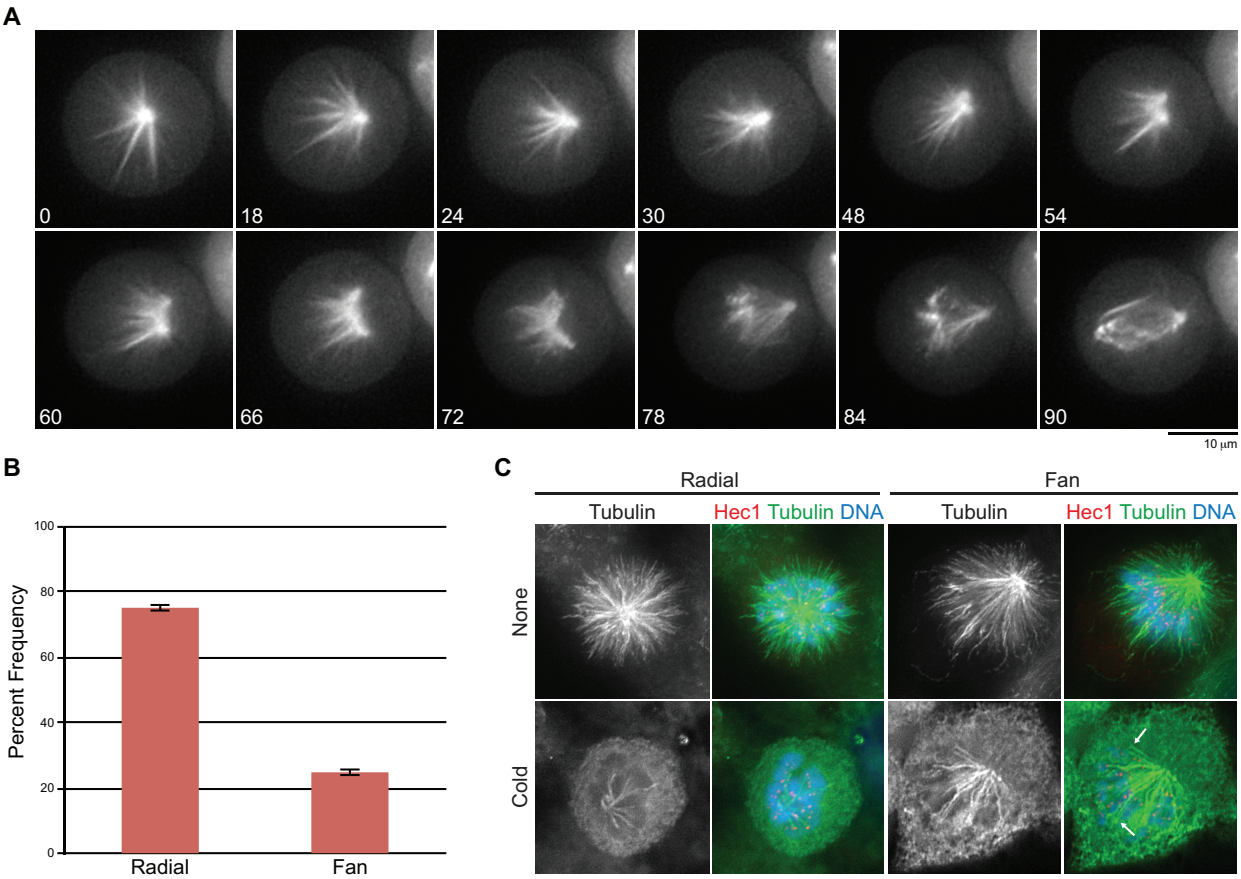

Figure 3.4: EIC cells are hypersensitive to MT stabilization. A) Spindles bipolarize by reverse jackknifing in EIC-1 cells. Still frames from a time-lapse movie of a representative EIC-1 cell expressing fluorescent tubulin. Time after initial frame is indicated in minutes. Scale bar, 10 μm. B) The majority of monopolar spindles in EIC-1 cells are radially-symmetric. Quantitation of monopolar spindle shape in EIC-1 cells, displayed as a percent frequency. Columns and error bars represent the average ± 1 SD. Radial, 75.2 ± 0.8; Fan, 24.8 ± 0.8. n = 500. C) Fan-shaped monopolar spindles have elevated MT stability. Representative images of radially-symmetric and fan-shaped monopolar spindles in unperturbed (top) or cold-treated (bottom) EIC-1 cells. Cells were fixed and stained with antibodies targeting Hec1 (red) and tubulin (green). DNA (blue) was detected with Hoechst-33342. Arrows indicate cold-stable MT bundles that do not terminate at a kinetochore. D) Low doses of Taxol increase the MI in EIC-1, -2, -3, and -5 cells. Quantitation of the MI in indicated cell types cultured in 0.3% DMSO or 2 nM Taxol for ~20 hours. Mitotic cells were identified as having a round cellular morphology. Columns and error bars represent the average ± 1 SD. DMSO data set is the same as in Figure 3.1. Taxol: HeLa, 9.4 ± 2.2; EIC-1, 39.4 ± 4.7; EIC-2, 79.3 ± 14.4; EIC-3, 30.8 ± 4.7; EIC-4, 18.2 ± 2.5; EIC-5, 80.7 ± 22.6. *, $p \leq 0.1$. $n \geq 825$.

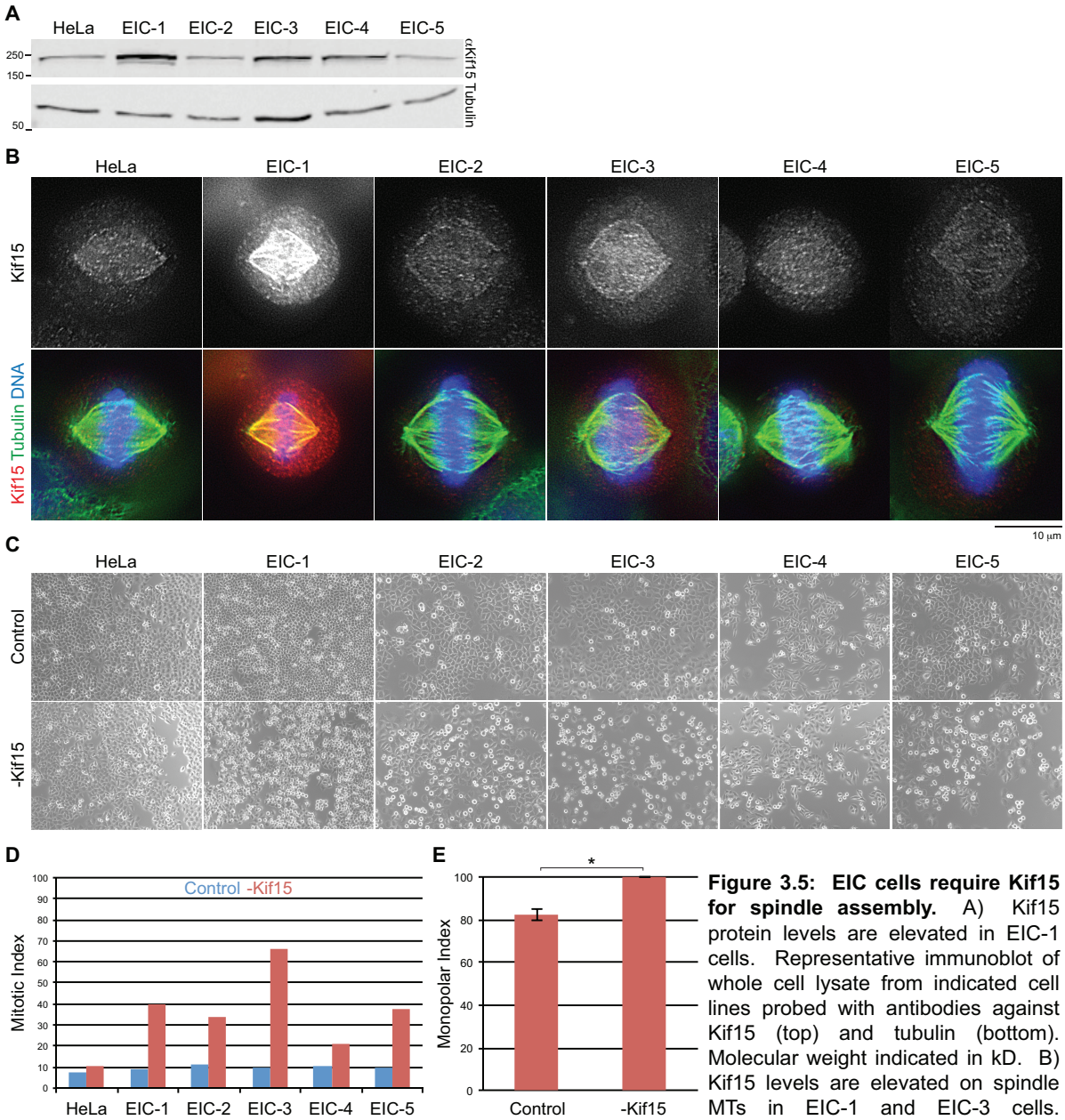

Figure 3.5: EIC cells require Kif15 for spindle assembly. A) Kif15 protein levels are elevated in EIC-1 cells. Representative immunoblot of whole cell lysate from indicated cell lines probed with antibodies against Kif15 (top) and tubulin (bottom). Molecular weight indicated in kD. B) Kif15 levels are elevated on spindle MTs in EIC-1 and EIC-3 cells. Images of representative mitotic cells in indicated cell types stained with antibodies targeting Kif15 (red) and tubulin (green). DNA (blue) was detected with Hoechst-33342. LUTs were scaled identically for Kif15 channel. Scale bar, 10 μm. C) Kif15 depletion increases the MI in all EIC lines. Representative fields of indicated cell types transfected with non-specific (top) or Kif15-targeting (bottom) siRNAs ~20 hours prior to imaging by DIC microscopy. D) Quantitation of experiment described in (C). Mitotic cells were identified as having a round cellular morphology. Columns represent the average. Control: HeLa, 7; EIC-1, 9; EIC-2, 11; EIC-3, 10; EIC-4, 10; EIC-5, 10. -Kif15: HeLa, 11; EIC-1, 40; EIC-2, 34; EIC-3, 66; EIC-4, 21; EIC-5, 38. $n \geq 295$. E) Kif15 depletion increases the monopolar index in EIC-1 cells. Quantitation of monopolar index in EIC-1 cells transfected with non-specific or Kif15-targeting siRNAs for ~24 hours. Spindle geometry was assessed by tubulin immunostaining. Columns and error bars represent the average ± 1 SD. Control, 82.1 ± 2.4; -Kif15, 100.0 ± 0.0. *, $p = 0.006$. $n \geq 600$.

EIC Cells Require Kif15 for Spindle Assembly

In addition to MT stabilization, forces from subsidiary mitotic motors likely contribute to spindle assembly in EIC cells. The kinesin-12 Kif15 has been shown to rescue spindle assembly in cells with compromised Eg5 activity when overexpressed (Tanenbaum et al. 2009; Vanneste et al. 2009). Along these lines, Kif15 levels in whole cell lysate and on spindle MTs are elevated in EIC-1 cells compared to HeLa cells (Figures 3.5A and B). However, Kif15 levels appear unchanged in EIC-2 through -5 cells (Figures 3.5A and B). Regardless, siRNA depletion of Kif15 increases the MI of all 5 EIC lines while having no effect on HeLa cells ($n \geq 295$, Figures 3.5C and D). This robust mitotic arrest appears to result from failed spindle assembly, as Kif15-depleted EIC-1 cells exhibit a MPI of 100.0 ± 0.0 compared to 82.1 ± 2.4 in unperturbed EIC-1 cells ($p = 0.006$, $n = 600$, Figure 3.5E). These data provide the first evidence for cancer cells naturally acquiring K5I resistance through a Kif15-dependent spindle assembly pathway, motivating further study into the combination of Eg5- and Kif15-inhibitors in the treatment of neoplastic diseases.

Discussion

This study identifies a major discrepancy between HeLa and K5I-resistant cells in the timing of centrosome separation. EIC-1 cells invariably form bipolar spindles through an intermediary monopolar geometry, which likely holds true for the other 4 EIC lines as they exhibit an unusual preponderance of monopolar spindles (data not shown). This work underscores the importance of Eg5 in avoiding spindle monopolarity, and defines a unique feature of K5I-resistant cells as the transient monopolar spindle. As

EIC cells are hypersensitive to MT stabilization and Kif15 depletion, the transient monopolar spindle serves as an Achilles' heel that can be exploited for therapeutic advantage.

Despite its therapeutic potential, the transient monopolar spindle may also serve to benefit the tumor in K5I-treated cancer patients. An abundance of kinetochore-MT attachment errors predisposes cells to accumulate chromosomal instability (CIN), or aneuploidy from whole chromosome loss and/or gain (Lengauer, Kinzler, and Vogelstein 1997; Silkworth et al. 2012; McClelland, Burrell, and Swanton 2009). Chronic low-grade CIN can accelerate disease progression through Darwinian type evolution (Kuukasjärvi et al. 1997; Kops, Weaver, and Cleveland 2005). This raises the haunting possibility that K5Is actually select for aggressive tumor phenotypes and confound disease management in cancer patients.

Ideally, chemotherapies would avoid CIN by inducing a full-proof mitotic arrest. But as this is a somewhat unrealistic expectation, therapies must be designed to create lethal doses of CIN in the event of mitotic slippage (Silk, Zasadil, and Holland 2013; Kops, Foltz, and Cleveland 2004). In the case of K5Is, this may be accomplished by slightly perturbing the machinery that corrects improper kinetochore-MT attachments. By transitioning through an intermediary monopolar spindle, K5I-resistant cells likely make erroneous kinetochore-MT attachments more frequently than Eg5-competent cells. Therefore, slight disruption of the error correction machinery may have devastating consequences on the genomic stability of K5I-resistant cells while leaving the genome of normal cells intact. In fact, the hypersensitivity of EIC cells to Taxol (Figure 3.4D) could be interpreted in this light, as MT dynamics are intimately involved in the

correction of kinetochore-MT mal-attachments (Andrews et al. 2004; Kline-Smith et al. 2004; Bakhoum et al. 2009). Future studies will more rigorously test the efficacy of pairing K5Is with inhibitors of the error correction machinery.

As a parallel strategy, combinatorial therapies can be designed to increase the strength of a K5I-induced mitotic arrest. This study unveils a non-canonical Kif15-dependent spindle assembly pathway that confers K5I resistance to cells, suggesting that pairing of Kif15- and Eg5-inhibitors may induce a complete block in spindle assembly. Moreover, Kif15 may serve as a universal target of K5I-resistant cells since all 5 EIC lines perish upon Kif15 depletion. And Kif15 likely offers a large therapeutic window becuase it is normally dispensable for viability. But despite its therapeutic promise, little is known about the molecular function of Kif15 on spindle MTs. EIC-1 cells offer a unique opportunity to study Kif15 during mitosis by circumventing the overpowering forces generated by Eg5.

Finally, this study has tremendous implications for the personalization of anti-mitotic chemotherapies. The role of genetics in drug response is gaining considerable interest with the advent of personalized medicine (Jayachandran et al. 2014). However, genetic variation has been largely ignored regarding the targets of cytotoxic chemotherapies. This study is suggestive of naturally occurring genetic heterogeneity in both *CENP-E* and *Kif15*. CENP-E shows altered localization and hypersensitivity to GSK-923295 in EIC-1 cells (Figure 3.3). Both of these phenotypes could be accounted for by mutations to amino acid 422, as this residue influences CENP-E partitioning to kinetochores *versus* MTs (Kim et al. 2010). And variation in the *Kif15* gene is evidenced by the Kif15 dependency absent of its overexpression in several EIC lines

(Figure 3.5). Activating mutations in Kif15 could predispose cells to K5I-resistance, similar to mutations in the kinesin-4 KIF21A that cause the onset of Congenital Fibrosis of the Extraocular Muscles Type 1 (CFEOM1, (van der Vaart et al. 2013; Cheng et al. 2014)). Given their validated and putative clinical significance, examining *CENP-E* and *Kif15* heterogeneity will be a priority going forward.

CHAPTER IV

KINESIN-12 KIF15 DIFFERENTIALLY AFFECTS SPINDLE ASSEMBLY DEPENDING ON ITS MT SUBSTRATE

Emma G. Sturgill and Ryoma Ohi

Department of Cell and Developmental Biology, Vanderbilt University Medical Center, Nashville, TN

Previously published in part as:

Sturgill EG and Ohi R. (2013). Kinesin-12 differentially affects spindle assembly depending on its microtubule substrate. *Current Biology* 23, 1280-1290.

Abstract

The work shown here provides the first insight into kinesin-12 Kif15 action on spindle microtubules (MTs). Instead of acting redundantly to the kinesin-5 Eg5 as previously suspected, Kif15 diverges in both localization and function. Kif15 localizes exclusively to kinetochore-MTs (K-MTs) in HeLa cells, where it modulates K-MT-generated forces to prevent excessive centrosome separation. And under pathological conditions wherein Eg5 activity is chronically inhibited, Kif15 catalyzes centrosome separation as a consequence of mislocalizing to non-K-MTs. Therefore, Kif15 differentially affects spindle assembly depending on its MT substrate.

Introduction

Spindle bipolarity must be established and maintained to ensure proper chromosome segregation (Walczak and Heald 2008). The prevailing “balance-of-forces” model posits that molecular motors of opposing directionality reach an equilibrium that determines spindle size and shape (Goshima et al. 2005). As plus-end directed motors, the kinesin-5 Eg5 and kinesin-12 Kif15 are thought to generate the primary outward pushing forces on the spindle poles, while the minus-end directed motors dynein and kinesin-14 HSET are believed to pull the spindle poles inward (Sharp, Rogers, and Scholey 2000). Remarkably, however, Eg5 inhibition does not collapse the bipolar geometry of fully assembled spindles (Tanenbaum et al. 2009). It therefore remains a largely unexplored problem as to how individual force components are integrated to build a spindle of constant shape and size during mitosis.

Kif15 is gaining considerable interest as a target for novel chemotherapies, yet its mechanism of action on spindle MTs is ill defined. Kif15 has been likened to Eg5 for its ability to power spindle assembly in Eg5-compromised cells (Tanenbaum et al. 2009). Moreover, the kinesin-12 KLP18 drives spindle assembly in *C. elegans* oocytes and the kinesin-12 Xklp2 is required for spindle maintenance in *Xenopus* egg extracts (Segbert et al. 2003; Wignall and Villeneuve 2009; Boleti, Karsenti, and Vernos 1996). But it has yet to be tested whether Kif15 is an anti-parallel MT slider like its Eg5 counterpart.

The previously described Eg5-independent cell line (EIC-1) serves as a valuable tool for exploring Kif15 activity on spindle MTs, as Kif15 assumes a commanding role during spindle assembly in these cells (Chapter III). The mechanics of Kif15-dependent spindle assembly are distinct from those of Eg5-powered spindle assembly, indicating that the molecular function of Kif15 differs from that of Eg5. Notably, spindles in EIC-1 cells transition through a monopolar geometry (Chapter III). Kinetochore-MTs (K-MTs), or the population of spindle MTs that physically attach chromosomes, have been suggested to aid in bipolarizing spindles from a monopolar geometry (Toso et al. 2009), suggesting that Kif15 may act on these parallel MT arrays. Also supporting this notion, both frog Xklp2 and human Kif15 localize to spindle MTs in a manner dependent on TPX2, a MT-associated protein (MAP) concentrated on K-MTs (Wittmann et al. 1998; Tanenbaum et al. 2009; Vanneste et al. 2009; Bird and Hyman 2008). These observations motivate further exploration into the MT population(s) that mediates Kif15-generated forces.

Results

KIF15 Localizes Specifically to K-MTs in HeLa Cells

Kif15 localization was monitored with affinity-purified antibodies against its C-terminus that recognize a band of ~160 kD from HeLa cell lysate (data not shown). Kif15 first localizes to spindle MTs during late prophase and enriches on metaphase spindles (Figure 4.1A). For comparison, Eg5 localizes to MTs preceding nuclear envelope breakdown (NEB), and dissipates from spindle MTs as mitosis progresses (Figure 4.1A). This agrees with Eg5 functioning at mitotic onset (Ferenz, Gable, and Wadsworth 2010), and suggests that Kif15 acts on more mature spindles.

To test whether Kif15 specifically targets K-MTs, its localization was monitored in Nuf2-depleted mitotic HeLa cells. Depletion of this outer-kinetochore component prevents K-MT formation (DeLuca et al. 2002). Strikingly, Nuf2 RNAi abrogates Kif15 spindle localization (Figure 4.1B). Similarly, the polo-like kinase inhibitor BI-2536, which induces K-MT disassembly (Lénárt et al. 2007), displaces Kif15 from spindles (data not shown). Neither Nuf2 RNAi nor BI-2536 prevents Eg5 from binding spindle MTs (Figure 4.1B and data not shown).

As a parallel approach, non-K-MTs were selectively depolymerized with cold temperatures (Brinkley and Cartwright 1975). Kif15 noticeably enriches on the residual K-MTs (Figure 4.1C), suggesting that non-K-MTs actually attenuate Kif15 spindle binding. Notably, a subpopulation of Kif15 enriches at the outer-kinetochore. Briefly extracting cells prior to fixation accentuates this pattern (Figures 4.1D and E), while depolymerizing MTs with nocodazole eliminates it (data not shown). Collectively, these data demonstrate that Kif15 specifically targets K-MTs.

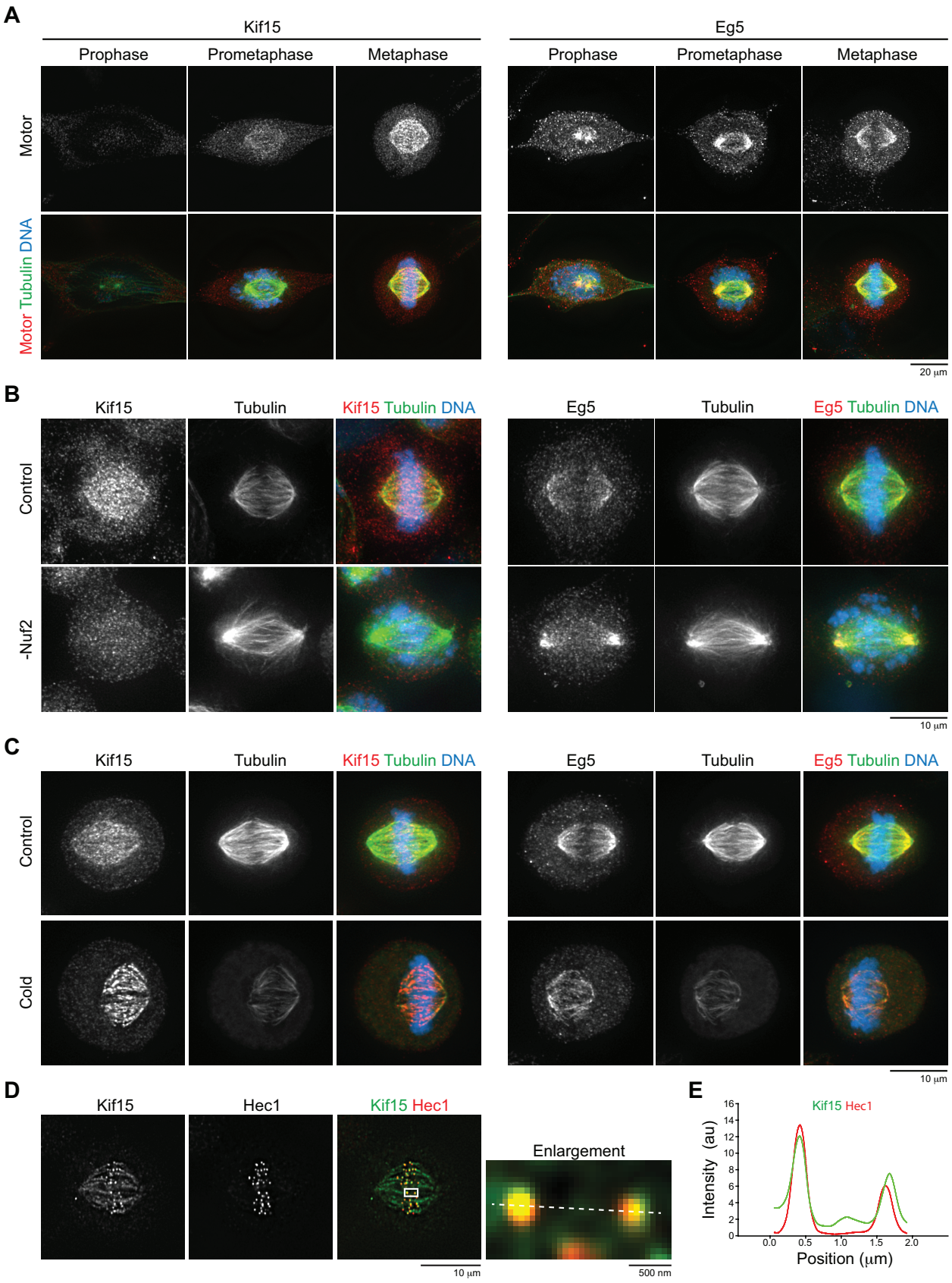
A
Kif15
Eg5
Prophase
Prometaphase
Metaphase
Prophase
Prometaphase
Metaphase
Motor
Motor Tubulin DNA
20 μm
B
Kif15
Tubulin
Kif15 Tubulin DNA
Eg5
Tubulin
Eg5 Tubulin DNA
Control
-Nuf2
10 μm
C
Kif15
Tubulin
Kif15 Tubulin DNA
Eg5
Tubulin
Eg5 Tubulin DNA
Control
Cold
10 μm
D
Kif15
Hec1
Kif15 Hec1
10 μm
Enlargement
500 nm
E
Kif15 Hec1
Intensity (au)
Position (μm)

Figure 4.1: Kif15 localizes specifically to K-MTs in HeLa cells. A) Kif15 localization to spindle MTs is delayed compared to Eg5. Maximum z-projections of representative HeLa cells in indicated mitotic phases fixed and stained with antibodies targeting Kif15 or Eg5 (red) and tubulin (green). DNA (blue) was detected with Hoechst-33342. LUTs were scaled identically for each channel. Scale bar, 20 μm. B) Nuf2 depletion abrogates Kif15 spindle localization. Maximum z-projections of representative HeLa cells transfected with non-specific (top) or Nuf2-targeting (bottom) siRNAs ~48 hours prior to being fixed and stained with antibodies targeting Kif15 or Eg5 (red) and tubulin (green). DNA (blue) was detected with Hoechst-33342. LUTs were scaled identically for each channel. Scale bar, 10 μm. C) Kif15 localization to spindle MTs is enhanced upon cold treatment. Maximum z-projections of representative HeLa cells left unperturbed (top) or exposed to cold temperatures (bottom) ~10 minutes prior to being fixed and stained with antibodies targeting Kif15 or Eg5 (red) and tubulin (green). DNA (blue) was detected with Hoechst-33342. LUTs were scaled identically for each channel. Scale bar, 10 μm. D) Kif15 colocalizes with Hec1. Images of representative HeLa cell briefly exctracted prior to fixation, and then stained with antibodies targeting Kif15 (green) and Hec1 (red). Enlarged image of boxed section is shown (right) to emphasize colocalization of Kif15 and Hec1 puncta. Dotted line was used for line scan in (E). Scale bars, 10 μm and 500 nm. E) Line scan from (D) showing Kif15 (green) and Hec1 (red) intensity relative to position.

Next, spindle morphology was monitored in cells singly- or co-depleted of Nuf2 and Kif15. None of these perturbations affects spindle bipolarity, as the monopolar index (MPI) in mock-, Nuf2-, Kif15-, and Nuf2/Kif15-depleted cells averages 6.0 ± 1.3, 5.1 ± 1.0, 4.3 ± 3.1, and 4.1 ± 0.8, respectively (average ± standard deviation (SD), $n \geq 588$, Figures 4.2A and C). However, these perturbations do impact spindle morphology. Spindles in Nuf2-depleted cells appear long and wispy, while spindles in Kif15-depleted cells present as short and stumpy. Importantly, spindles in cells co-depleted of Nuf2 and Kif15 resemble the Nuf2 single-depletion morphology, suggesting that Kif15 functions solely on K-MTs (Figure 4.2A). For comparison, treatment of Nuf2-depleted cells with the Eg5 inhibitor S-trityl-L-cysteine (STLC) yields a MPI of 93.8 ± 5.3 ($p \leq 0.001$, $n = 600$, Figures 4.2B and C), indicating that Eg5 supports spindle bipolarity by acting on non-K-MTs. These data do not exclude a possible function of Eg5 on K-MTs; rather, they provide strong evidence that Kif15 acts exclusively on K-MTs.

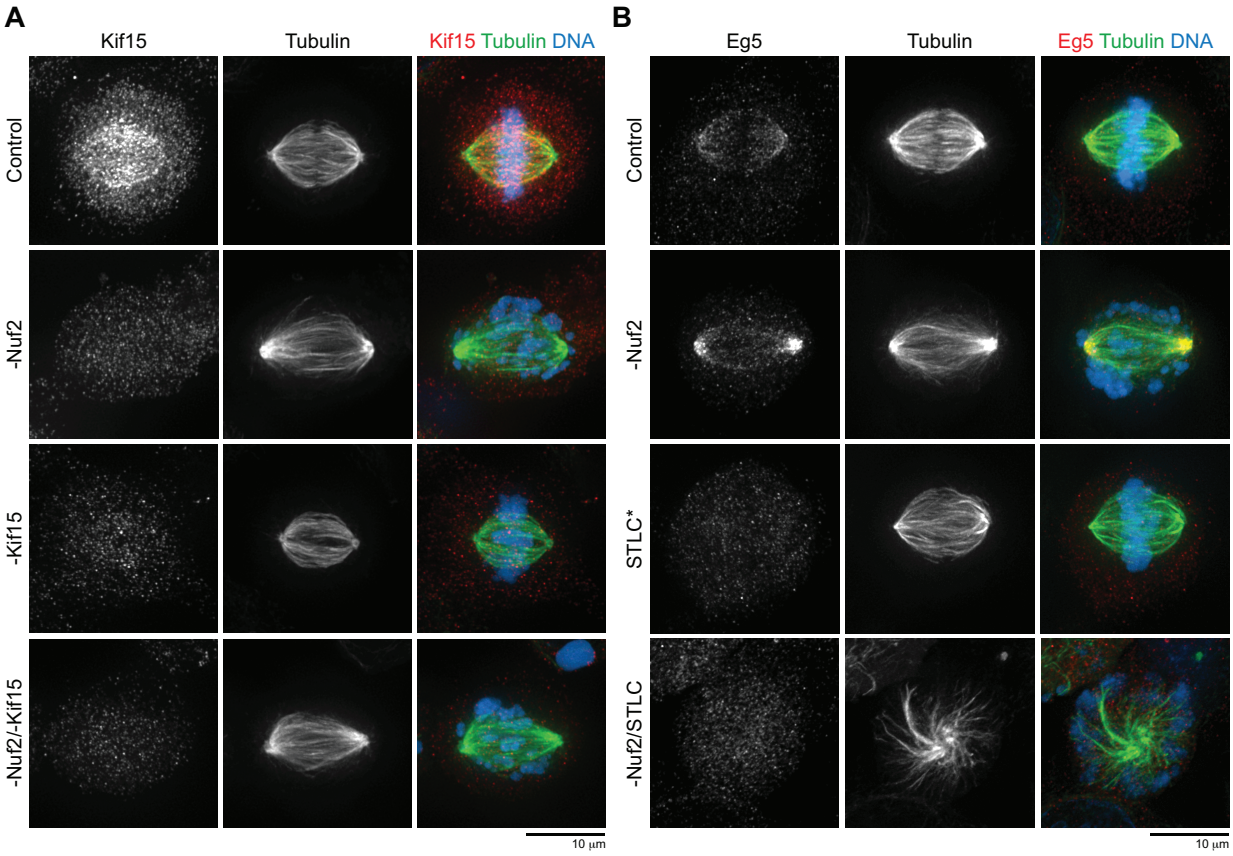

Figure 4.2: Kif15 acts specifically on K-MTs in HeLa cells. A) Kif15/Nuf2 codepletion phenocopies Nuf2 single depletion. Maximum z-projections of representative HeLa cells transfected with the indicated siRNAs ~48 hours prior to being fixed and stained with antibodies targeting Kif15 (red) and tubulin (green). DNA (blue) was detected with Hoechst-33342. LUTs were scaled identically for each channel. Scale bar, 10 μm. B) STLC collapses bipolar spindles in Nuf2-depleted cells. Maximum z-projections of representative HeLa cells transfected with non-specific or Nuf2-targeting siRNAs ~48 hours prior to being fixed. STLC* indicates cells were blocked in metaphase with MG-132 prior to treatment with 10 μM STLC for 1 hour. -Nuf2/STLC indicates Nuf2-depleted cells were treated with 10 μM STLC for 1 hour. Cells were then fixed and stained with antibodies targeting Eg5 (red) and tubulin (green). DNA (blue) was detected with Hoechst-33342. LUTs were scaled identically for each channel. Scale bar, 10 μm. C) Quantitation of monopolar index from experiments described in (A) and (B). Columns and error bars represent the average ± 1 SD. Control, 6.0 ± 1.3; -Nuf2, 5.1 ± 1.0; -Kif15, 4.3 ± 3.2; STLC*, 13.3 ± 8.9; -Nuf2/-Kif15, 4.1 ± 0.8; -Nuf2/STLC, 93.8 ± 5.3. **, $p \leq 0.001$. $n \geq 588$.

Kif15 Modulates K-MT-Generated Forces to Limit Centrosome Separation in HeLa Cells

Spindle lengths were next measured in cells singly- or co-depleted of Nuf2 and Kif15. Spindles in mock-depleted cells average 13.7 ± 1.2 μm (n = 64, Figure 4.3A). Nuf2 RNAi generates significantly longer spindles averaging 16.5 ± 1.4 μm, while Kif15 RNAi produces significantly shorter spindles averaging 11.7 ± 0.9 μm ($p \leq 0.001$, $n \geq 62$, Figure 4.3A). Again, spindles in cells co-depleted of Nuf2 and Kif15 phenocopy those in cells singly depleted of Nuf2, averaging 16.8 ± 1.7 μm in length (n = 77, Figure 4.3A). These data reveal that Kif15 influences spindle length in a K-MT-dependent manner.

To approximate K-MT length, pole-to-pole distances were halved in cold-treated cells. By this metric, Kif15 RNAi produces significantly short K-MTs averaging 3.0 ± 0.6 μm compared to 3.9 ± 0.8 μm in mock-depleted cells ($p \leq 0.001$, $n \geq 76$, Figures 4.3B and C). As a parallel approach, K-MT length was approximated as the radius of kinetochore rosettes in Monastrol-induced monopolar spindles. Kinetochores radiate a mere 4.3 ± 0.6 μm from monoaster centers in Kif15-depleted cells compared to 5.6 ± 0.7 μm in mock-depleted cells ($p \leq 0.001$, $n \geq 77$, Figures 4.3D and E). As proof of principle, cold treatment also yields short K-MTs approximating 3.4 ± 0.5 μm in length ($p \leq 0.001$, n = 89, Figures 4.3D and E). These perturbations are additive, as kinetochores radiate 2.8 ± 0.5 μm from monoaster centers in Kif15-depleted cells exposed to cold ($p \leq 0.001$, n = 86, Figures 4.3D and E). Notably, outlying kinetochores in these double-perturbed cells stain positive for residual Kif15, suggesting that Kif15 protects K-MTs from cold-induced depolymerization (Figure 4.3D). Collectively, these data indicate that Kif15 stabilizes K-MTs to influence steady-state spindle length.

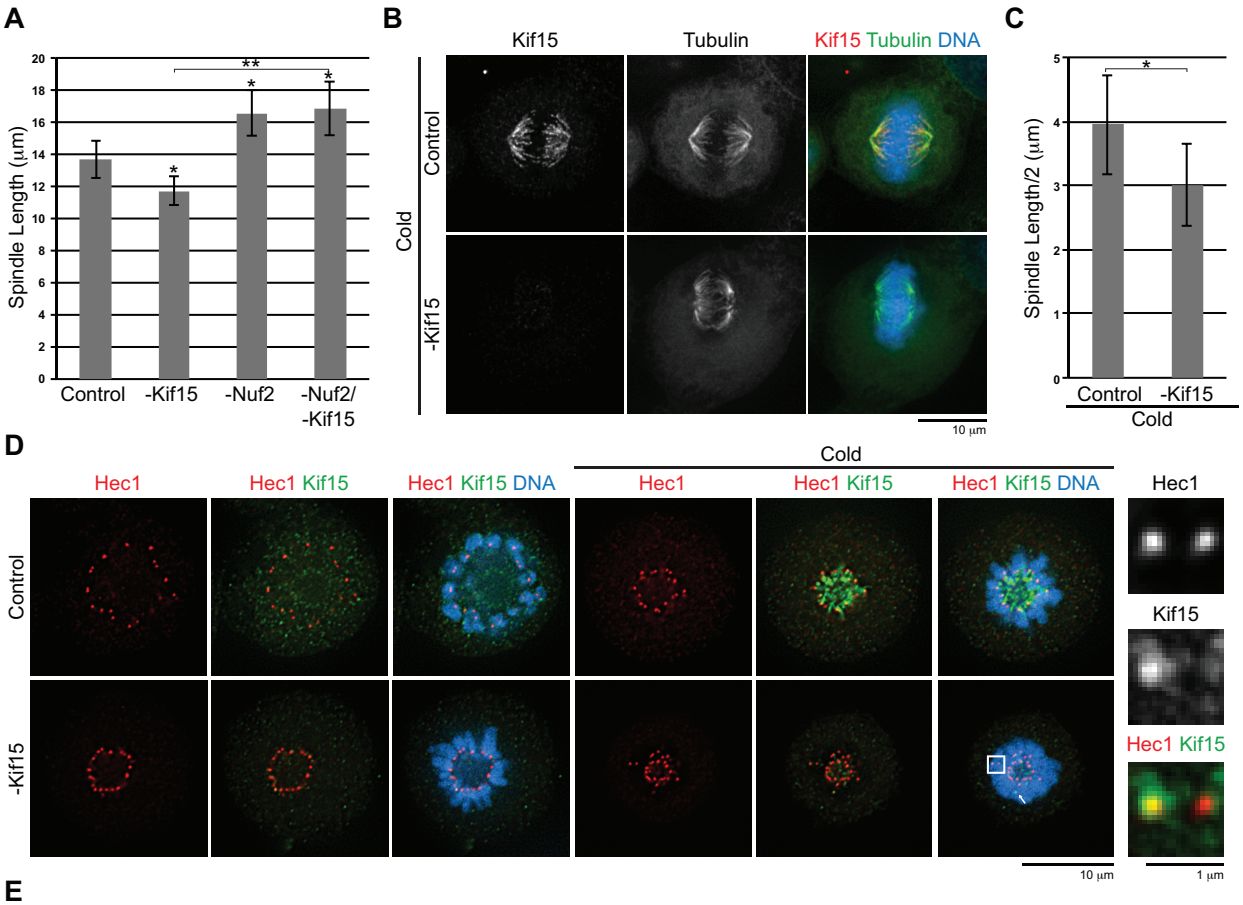

Figure 4.3: Kif15 influences spindle and K-fiber length in HeLa cells. A) Kif15 depletion shortens spindles in a K-MT-dependent manner. Quantitation of spindle length in μm in HeLa cells transfected with indicated siRNAs. Spindle length was assessed by tubulin immunostaining. Columns represent the mean ± SD. Control, 13.7 ± 1.2; -Kif15, 11.7 ± 0.9; -Nuf2, 16.6 ± 1.4; -Nuf2/-Kif15, 16.9 ± 1.7. *, $p \leq 0.001$ with respect to control. **, $p \leq 0.001$. $n \geq 62$. B) Kif15 protects K-MTs from cold. Maximum z-projections of representative HeLa cells transfected with non-specific or Kif15-targeting siRNAs for ~48 hours, released from an RO-3306-induced G2 block, and treated with cold temperatures upon reaching metaphase. Cells were then fixed and stained with antibodies targeting Kif15 (red) and tubulin (green). DNA (blue) was detected with Hoechst-33342. LUTs were scaled identically for Kif15 channel. Scale bar, 10 μm. C) Quantitation of half-spindle lengths in μm from experiment described in (B). Spindle length was assessed by tubulin immunostaining. Columns and error bars represent the average ± SD. Control, 4.0 ± 0.8; -Kif15, 3.0 ± 0.6. *, $p \leq 0.001$. $n \geq 76$. D) Kif15 depletion shortens K-fibers. Images of representative HeLa cells transfected with non-specific or Kif15-targeting siRNAs for ~48 hours prior, induced to form monopolar spindles by 100 μM Monastrol for 1 hour, and either fixed or exposed to cold temperatures prior to being fixed. Cells were stained with antibodies targeting Hec1 (red) and Kif15 (green). DNA (blue) was detected with Hoechst-33342. The boxed region is enlarged (right) to show residual Kif15 on distal kinetochore of outlying pair in Kif15-depleted cell exposed to cold. LUTs were scaled identically for Kif15 channel, excluding enlarged images. Scale bars,10 μm and 1 μm. E) Quantitation of kinetochore rosette diameter in μm from experiment described in (D). Columns represent the mean ± SD. Control, 5.7 ± 0.7; -Kif15, 4.3 ± 0.+6; Cold, 3.5 ± 0.5; Cold/-Kif15, 2.8 ± 0.5. *, $p \leq 0.001$ with respect to control. **, $p \leq 0.001$. $n \geq 77$.

To gain insight into how Kif15 affects the dynamics of spindle assembly, cells expressing fluorescent tubulin were imaged by time-lapse fluorescence microscopy upon release from a Monastrol block. Spindles in mock-depleted cells elongate at 0.8 ± 0.2 μm min^{-1} until reaching a steady-state length (n = 4, Figures 4.4A-C). Spindles in Kif15-depleted cells similarly elongate at 0.8 ± 0.1 μm $minute^{-1}$, but overshoot their steady-state length (n = 4, Figure 4.4A-C). A contraction phase subsequently shortens the pole-to-pole distance at 0.4 ± 0.1 μm $minute^{-1}$ until spindles reach a characteristically short length (n = 4, Figures 4.4A-C). Spindles in Nuf2-depleted cells also experience an extended elongation phase without a postliminary contraction, resulting in abnormally long steady-state lengths (Figures 4.4A-C). These data align with the fixed cell analyses and reveal that K-MTs have the propensity to reel the spindle poles inwards. Ultimately, these data demonstrate that Kif15 modulates K-MT-mediated forces to limit centrosome separation in HeLa cells.

Kif15 Bundles Non-K-MTs to Drive Spindle Assembly in EIC-1 Cells

Kif15 activity in HeLa cells seemingly opposes centrosome separation, yet Eg5-independent cells (EIC-1) require Kif15 for spindle assembly (Chapter III). To account for this discrepancy, Kif15 localization in EIC-1 cells was monitored. Strikingly, Nuf2-depletion does not abrogate Kif15 spindle localization in EIC-1 cells, indicating that Kif15 atypically localizes to non-K-MTs (Figure 4.5A). Nuf2 depletion does not affect spindle bipolarity in EIC-1 cells, as the MPI after mock- and Nuf2-depletion averages 82.1 ± 2.4 and 79.6 ± 4.6, respectively (n ≥ 1007, Figure 4.5B). These data indicate that non-K-MTs mediate Kif15-generated centrosome separation forces in EIC-1 cells.

As EIC-1 cells uniquely exhibit Kif15 on non-K-MTs and non-K-MT bundling (Chapter III), Kif15 may drive the rate-limiting step of monoaster symmetry breaking during Eg5-indpendent spindle assembly (Chapter III). Consistent with this notion, Kif15 enriches on fan-shaped *versus* radially-symmetric monoasters in pre-metaphase EIC-1 cells (Figure 4.5C). Perhaps more convincingly, Kif15 depletion from EIC-1 cells results in 98.1% ± 0.2% of monoasters exhibiting radial symmetry, indicative of near total failure in symmetry breaking ($p \leq 0.001$, $n \geq 420$, Figures 4.5D and E). Altogether, these data suggest that Kif15 performs the essential function of monoaster symmetry breaking in EIC-1 cells by mislocalizing to and bundling non-K-MTs.

Non-K-MTs also mediate the centrosome separation forces in HeLa cells, as Eg5 acts on anti-parallel non-K-MTs (Kapitein et al. 2005; Ferenz, Gable, and Wadsworth 2010). But given the geometry of monopolar spindles, non-K-MTs involved in Eg5-independent spindle assembly are likely oriented in parallel. To visualize non-K-MT orientation, a MT plus-end tracker, GFP-EB3 (Akhmanova and Steinmetz 2008), was imaged by fluorescence time-lapse microscopy in Nuf2-depleted pre-metaphase EIC-1 cells. Indeed, all observed GFP-EB3 comets radiate away from the monoaster centers, revealing that non-K-MTs are arranged in parallel with their plus-ends extending toward the cell periphery (Figures 4.5F and G). Therefore, Kif15 commonly acts on parallel MT arrays but differentially affects spindle assembly depending on its partitioning to K-MTs *versus* non-K-MTs.

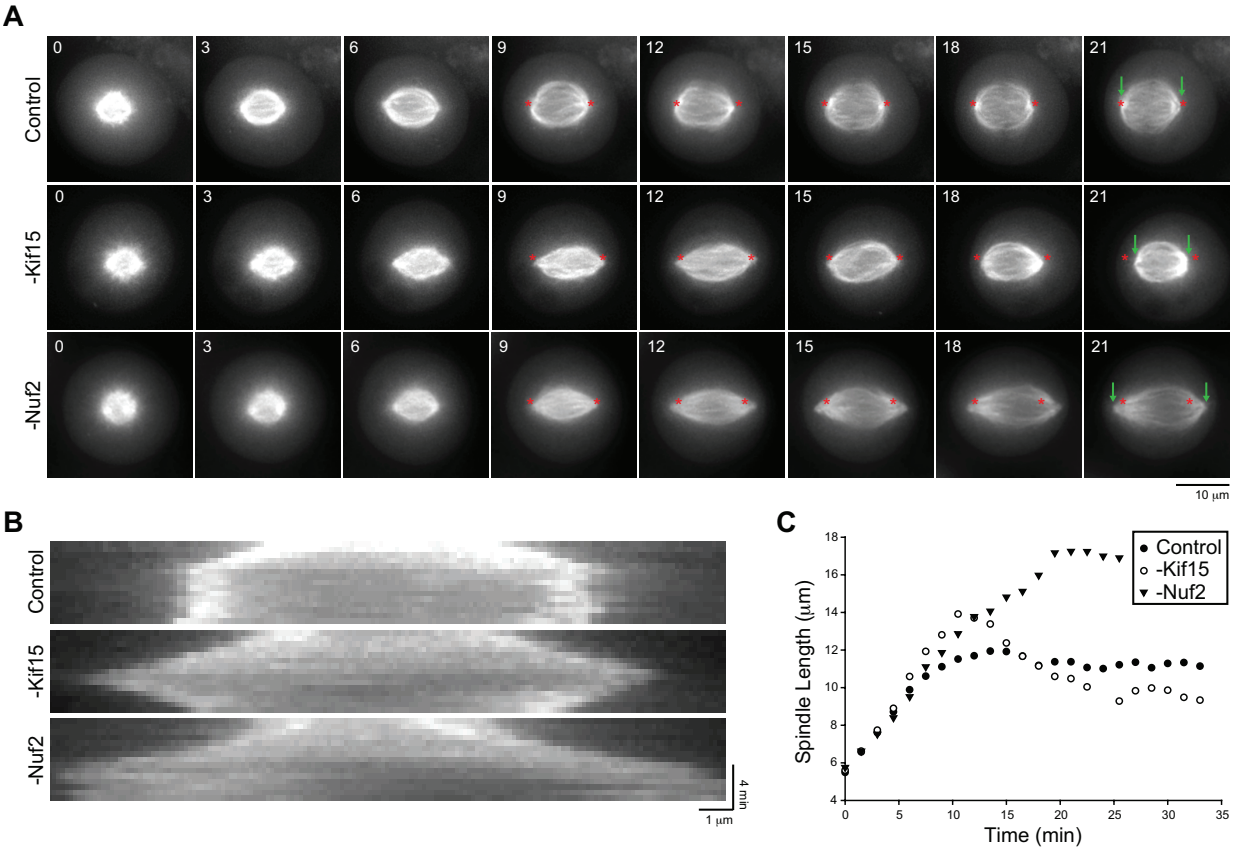

Figure 4.4: Kif15 modulates K-fiber-generated forces in HeLa cells. A) Kif15 depletion contracts spindles in a K-MT-dependent manner. Maximum z-projections from time-lapse movies in representative HeLa cells transfected with indicated siRNA for ~48 hours. Cells stably expressed fluorescent tubulin and were released from a Monoastrol-induced mitotic block prior to imaging. Time relative to the initial frame is indicated in minutes. Asterisks, spindle poles at 9 minutes. Arrows, spindle poles at 21 minutes. Scale bar, 10 μm. B) Kymographs of movies in (A). Scale bars, 1 μm and 4 minutes. C) Quantitation of experiment described in (A). Data points represent average spindle length in μm relative to time in minutes after Monoastrol washout. n ≥ 4.

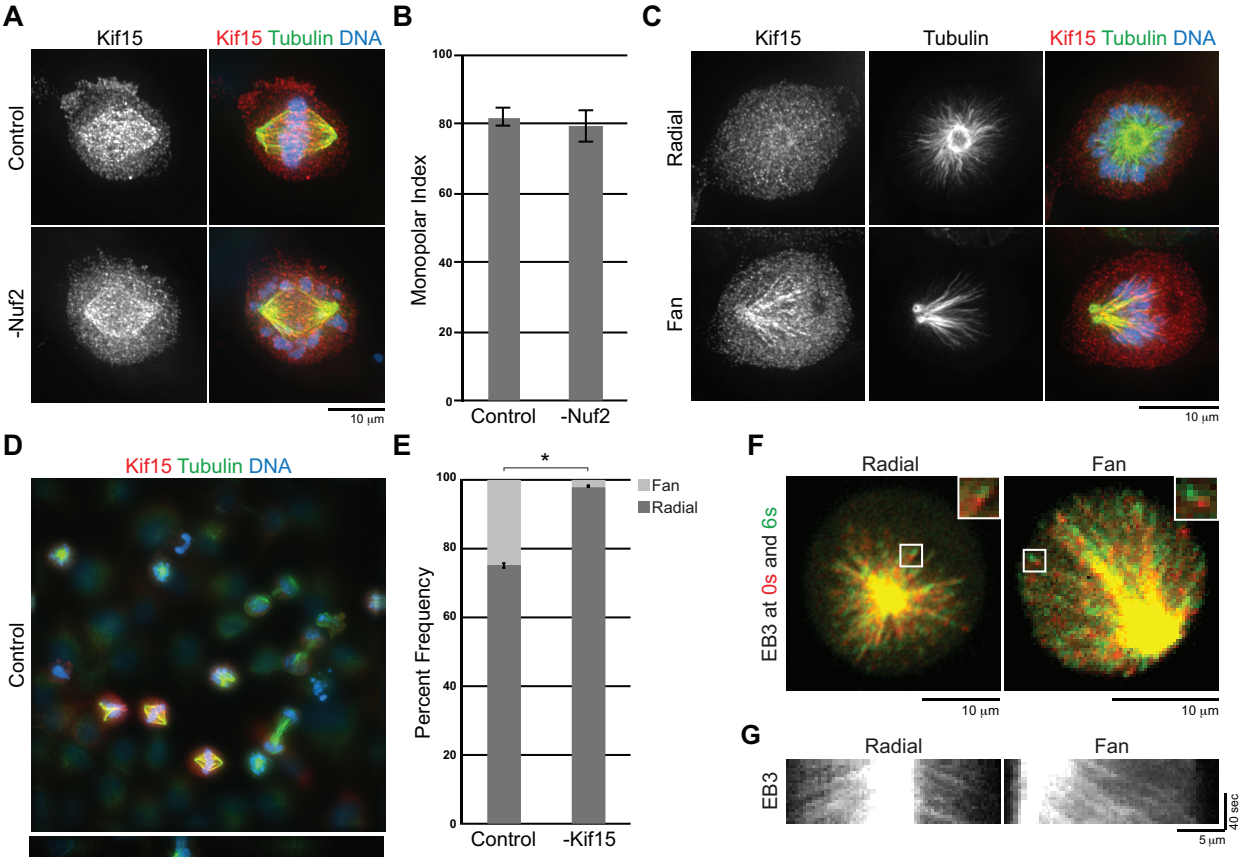

Figure 4.5: Kif15 drives spindle bipolarization in EIC-1 cells by acting on parallel non-K-MTs. A) Kif15 localizes to non-K-MTs in EIC-1 cells. Maximum z-projections of representative EIC-1 cells transfected with non-specific or Nuf2-targeting siRNAs for ~48 hours. Cells were fixed and stained with antibodies targeting Kif15 (red) and tubulin (green). DNA (blue) was detected with Hoechst-33342. LUTs were scaled identically for each channel. Scale bar, 10 μm. B) Nuf2 depletion does not affect spindle bipolarization in EIC-1 cells. Quantitation of monopolar index in EIC-1 cells transfected with non-specific or Nuf2-targeting siRNAs for ~48 hours. Spindle geometry was assessed by tubulin immunostaining. Columns represent average ± SD. Control, 79.6 ± 4.6; -Nuf2, 82.1 ± 2.4. n ≥ 1000. C) Kif15 enriches on fan-shaped monopolar spindles in EIC-1 cells. Maximum z-projections of representative EIC-1 cells containing a radially symmetric or fan-shaped monopolar spindle. Cells were fixed and stained with antibodies targeting Kif15 (red) and tubulin (green). DNA (blue) was detected with Hoechst-33342. LUTs were scaled identically for each channel. Scale bar, 10 μm. D) Kif15 depletion prevents monoaster symmetry-breaking in EIC-1 cells. Maximum z-projections of representative fields of EIC-1 cells transfected with non-specific or Kif15-targeting siRNAs for ~24 hours. Cells were fixed and stained with antibodies targeting Kif15 (red) and tubulin (green). DNA (blue) was detected with Hoechst-33342. LUTs were scaled identically for each channel. Scale bar, 40 μm. E) Quantitation of experiment described in (D). Monopolar spindle geometry was assessed by tubulin immunostaining. Columns represent average ± SD. Radial: Control, 24.8 ± 0.8; -Kif15, 1.9 ± 0.2. Fan: Control, 75.2 ± 0.8; -Kif15, 98.1 ± 0.2. *, $p \leq 0.001$. n ≥ 420. F) Non-K-MTs orient in parallel in EIC-1 cell monoasters. Time squash of Nuf2-depleted EIC-1 cells expressing fluorescent-EB3. Monoaster shape is indicated. Red, time = 0 seconds; green, time = 6 seconds. Enlargements of the boxed regions are shown to emphasize the red-to-green pattern tracking away from the centrosome. Scale bars, 10 μm. G) Kymographs of movies in (F). Scale bars, 5 μm and 40 seconds.

Discussion

K-MTs have long been known to influence chromosome positioning with their dynamic plus-ends (Inoué and Salmon 1995; Howard and Hyman 2003). As their minus-ends are embedded in the centrosomes (Brinkley 1985), logic would hold that K-MTs also exert force on the spindle poles. However, this notion has not been rigorously tested. The work described here demonstrates that K-MTs maintain spindle bipolarity in the absence of Eg5 activity, but normally oppose Eg5-generated forces to prevent excessive spindle elongation. Thus, K-MTs can both push the spindle poles apart and pull the spindle poles together. These findings prove the balance-of-forces model to be over simplified, as K-MTs must be taken into account as active force generators and not merely passive substrates for molecular motors.

This work also questions the binning of motors into “outward” or “inward” force generators based on their directionality (Sharp, Rogers, and Scholey 2000; Goshima et al. 2005). Shown here, Eg5 and Kif15 have vastly divergent roles during spindle assembly despite both having plus-end directionality. Under normal conditions, Kif15 modulates K-MT generated forces to set an upper limit to spindle length. The mechanism by which it does so remains unclear, but its enrichment at the kinetochore-MT interface suggests that Kif15 may regulate K-MT plus-end dynamics. Alternatively, Kif15 may crosslink adjacent K-MTs along their lattices to coordinate the polymerization dynamics of neighboring K-MTs. Distinguishing between these non-mutually-exclusive hypotheses will be the subject of future work.

In cells with compromised Eg5 activity, Kif15 spills onto non-K-MTs and drives centrosome separation. Similarly, the kinesin-12 KLP18 acts on non-K-MTs to drive

centrosome separation in *C. elegans* oocytes (Segbert et al. 2003; Wignall and Villeneuve 2009). Comparing these cellular contexts indicates that Kif15 differentially affects spindle assembly depending on its MT substrate. Thus, mechanisms that regulate Kif15 localization are key in understanding spindle length homeostasis and the emergence of Eg5-inhibitor resistant cancer cells.

CHAPTER V

KINESIN-12 KIF15 TARETS KINETOCHORE-FIBERS THROUGH AN INTRINSIC TWO-STEP MECHANISM

Emma G. Sturgill[1], Dibyendu Kumar Das[2], Yoshimasa Takizawa[1], Yongdae Shin[3], Scott Collier[1], Melanie D. Ohi[1], Wonmuk Hwang[4,5], Matthew J. Lang[2], and Ryoma Ohi[1*]
[1]Department of Cell and Developmental Biology, Vanderbilt University Medical Center, Nashville, TN 37232, [2]Department of Chemical and Biomolecular Engineering, Vanderbilt University, Nashville, TN, 37235, [3]Department of Mechanical Engineering, Massachusetts Institute of Technology, Cambridge, MA, 02139, [4]Department of Biomedical Engineering, Texas A&M, College Station, TX 77843, and [5]School of Computational Sciences, Korea Institute for Advanced Study, Seoul, Korea 130-722

Previously published as:

Sturgill EG, Das DK, Takizawa Y, Shin Y, Collier SE, Ohi MD, Hwang W, Lang MJ, and Ohi R. (2014). Kinesin-12 Kif15 targets kinetochore fibers through an intrinsic two-step mechanism. *Current Biology* 24, 2307-2313.

Abstract

Documented here is the first account of Kif15 temporal and spatial regulation. Kif15 selectively activates on MT bundles during mitosis as a consequence of two inherent biochemical properties. First, Kif15 is self-repressed by its C-terminus. Second, Kif15 harbors a second MT-binding site adjacent to its motor domain which enables dimeric Kif15 to crosslink and slide MTs. Two-MT-binding locks Kif15 in an active conformation, causing its accumulation on bundled MTs. As K-fibers represent the primary source of bundled spindle MTs, Kif15 autonomously targets this population during mitosis. This study challenges the current model of Kif15 regulation and provides a new paradigm as to how kinesin auto-regulation can impact motor distribution in cells.

Introduction

Proteins that recognize and act on specific subsets of microtubules (MTs) enable the varied functions of the MT cytoskeleton (Sawin and Scholey 1991). The design principles of each mitotic kinesin appear optimally tuned for a specific task (Welburn 2013). For example, the kinesin-5 Eg5 tetramerizes to slide anti-parallel MTs apart during mitotic onset, an activity that establishes spindle bipolarity (Kapitein et al. 2005; Ferenz, Gable, and Wadsworth 2010). In contrast to Eg5, Kif15 functions on parallel MT arrays (Chapter IV). Kif15 normally modulates spindle length by acting on kinetochore-fibers (K-fibers), or bundles of spindle MTs that attach end-on to kinetochores (Rieder and Salmon 1998; Hayden, Bowser, and Rieder 1990). In cells that have evolved Eg5 independence, Kif15 functions on parallel non-K-MTs to drive

spindle assembly (Chapter III and IV). Given the rarity of K-fiber-specific localization, the duality of Kif15 function on spindle MTs, and the clinical implications of Kif15-dependent spindle assembly, it is important to understand the temporal and spatial control of Kif15 activity.

In order to prevent futile ATP consumption, mitotic kinesins are often inhibited during interphase. For example, the kinesin-10 Kid and kinesin-8 Kif18A are sequestered in the nucleus away from MTs during interphase (Tokai et al. 1996; Du, English, and Ohi 2010). Other mitotic kinesins remain cytoplasmic during interphase, but are inhibited by intramolecular interactions (Verhey and Hammond 2009). The canonical mechanism for self-repression, as detailed for kinesin-1, involves direct binding of the C-terminal tail to the N-terminal motor heads (Hackney, Levitt, and Suhan 1992). Tail-head interactions trap ADP in the nucleotide binding pocket, locking the kinesin in a low-affinity MT-binding state (Kaan, Hackney, and Kozielski 2011). Tail-head interactions inhibit kinesin-7 CENP-E activity in a manner that is relieved by cell-cycle dependent phosphorylation (Espeut et al. 2008). In this way, CENP-E activates only during mitosis. As cytoplasmic Kif15 fails to bind MTs during interphase, its temporal activation may be subjected to similar cell-cycle dependent control (Vanneste et al. 2009).

The spatial partitioning of kinesins to K-fibers is unusual, demonstrated by a small cohort of molecular motors and MT-associated proteins (MAPs) including TPX2, Astrin, Kif18A, and HURP (Bird and Hyman 2008; Mack and Compton 2001; Mayr et al. 2007; Silljé et al. 2006; Wong and Fang 2006). Generally, the mechanisms governing K-fiber-specific localization are not well understood, but are of obvious importance given

the functional significance of K-fibers during mitosis (Howard and Hyman 2003). Intrinsic biophysical properties could drive K-fiber specific accumulation. Such is the case for Kif18A, as it enriches on K-fibers as a consequence of its ultra-processive motility (Mayr et al. 2007; Stumpff et al. 2011). Alternatively, intermediary factors could facilitate MT recruitment. In the case of Kif15, the MAP TPX2 has been suggested to function in this capacity (Wittmann et al. 2000; Tanenbaum et al. 2009; Vanneste et al. 2009). Despite the prevalence of this model, no evidence for a direct TPX2-Kif15 interaction has been shown.

Results

Kif15-MT Binding Is Prevented by its C-Terminus during Interphase

To test whether Kif15 can transiently bind MTs during interphase, cells were infused with AMPPNP. Kinesins lock onto MTs when bound with this non-hydrolyzable ATP analog, making brief MT-binding events detectable by fix-and-stain methodology (Cai et al. 2007; Hammond et al. 2009). Endogenous Kif15 fails to co-localize with interphase MTs in AMPPNP-infused cells (data not shown). Exogenously expressed full-length Kif15 (GFP-Kif15-FL, Figure 5.1A) also remains diffuse in AMPPNP-infused interphase cells, indicating that the motor heads are completely blocked from engaging MTs (Figure 5.1B). In contrast, a C-terminally truncated Kif15 construct (GFP-Kif15-N700, Figure 5.1A) decorates interphase MTs in a manner enhanced by AMPPNP (Figure 5.1B). These data suggest that Kif15-MT binding is inhibited by its C-terminus during interphase.

Kif15 Motility Is Self-Repressed by Coil-2 *in vitro*

Motivated by these cellular data, the possibility of Kif15 self-repression was next tested *in vitro*. Antibodies targeting the C-terminal Coil-2 (Figure 5.1A) were utilized, reasoning that they would activate Kif15 by preventing inhibitory tail-head interactions (αC2, Chapter IV). In conventional MT gliding assays, recombinant GFP-Kif15-FL moves MTs at 0.059 ± 0.029 μm second^{-1} (average ± standard deviation (SD), n = 1374, Figures 5.1A, C, and D). But when anchored to flow cells by αC2, GFP-Kif15-FL glides MTs at 0.123 ± 0.071 μm second^{-1} (n = 1804, Figures 5.1C and D). The relatively large spread in gliding velocities may be attributable to the co-existence of active and repressed GFP-Kif15-FL molecules.

While these data suggest that αC2 activates Kif15, adverse effects from nonspecifically adsorbing GFP-Kif15-FL to flow cells cannot be ruled out. As a more rigorous test, single GFP-Kif15-FL molecules bound to MTs were imaged by time-lapse total internal reflection fluorescence (TIRF) microscopy. GFP-Kif15-FL appears dimeric, as the fluorescence of single molecules reduces to background in two steps (data not shown). Single GFP-Kif15-FL molecules bind MTs for 1.9 ± 0.3 seconds and are immotile (n = 194, Figures 5.1E and F). AMPPNP increases this dwell time to 12.2 ± 2.3 seconds, which may actually be an underestimation due to photobleaching (n = 215, Figures 5.1E and F). In the presence of αC2, GFP-Kif15-FL binds MTs for 4.0 ± 1.1 seconds and walks 0.6 ± 0.1 μm at 0.19 ± 0.07 μm second^{-1} (n ≥ 83, Figures 5.1E-H). αC2 does not alter the fluorescence distribution or bleaching kinetics of single GFP-Kif15-FL molecules (data not shown). Taken together, these data show that Kif15 is self-repressed by its C-terminal Coil-2.

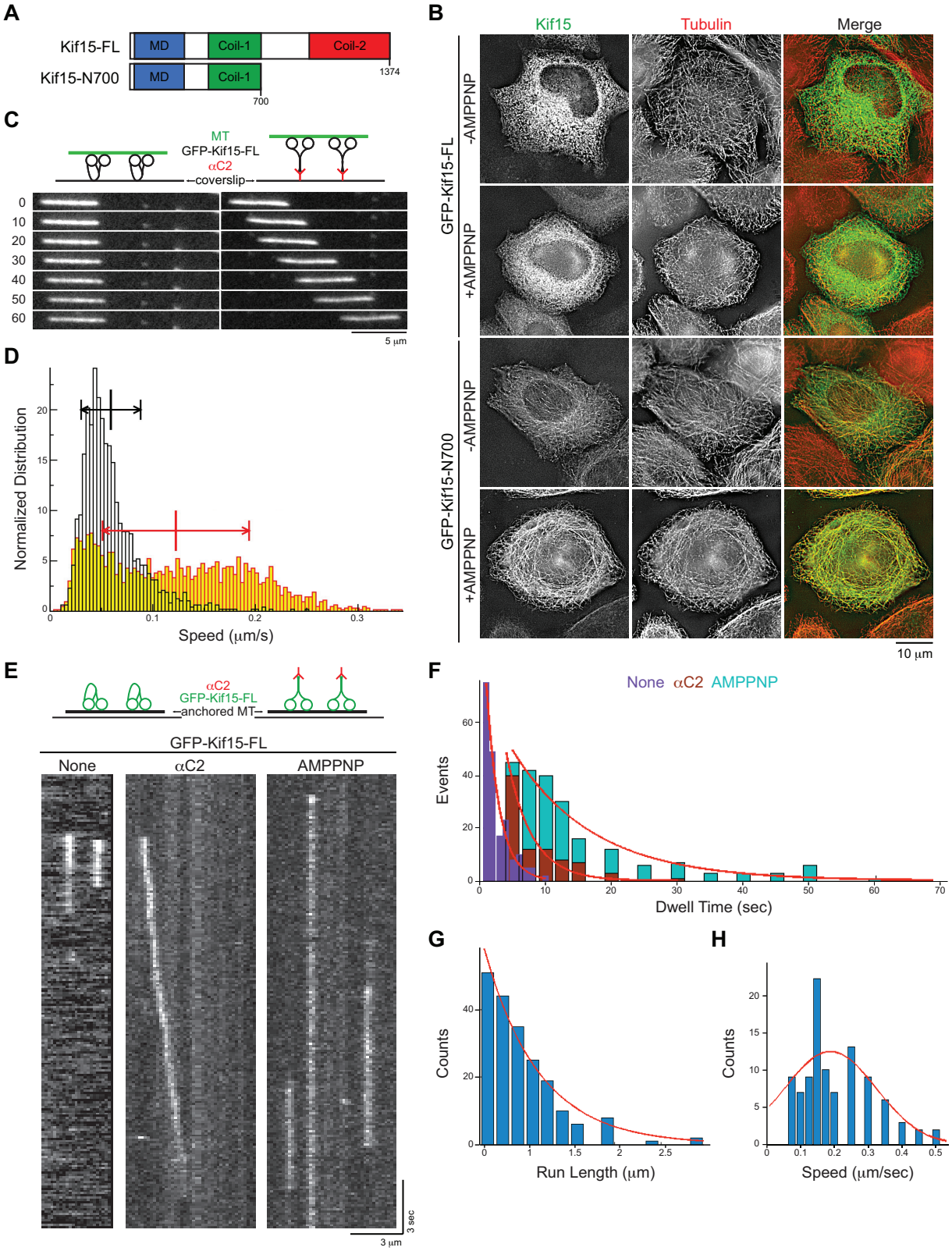
A
Kif15-FL
MD
Coil-1
Coil-2
1374
Kif15-N700
MD
Coil-1
700
B
Kif15
Tubulin
Merge
GFP-Kif15-FL
-AMPPNP
+AMPPNP
GFP-Kif15-N700
-AMPPNP
+AMPPNP
10 μm
C
MT
GFP-Kif15-FL
αC2
–coverslip–
0
10
20
30
40
50
60
5 μm
D
Normalized Distribution
Speed (μm/s)
E
αC2
GFP-Kif15-FL
–anchored MT–
GFP-Kif15-FL
None
αC2
AMPPNP
3 μm
3 sec
F
None αC2 AMPPNP
Events
Dwell Time (sec)
G
Counts
Run Length (μm)
H
Counts
Speed (μm/sec)

Figure 5.1: Kif15 is self-repressed by its C-terminal Coil-2. A) Schematic of Kif15 constructs. Motor domain (MD), blue; Coil-1, green; Coil-2, red. Amino acid residues are indicated. B) Kif15 fails to bind interphase MTs. Images of representative HeLa cells expressing GFP-Kif15-FL or GFP-Kif15-N700. Cells were unperturbed (top) or infused with 1 mM AMPPNP (bottom). Cells were fixed and stained with antibodies targeting tubulin (red). Kif15 (green) was detected by GFP fluorescence. LUTs were scaled identically for each channel. Scale bar, 10 μm. C) αC2 activates GFP-Kif15-FL in gliding assays. Top, schematic of experimental conditions. Coverslip, black line; GFP-Kif15-FL, black; fluorescent MTs, green; αC2, red. Bottom, montages of fluorescent MTs in gliding assays powered by GFP-Kif15-FL non-specifically adsorbed to a flow cell (left) or anchored to a flow cell by αC2 (right). Time in seconds after initial frame is indicated. Scale bar, 5 μm. D) Quantitation of experiment described in (C). Normalized distribution of gliding speeds in μm sec^{-1}. Black/white, GFP-Kif15-FL non-specifically adsorbed to flow cells; red/yellow, GFP-Kif15-FL anchored to flow cells by αC2. Vertical lines and horizontal arrows indicate average ± standard deviation. n ≥ 1804. E) αC2 activates GFP-Kif15-FL in single molecule motility assays. Top, schematic of experimental conditions. Coverslip, thin black line; anchored MT, thick black line; GFP-Kif15-FL, green; αC2, red. Bottom, kymographs of single GFP-Kif15-FL molecules on MTs in the presence of ATP (left), ATP and αC2 (middle), or AMPPNP (right). F-H) Quantitation of experiment described in (E). F) Dwell time distributions in seconds. GFP-Kif15-FL alone, purple; GFP-Kif15-FL with αC2, red; and GFP-Kif15-FL with AMPPNP instead of ATP, teal. Average dwell times were calculated from exponential fits (red) to the distributions. G) Run-length distribution in μm of single GFP-Kif15-FL molecules with αC2 . Average run-length was calculated from an exponential fit (red) to the distribution. H) Speed distribution in μm sec^{-1} of single GFP-Kif15-FL molecules with α C2. Average speed was calculated from a fit of the distribution to a single Gaussian (red).

The Hydrodynamic Properties of Kif15 Are Salt-Sensitive

Previous reports highlight the importance of conformational folding in facilitating inhibitory tail-head interactions (Hackney, Levitt, and Suhan 1992; Verhey and Hammond 2009). To test for this possibility, the hydrodynamic properties of Kif15 were probed by sizing chromatography and sedimentation velocity analytical ultracentrifugation (SVAU). During sizing chromatography, GFP-Kif15-FL elutes near the void volume in buffers of high ionic strength (300 mM KCl), peaking at an elution volume of 60.3 mls of a sizing column optimized to resolve proteins under 600 kD (Figures 5.2A and B). In buffers of low ionic strength (50 mM KCl), GFP-Kif15-FL shifts to an elution volume of 69 mls (Figures 5.2A and C), suggesting that intramolecular electrostatic interactions fold Kif15 into a compact conformation. Notably, the elution profile of GFP-Kif15-FL in low salt displays a “shoulder” left of the peak (Figure 5.2A). This likely represents a subpopulation of GFP-Kif15-FL in transitory conformations, as

no impurities are evident by SDS-PAGE (Figure 5.2C). During SVAU, GFP-Kif15-FL sediments with a Svedberg value of 4.0 (r.m.s.d. = 0.0041, Figure 5.2D). At 376.4 kD, this is consistent with GFP-Kif15-FL existing as a dimer in solution and agrees with the single molecule analysis. Additionally, the high frictional ratio of 2.7 indicates that GFP-Kif15-FL is an elongated molecule, accounting for its anomalous migration during sizing chromatography in high salt (Figures 5.2A and B).

Two short disordered regions are predicted to interrupt the otherwise coiled-coil stalk of Kif15 (Boleti, Karsenti, and Vernos 1996; Tanenbaum et al. 2009; Klejnot, Falnikar, and Ulaganathan 2013). These regions could serve as flexible hinges to enable conformational folding, so GFP-Kif15-FL molecules were next visualized by single particle negative stain electron microscopy (EM). Single GFP-Kif15-FL molecules exhibit two globular domains, likely corresponding to two GFP-fused motor heads of a Kif15 homodimer (Figure 5.2E). Consistent with the notion of a flexible hinge region, the stalks of single GFP-Kif15-FL molecules are commonly punctuated by a kink (Figure 5.2E). To ensure that kinks are not artifacts introduced during sample preparation, the kinesin-14 GFP-HSET was visualized by the same methodology. The cherry-like appearance of single GFP-HSET molecules likely represents two C-terminal motor heads dimerized by a coiled-coil stalk extending to two N-terminal GFP-tagged globular domains (Figure 5.2D, (Bieling, Telley, and Surrey 2010)). Importantly, no kinks are evident within single GFP-HSET molecules (Figure 5.2E). Altogether, these data suggest that Kif15 toggles between open and closed conformations in an electrostatic-dependent manner.

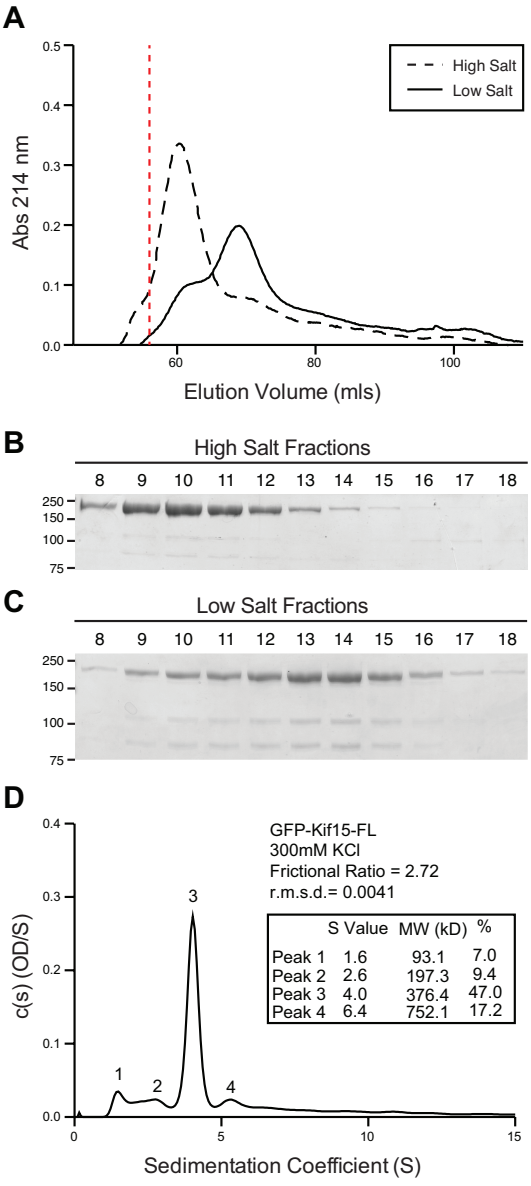

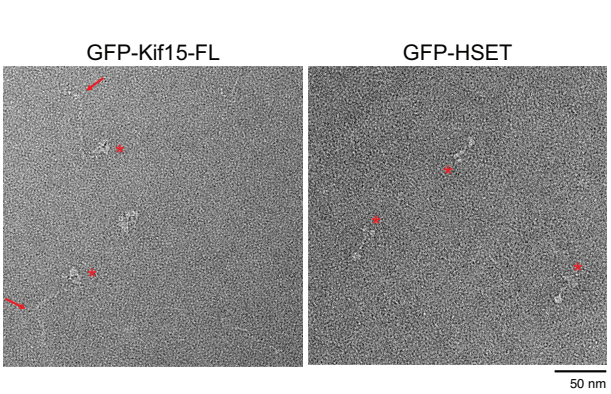

Figure 5.2: The hydrodynamic properties of Kif15 are salt-sensitive. A) Elution profiles of GFP-Kif15-FL from Superdex 200 16/60 sizing column runs in buffers of high salt (300 mM KCl, dashed line) and low salt (50 mM KCl, solid line). The void volume for the column is indicated by the red stippled line. B) and C) SDS-PAGE of the indicated sizing column fractions run in buffers of high salt (B) or low salt (C) stained with Coomassie blue. Fractions 8-18 correspond to column eluates that span 57-79 mls. Molecular weight markers are indicated in kD. D) GFP-Kif15-FL is an extended rod-like dimer in high salt buffer by SVAU. The calculated s [c(s)] is plotted versus the sedimentation coefficient (S) for GFP-Kif15-FL. The sedimentation velocity profile was fit to a continuous sedimentation distribution. E) Representative fields of GFP-Kif15-FL (top) and GFP-HSET (bottom) particles as seen by negative stain EM. Asterisks mark globular head regions and arrows indicate flexible regions. Scale bar, 50 nm.

Kif15 Crosslinks and Slides MTs through a Second MT-Binding Site

To study the motile properties of constitutively active Kif15, a recombinant C-terminally truncated construct (Kif15-N700, Figure 5.1A) was analyzed *in vitro*. Like GFP-Kif15-FL, Kif15-N700 dimerizes as assessed by sizing chromatography (data not shown). In conventional gliding assays, Kif15-N700 moves MTs at 0.184 ± 0.084 μm second^{-1} (n = 368, Figures 5.3A and B). Polarity marked MTs lead with their minus ends (data not shown), validating that Kif15 is plus-end-directed like its *Xenopus* ortholog Xklp2 (Boleti, Karsenti, and Vernos 1996).

Kif15-N700 robustly bundles MTs in solutions devoid of nucleotide (Figure 5.3C). In solutions containing ATP, Kif15-N700 crosslinks MTs with minimal overlap. This end-to-end MT "tiling" is detectable with two populations of monochromatically labeled MTs (Figure 5.3D). To visualize the remodeling of MT bundles into tiled arrays, Kif15-N700 was sandwiched between a coverslip-anchored red MT and a solution-derived green MT in flow cells. Kif15-N700 slides the cargo MT along the anchored MT upon ATP addition (Figure 5.3E), accounting for the nucleotide-dependent change in MT organization.

The ability of Kif15-N700 to bundle MTs independently of ATP suggests the presence of a non-motor MT-binding site. So the MT-binding capabilities of Coil-1 (Figure 5.1A) were next tested. Kif15-Coil-1 fractionates with MTs in conventional co-pelleting assays, revealing that Kif15 harbors a non-motor MT-binding site (Figure 5.3F). For comparison, Kif15-Coil-2 does not co-pellet with MTs (Figure 5.3G). Altogether, these data show that dimeric Kif15 crosslinks and slides MTs as a function of its two MT-binding sites.

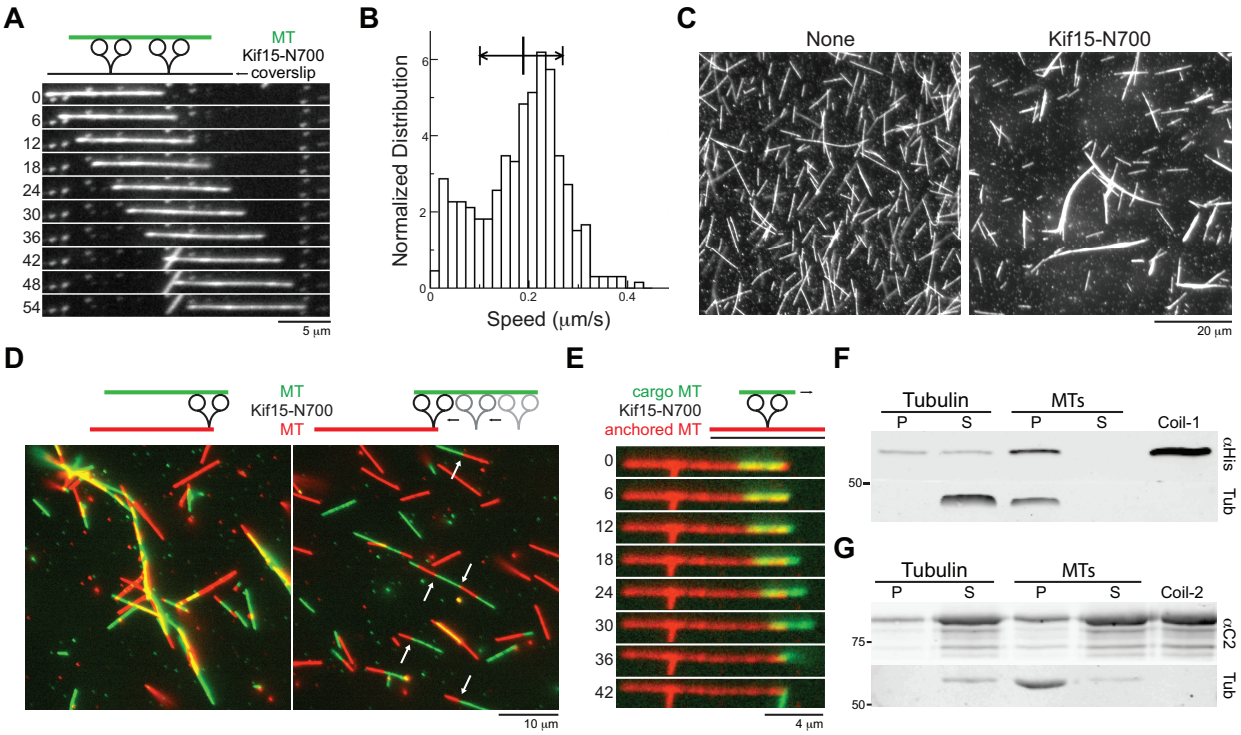

Figure 5.3: Kif15 crosslinks and slides MTs with a second MT-binding site. A) Kif15-N700 robustly glides MTs. Top, schematic of experimental conditions. Coverslip, black line; GFP-Kif15-N700, black; fluorescent MT, green. Bottom, montage of a fluorescent MT in gliding assay powered by Kif15-N700. Time in seconds after initial frame is indicated. Scale bar, 5 μm. B) Quantitation of experiment described in (A). Normalized distribution of gliding speeds in μm s^{-1}. Vertical lines and horizontal arrows indicate average ± standard deviation. 0.184 ± 0.084. n = 368. C) Kif15-N700 bundles MTs. Images of fluorescent MTs incubated in solution devoid of nucleotide in the absence (left) or presence (right) of Kif15-N700. Scale bar, 20 μm. D) Kif15-N700 tiles MTs. Top, schematic of experimental conditions. Fluorescent MTs, red and green; Kif15-N700, black. Bottom, images of red and green fluorescent MTs incubated in solution with Kif15-N700 in the absence (left) or presence (right) of 1 mM ATP. Arrows indicate examples of MT "tiling". Scale bar, 10 μm. E) Kif15-N700 slides MTs. Top, schematic of experimental conditions. Coverslip, black line; anchored MT, red; Kif15-N700, black; solution-derived cargo MT, green. Bottom, montage of red and green MTs in a two MT sliding assay with Kif15-N700 in 750 μM ATP. Time in seconds after initial frame is indicated. Scale bar, 4 μm. F) Kif15-Coil-1 contains a MT-binding site. Immunoblot of fractions from a MT co-pelleting assay with Kif15-Coil-1. Supernatant "S" and pellet "P" fractions are indicated. Kif15-Coil-1 was detected with α-His antibodies. Tubulin is also shown. Molecular weight markers are indicated in kD. G) Kif15-Coil-2 does not contain a MT-binding site. Immunoblot of fractions from a MT co-pelleting assay with Kif15-Coil-2. Supernatant "S" and pellet "P" fractions are indicated. Kif15-Coil-2 was detected with αC2. Tubulin is also shown. Molecular weight markers are indicated in kD.

Kif15 Accumulates on MT Bundles

In the case of kinesin-1, cargo binding activates motility (Cai et al. 2007). Kif15 lacks a conventional globular tail domain, but a second MT could theoretically serve to activate Kif15 by engaging Coil-1. In this scenario, MT bundles would induce robust Kif15 activity by simultaneously providing substrate for Coil-1 and the motor heads. To test this notion, GFP-Kif15-FL was monitored on MT bundles induced by PRC1, a MAP that bundles midzone MTs (Subramanian et al. 2010). In agreement with the single molecule data (Figure 5.1), GFP-Kif15-FL does not detectably associate with individual MTs in solution (Figure 5.4A). In contrast, GFP-Kif15-FL accumulates on PRC1-induced MT bundles (Figure 5.4A). Like PRC1, TPX2 exhibits MT-bundling activity (Wittmann et al. 2000). TPX2 has been proposed to be a loading factor for Kif15 (Wittmann et al. 2000; Tanenbaum et al. 2009; Vanneste et al. 2009), but both PRC1 and TPX2 fail to recruit Kif15 to individual coverslip-bound MTs (Figure 5.4B). These data question the current model of Kif15 regulation, instead indicating that Kif15 has an inherent affinity for MT bundles *in vitro*.

In addition to localization, the motility of GFP-Kif15-FL within PRC1-induced MT bundles was monitored. Single GFP-Kif15-FL molecules within PRC1-induced MT bundles dwell for 9.0 ± 1.3 seconds and move 0.4 ± 0.1 μm at 0.14 ± 0.03 μm second^{-1} as assessed by TIRF microscopy (n ≥ 91, Figures 5.4C-E). These motility parameters contrast those of GFP-Kif15-FL on single MTs, demonstrating that MT bundles activate Kif15.

In mitotic cells, Kif15 enriches on K-fibers (Chapter IV). To test whether Kif15 recognizes this spindle MT population for their bundled configuration, non-K-MT were made to bundle with the Eg5 rigor drug FCPT (Groen et al. 2008; Vladimirou et al. 2013). As previously described, siRNA-depletion of the outer kinetochore component Nuf2 abrogates Kif15 spindle localization by blocking K-MT formation (Figure 5.4F, Chapter IV, (DeLuca et al. 2002)). Strikingly, FCPT restores Kif15 spindle localization in Nuf2-depleted cells, revealing that Kif15 binds bundled non-K-MTs (Figures 5.4F). Therefore, Kif15 normally targets K-fibers because of its inherent affinity for MT bundles.

To model these data, Kif15 autonomously targets K-fibers by 1) molecular unfolding and 2) two-MT binding (Figure 5.4G). First, cytosolic Kif15 toggles between closed and open conformations, with a tendency for the closed conformation. Mediated by intramolecular electrostatic interactions, the closed conformation juxtaposes Coil-2 and the motor heads to hinder MT binding. A non-motor MT-binding site becomes exposed when Kif15 transiently unfolds, allowing Kif15 to engage MTs with its motor heads and/or Coil-1. If Kif15 engages a single MT with one binding site, it rapidly unbinds and collapses back to a closed conformation. As most non-K-MTs are solitary and short-lived, Kif15 does not appreciably concentrate on this spindle MT population. On the other hand, if Kif15 simultaneously engages two MTs with both binding sites, it becomes locked in an open and active conformation. As MTs within a K-fiber are bundled and long-lived, they are conducive to two-MT-binding and promote Kif15 activation. Kif15 therefore accumulates on K-fibers. When overexpressed or constitutively active, as in Eg5-independent cells (Chapter III, (Tanenbaum et al. 2009)), Kif15 may be able to create its own substrate through its MT-bundling activity.

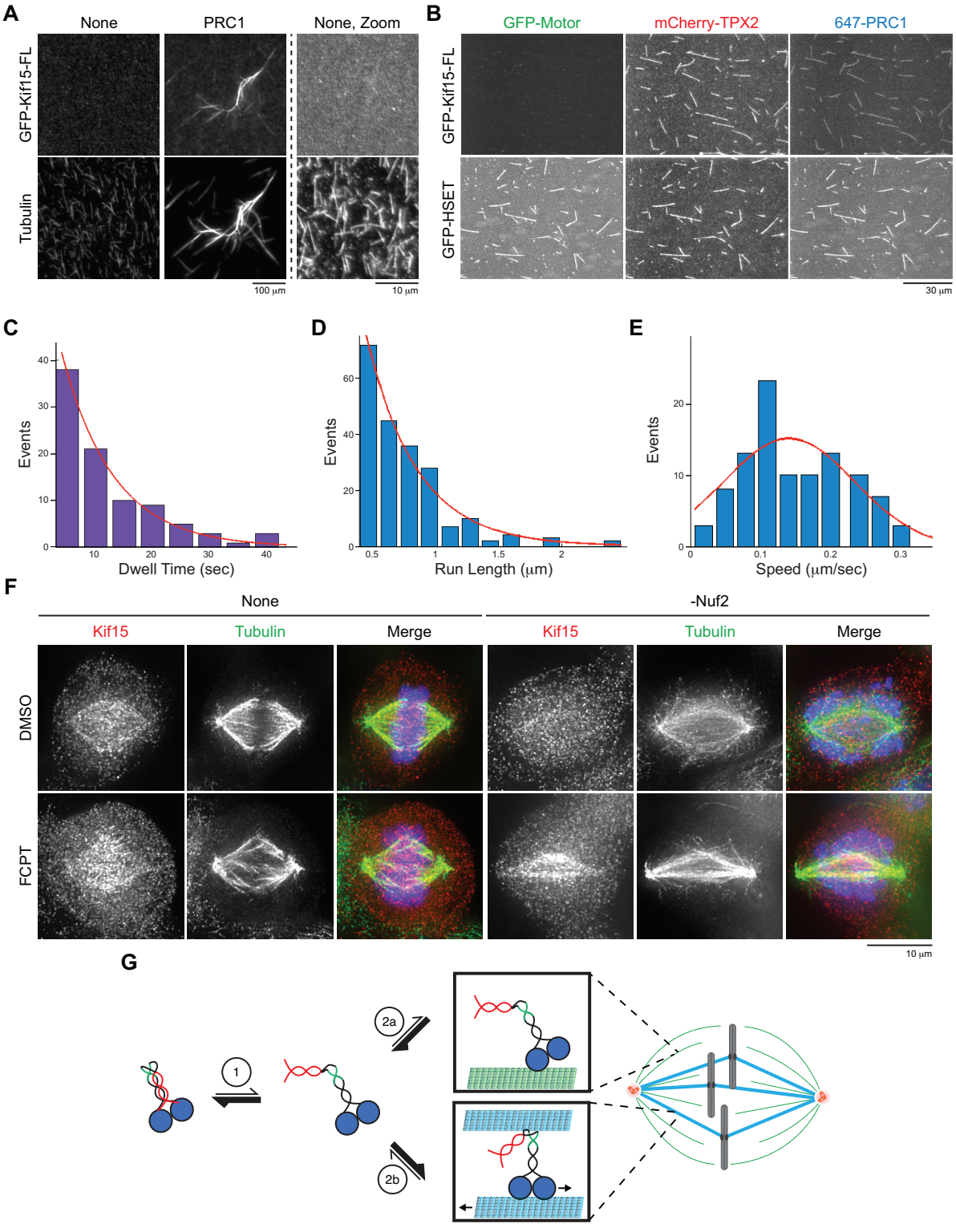
A
None
PRC1
None, Zoom
GFP-Kif15-FL
Tubulin
100 μm
10 μm
B
GFP-Motor
mCherry-TPX2
647-PRC1
GFP-Kif15-FL
GFP-HSET
30 μm
C
Events
Dwell Time (sec)
D
Events
Run Length (μm)
E
Events
Speed (μm/sec)
F
None
-Nuf2
Kif15
Tubulin
Merge
DMSO
FCPT
10 μm
G
1
2a
2b

Figure 5.4: Kif15 accumulates on MT bundles. A) GFP-Kif15-FL accumulates on PRC1-bundled MTs. Images of GFP-Kif15-FL on individual (left) or PRC1-bundled (middle) fluorescent MTs in solution. Individual MTs are also shown at higher magnification (right). LUTs were scaled identically for individual channels. Scale bars, 100 μm and 10 μm (right). B) Neither TPX2 nor PRC1 recruits GFP-Kif15-FL to single MTs. Representative images of GFP-Kif15-FL (top) or GFP-HSET (bottom) on single MTs decorated with mCherry-TPX2 and 647-labeled-PRC1. Non-fluorescent, biotinylated-MTs were anchored to coverslip surfaces through a biotin-streptavidin linkage. Scale bar, 30 μm. C-F) GFP-Kif15-FL moves within PRC1-bundled MTs. C) Dwell time distribution in seconds of single GFP-Kif15-FL molecules within PRC1-bundled MTs. Average dwell time was calculated from an exponential fit (red) to the distribution. D) Run-length distribution in μm of single GFP-Kif15-FL molecules within PRC1-bundled MTs. Average run-length was calculated from an exponential fit (red) to the distribution. E) Speed distribution in μm sec^{-1} of single GFP-Kif15-FL molecules within PRC1-bundled MTs. Average speed of single GFP-Kif15-FL molecules was calculated from a fit of the distribution to a single Gaussian (red). F) Maximum z-projections of representative HeLa cells left unperturbed (left) or transfected with Nuf2 targeting siRNAs (right) for ~48 hours. Cells were then treated with DMSO (top) or 200 μM FCPT (bottom) for 30 minutes prior to fixation. Cells were stained with antibodies targeting Kif15 (red) and tubulin (green). DNA (blue) was detected with Hoeschst-33342. LUTs were scaled identically for individual channels. Scale bar, 10 μm. G) Model: Kif15 targets K-fibers through an intrinsic two-step mechanism. Motor heads, blue; Coil-1, green; Coil-2, red. See text for details.

Discussion

Most kinesin-targeting mechanisms rely on motor-track affinity or extrinsic targeting factors. For example, kinesin-1 selectively binds MTs that are acetylated or GTP-tubulin rich (Nakata et al. 2011). On the other hand, the mitotic kinesin Xklp1 accumulates on anti-parallel midzone MTs through transient interactions with PRC1 (Bieling, Telley, and Surrey 2010). In contrast to these previously described mechanisms, the data shown here suggest that Kif15 targets K-fibers as a function of its inherent affinity for MT bundles. This conclusion is supported by two key findings. First, Kif15 binds non-K-MTs only when they are bundled, as in Eg5-independent cells and FCPT-treated HeLa cells (Chapter IV, Figure 5.4). Second, Kif15 selectively accumulates on MT bundles *in vitro*, such as those formed by PRC1 and TPX2 (Figure 5.4, (Drechsler et al. 2014)).

While PRC1 has no known physiological interaction with Kif15, TPX2 has been proposed to recruit Kif15 to spindle MTs through a specific protein-protein interaction (Wittmann et al. 2000; Tanenbaum et al. 2009; Vanneste et al. 2009). In support of this

notion, TPX2 depletion abrogates Kif15 spindle localization (Tanenbaum et al. 2009; Vanneste et al. 2009). However, spindles in TPX2-dpeleted cells lack K-fibers (Tulu et al. 2006; Bird and Hyman 2008). Therefore a loss of Kif15 spindle localization in TPX2-depleted cells may be an indirect consequence of failed K-fiber formation, as is the case in Nuf2-depleted cells (Chapter IV). Previous experiments implicating a direct TPX2-Kif15 interaction *in vitro* required the presence of MTs (Wittmann et al. 2000). In light of these new data, Kif15 likely binds to the bundled MTs under these conditions instead of TPX2 itself. Indeed, TPX2 fails to recruit Kif15 to individual MTs, and a direct TPX2-Kif15 interaction cannot be detected by conventional pull-down assays (Figure 5.4, data not shown). Therefore, this study undermines the current model of Kif15 regulation by TPX2, instead suggesting that Kif15 autonomously targets K-fibers through an intrinsic two-step mechanism.

These findings have interesting implications for mechanisms of kinesin self-repression. To date, the molecular details of kinesin self-repression have only been described for kinesin-1, so it remains to be seen whether all kinesins use the same strategy to modulate their activity (Verhey and Hammond 2009). Kif15 potentially offers a novel mechanism because of its two MT-binding sites. So while kinesin-1 is repressed by tail-head interactions, Kif15 may be inhibited by tail-stalk interactions. Future work detailing the mechanism of Kif15 self-repression will be of broad interest to students of the cytoskeleton.

Another important direction for future work concerns the activity of Kif15 within MT bundles. This study demonstrate that dimeric Kif15 can combine its motor and non-motor MT-binding sites to slide two MTs apart. Analogous to the kinesin-14 Ncd and

kinesin-8 Kip3 (Braun et al. 2009; Su et al. 2013), Kif15 might accomplish this by engaging one MT with its motor heads while holding a second MT with Coil-1. In this scenario, the strength of the Coil-1-MT interaction would dictate the consequence of Kif15 motility within a MT bundle. For example, diffusive Coil-1-MT interactions would allow Kif15 to move within a MT bundle, similar to Xklp1 (Bieling, Telley, and Surrey 2010). On the other hand, strong Coil-1-MT interactions that exceed the Kif15 stall force would cause energy to be stored in the MT bundle as mechanical strain. Differentiating between these possibilities is key to understanding the mechanics underlying the Kif15-dependent spindle assembly pathway in K5I-resistant cells (Chapter III and IV).

CHAPTER VI

CONCLUDING REMARKS

The failure of kinesin-5 Eg5-inhibitors (K5Is) to generate a clinical response has called into question the therapeutic potential of anti-mitotics in the treatment of neoplastic diseases. It came as a sobering realization that the proliferation rates of tumor cells *in vivo* are not as rapid as those in cell culture and murine xenografts (Komlodi-Pasztor, Sackett, and Fojo 2012; Mitchison 2012). But in contrast to solid tumors, liquid cancers proliferate rapidly *in vivo*, suggesting anti-mitotics may be a powerful line of defense for leukemias and lymphomas (K. S. Chan, Koh, and Li 2012; Rath and Kozielski 2012). This notion is supported by the detection of monopolar spindles in acute myeloid leukemia patients treated with K5Is (Kantarjian 2011, Infante 2011).

Despite this evidence that K5Is work pharmacologically, patients treated with K5Is do not experience disease regression. This discontinuity may arise from monoasters representing an intermediate spindle morphology rather than an end-point. The Eg5-independent cell lines described in Chapter III support this notion, as monopolar spindles do not equate death in these cells. Instead, monopolar spindles bipolarize through a kinesin-12 Kif15-dependent mechanism detailed in Chapter IV. Whether this non-canonical spindle assembly pathway confers K5I-resistance to cancer cells *in vivo* remains untested, as tumor biopsies from K5I-treated patients have been unavailable. However, whole exome and RNA sequencing of tumor cells isolated from

a glioblastoma patient show spontaneous deletion in the *EG5* gene and duplication of the *Kif15* gene (Dr. Steven Rosenfeld, personal communication). These findings suggest that the full potency of K5Is will not be realized until the development of Kif15 inhibitors.

The biochemical work described in Chapter V provides opportunity for the discovery of Kif15 inhibitors. For example, large-biomolecules can be designed to mimic Kif15 inhibition by its C-terminus. To realize this possibility, experiments in the near future will focus on mapping the inhibitory domain, reconstituting inhibition *in trans*, and detailing the structural underpinnings of Kif15 self-repression. As a parallel approach, a high-throughput screen for small-molecule inhibitors will be conducted at the Vanderbilt Institute of Chemical Biology using the constitutively active Kif15-N700 construct in a pure-protein based ATPase assay. Both of these strategies offer a potential means to synthetically control Kif15 activity, an essential step toward testing the efficacy of combining Eg5- and Kif15-inhibitors in the treatment of hematological neoplasias.

In addition to pursuing pharmacological inhibitors of Kif15, future efforts will address questions regarding the Kif15-driven “reverse-jackknifing” spindle assembly pathway described in Chapter IV. First, how does Kif15 activity become elevated in Eg5-independent cells? Kif15 is overexpressed in EIC-1 cells, and may therefore create its own substrate by bundling and accumulating on spindle microtubules (MTs). But in the remaining 4 EIC lines, Kif15 protein levels remain unchanged. It is possible that Kif15 has accrued activatory mutations that interfere with its self-repression, or that changes to MT-bundling factors create more spindle MT substrate for Kif15. A first pass

at testing these non-mutually exclusive hypotheses will involve RNA sequencing of the 5 EIC lines and parental HeLa line by the Vanderbilt Technologies for Advanced Genomics. Second, does Kif15 indeed drive reverse jackknifing by a sliding-filament mechanism similar to ciliary dynein? The biophysical properties of Kif15 will be studied in collaboration with Dr. Matthew Lang at the Vanderbilt School of Engineering. More details regarding the hyperactivation and mechanics of Kif15 are key to understanding the emergence of K5I resistance in human tumor cells.

Ultimately, this study addressed three questions. How do cells adapt to a loss of their primary means of centrosome separation? How does this altered physiology relate to disease progression? And can these changes be exploited in the design of more intelligent strategies for anti-mitotic chemotherapies? By developing a means to study K5I-resistance in cell-culture, this work shed light on the physiology, pathology, and pharmacology of the mitotic spindle.

REFERENCES

Akhmanova, Anna, and Michel O Steinmetz. 2008. “Tracking the Ends: a Dynamic Protein Network Controls the Fate of Microtubule Tips..” *Nature Reviews. Molecular Cell Biology* 9 (4) (April): 309–322. doi:10.1038/nrm2369.

Akiyoshi, Bungo, Krishna K Sarangapani, Andrew F Powers, Christian R Nelson, Steve L Reichow, Hugo Arellano-Santoyo, Tamir Gonen, Jeffrey A Ranish, Charles L Asbury, and Sue Biggins. 2010. “Tension Directly Stabilizes Reconstituted Kinetochore-Microtubule Attachments..” *Nature* 468 (7323) (November 25): 576–579. doi:10.1038/nature09594.

Alberts, B, D Bray, J Lewis, M Raff, and K Roberts. “[Citation][C].” *Garland*.

Allen, C, and G G Borisy. 1974. “Structural Polarity and Directional Growth of Microtubules of Chlamydomonas Flagella..” *Journal of Molecular Biology* 90 (2) (December 5): 381–402.

Amos, L, and A Klug. 1974. “Arrangement of Subunits in Flagellar Microtubules..” *Journal of Cell Science* 14 (3) (May): 523–549.

Andersen, S S, and E Karsenti. 1997. “XMAP310: a Xenopus Rescue-Promoting Factor Localized to the Mitotic Spindle..” *The Journal of Cell Biology* 139 (4) (November 17): 975–983.

Andersen, S S, B Buendia, J E Domínguez, A Sawyer, and E Karsenti. 1994. “Effect on Microtubule Dynamics of XMAP230, a Microtubule-Associated Protein Present in Xenopus Laevis Eggs and Dividing Cells..” *The Journal of Cell Biology* 127 (5) (December): 1289–1299.

Andersen, SSL. 2000. “Spindle Assembly and the Art of Regulating Microtubule Dynamics by MAPs and Stathmin/Op18.” *Trends in Cell Biology*.

Anderson, H Bowne, M Zanic, M Kauer, and J Howard. 2013. “Microtubule Dynamic Instability: a New Model with Coupled GTP Hydrolysis and Multistep Catastrophe - Bowne-Anderson - 2013 - BioEssays - Wiley Online Library.” *Bioessays*.

Andrews, P D, Y Ovechkina, N Morrice, and M Wagenbach. 2004. “Aurora B Regulates MCAK at the Mitotic Centromere.” *Developmental Cell*.

Antonio, C, I Ferby, H Wilhelm, M Jones, E Karsenti, A R Nebreda, and I Vernos. 2000. “Xkid, a Chromokinesin Required for Chromosome Alignment on the Metaphase Plate..” *Cell* 102 (4) (August 18): 425–435.

Asbury, Charles L, Adrian N Fehr, and Steven M Block. 2003. “Kinesin Moves by an Asymmetric Hand-Over-Hand Mechanism..” *Science (New York, N.Y.)* 302 (5653) (December 19): 2130–2134. doi:10.1126/science.1092985.

Bakhoum, Samuel F, Sarah L Thompson, Amity L Manning, and Duane A Compton. 2009. “Genome Stability Is Ensured by Temporal Control of Kinetochore-Microtubule Dynamics..” *Nature Cell Biology* 11 (1) (January): 27–35. doi:10.1038/ncb1809.

Belmont, L D, A A Hyman, K E Sawin, and T J Mitchison. 1990. “Real-Time Visualization of Cell Cycle-Dependent Changes in Microtubule Dynamics in Cytoplasmic Extracts..” *Cell* 62 (3) (August 10): 579–589.

Bieling, Peter, Ivo A Telley, and Thomas Surrey. 2010. “A Minimal Midzone Protein Module Controls Formation and Length of Antiparallel Microtubule Overlaps..” *Cell* 142 (3) (August 6): 420–432. doi:10.1016/j.cell.2010.06.033.

Bird, A W, and A A Hyman. 2008. “Building a Spindle of the Correct Length in Human Cells Requires the Interaction Between TPX2 and Aurora A.” *The Journal of Cell Biology*.

Boleti, H, E Karsenti, and I Vernos. 1996. “Xklp2, a Novel Xenopus Centrosomal Kinesin-Like Protein Required for Centrosome Separation During Mitosis.” *Cell*.

Braun, Marcus, Douglas R Drummond, Robert A. Cross, and Andrew D. McAinsh. 2009. “The Kinesin-14 Klp2 Organizes Microtubules Into Parallel Bundles by an ATP-Dependent Sorting Mechanism.” *Nature Cell Biology* 11 (6) (May 10): 724–730. doi:10.1038/ncb1878.

Brinkley, B R. 1985. “Microtubule Organizing Centers.” *Annual Review of Cell Biology*.

Brinkley, B R, and J Cartwright. 1975. “Cold-Labile and Cold-Stable Microtubules in the Mitotic Spindle of Mammalian Cells..” *Annals of the New York Academy of Sciences* 253 (June 30): 428–439.

Brinkley, B R, E Stubblefield, and T C Hsu. 1967. “The Effects of Colcemid Inhibition and Reversal on the Fine Structure of the Mitotic Apparatus of Chinese Hamster Cells in Vitro..” *Journal of Ultrastructure Research* 19 (1) (July): 1–18.

Brito, Daniela A, and Conly L Rieder. 2006. “Mitotic Checkpoint Slippage in Humans Occurs via Cyclin B Destruction in the Presence of an Active Checkpoint..” *Current Biology : CB* 16 (12) (June 20): 1194–1200. doi:10.1016/j.cub.2006.04.043.

Brouhard, G J, and A J Hunt. 2005. “Microtubule Movements on the Arms of Mitotic Chromosomes: Polar Ejection Forces Quantified in Vitro.” *… Academy of Sciences of the United ….*

Brunet, Stéphane, Teresa Sardon, Timo Zimmerman, Torsten Wittmann, Rainer

Pepperkok, Eric Karsenti, and Isabelle Vernos. 2004. “Characterization of the TPX2 Domains Involved in Microtubule Nucleation and Spindle Assembly in Xenopus Egg Extracts..” *Molecular Biology of the Cell* 15 (12) (December): 5318–5328. doi:10.1091/mbc.E04-05-0385.

Cai, Dawen, Adam D Hoppe, Joel A Swanson, and Kristen J Verhey. 2007. “Kinesin-1 Structural Organization and Conformational Changes Revealed by FRET Stoichiometry in Live Cells..” *The Journal of Cell Biology* 176 (1) (January 1): 51–63. doi:10.1083/jcb.200605097.

Cameron, Lisa A, Ge Yang, Daniela Cimini, Julie C Canman, Olga Kisurina-Evgenieva, Alexey Khodjakov, Gaudenz Danuser, and E D Salmon. 2006. “Kinesin 5-Independent Poleward Flux of Kinetochore Microtubules in PtK1 Cells..” *The Journal of Cell Biology* 173 (2) (April 24): 173–179. doi:10.1083/jcb.200601075.

Caplow, M, R L Ruhlen, and J Shanks. 1994. “The Free Energy for Hydrolysis of a Microtubule-Bound Nucleotide Triphosphate Is Near Zero: All of the Free Energy for Hydrolysis Is Stored in the Microtubule Lattice..” *The Journal of Cell Biology* 127 (3) (November): 779–788.

Carlier, M F, T L Hill, and Y Chen. 1984. “Interference of GTP Hydrolysis in the Mechanism of Microtubule Assembly: an Experimental Study..” *Proceedings of the National Academy of Sciences of the United States of America* 81 (3) (February): 771–775.

Cassimeris, Lynne. 2006. “Mitosis: Riding the Protofilament Curl..” *Current Biology : CB* 16 (6) (March 21): R214–6. doi:10.1016/j.cub.2006.02.025.

Chan, Gordon K, Song-Tao Liu, and Tim J Yen. 2005. “Kinetochore Structure and

Function." *Trends in Cell Biology* 15 (11) (November): 589–598. doi:10.1016/j.tcb.2005.09.010.

Chan, K S, C G Koh, and H Y Li. 2012. "Mitosis-Targeted Anti-Cancer Therapies: Where They Stand." *Cell Death & Disease*.

Cheng, Long, Jigar Desai, Carlos J Miranda, Jeremy S Duncan, Weihong Qiu, Alicia A Nugent, Adrianne L Kolpak, et al. 2014. "Human CFEOM1 Mutations Attenuate KIF21A Autoinhibition and Cause Oculomotor Axon Stalling." *Neuron* 82 (2) (April): 334–349. doi:10.1016/j.neuron.2014.02.038.

Chung, Vincent, Elisabeth I Heath, William R Schelman, Brendan M Johnson, Lyndon C Kirby, Kerlin M Lynch, Jeffrey D Botbyl, Thomas A Lampkin, and Kyle D Holen. 2012. "First-Time-in-Human Study of GSK923295, a Novel Antimitotic Inhibitor of Centromere-Associated Protein E (CENP-E), in Patients with Refractory Cancer.." *Cancer Chemotherapy and Pharmacology* 69 (3) (March): 733–741. doi:10.1007/s00280-011-1756-z.

Cimini, Daniela, Daniela Fioravanti, E D Salmon, and Francesca Degrassi. 2002. "Merotelic Kinetochore Orientation Versus Chromosome Mono-Orientation in the Origin of Lagging Chromosomes in Human Primary Cells.." *Journal of Cell Science* 115 (Pt 3) (February 1): 507–515.

Cleveland, Don W, Yinghui Mao, and Kevin F Sullivan. 2003. "Centromeres and Kinetochores: From Epigenetics to Mitotic Checkpoint Signaling.." *Cell* 112 (4) (February 21): 407–421.

Cross, Robert A., and Andrew McAinsh. 2014. "Prime Movers: the Mechanochemistry of Mitotic Kinesins." *Nature Reviews. Molecular Cell Biology* 15 (4) (March 21): 257–

271. doi:10.1038/nrm3768.

David-Pfeuty, T, H P Erickson, and D Pantaloni. 1977. “Guanosinetriphosphatase Activity of Tubulin Associated with Microtubule Assembly.”

De Brabander, M, G Geuens, R Nuydens, R Willebrords, and J De Mey. 1981. “Microtubule Assembly in Living Cells After Release From Nocodazole Block: the Effects of Metabolic Inhibitors, Taxol and PH..” *Cell Biology International Reports* 5 (9) (September): 913–920.

de Cuevas, M, T Tao, and L S Goldstein. 1992. “Evidence That the Stalk of Drosophila Kinesin Heavy Chain Is an Alpha-Helical Coiled Coil..” *The Journal of Cell Biology* 116 (4) (February): 957–965.

DeBonis, Salvatore, Dimitrios A Skoufias, Luc Lebeau, Roman Lopez, Gautier Robin, Robert L Margolis, Richard H Wade, and Frank Kozielski. 2004. “In Vitro Screening for Inhibitors of the Human Mitotic Kinesin Eg5 with Antimitotic and Antitumor Activities..” *Molecular Cancer Therapeutics* 3 (9) (September): 1079–1090.

DeLuca, Jennifer G, Ben Moree, Jennifer M Hickey, John V Kilmartin, and E D Salmon. 2002. “hNuf2 Inhibition Blocks Stable Kinetochore-Microtubule Attachment and Induces Mitotic Cell Death in HeLa Cells..” *The Journal of Cell Biology* 159 (4) (November 25): 549–555. doi:10.1083/jcb.200208159.

Desai, Arshad, and Timothy J Mitchison. 1997. “Microtubule Polymerization Dynamics.” *Annual Review of Cell and Developmental Biology* 13 (1) (November): 83–117. doi:10.1146/annurev.cellbio.13.1.83.

Drechsler, Hauke, Toni McHugh, Martin R Singleton, Nicholas J Carter, and Andrew D.

McAinsh. 2014. “The Kinesin-12 Kif15 Is a Processive Track-Switching Tetramer..” *eLife* 3: e01724.

Du, Yaqing, Chauca A English, and Ryoma Ohi. 2010. “The Kinesin-8 Kif18A Dampens Microtubule Plus-End Dynamics.” *Current Biology* 20 (4) (February): 374–380. doi:10.1016/j.cub.2009.12.049.

Dumont, Julien, and Arshad Desai. 2012. “Acentrosomal Spindle Assembly and Chromosome Segregation During Oocyte Meiosis..” *Trends in Cell Biology* 22 (5) (May): 241–249. doi:10.1016/j.tcb.2012.02.007.

Dumont, Sophie, and Timothy J Mitchison. 2009. “Force and Length in the Mitotic Spindle.” *Current Biology* 19 (17) (September): R749–R761. doi:10.1016/j.cub.2009.07.028.

Engelhardt, W A, and M N LJUBIMOWA. 1939. “Myosine and Adenosinetriphosphatase.” *Nature* 144 (3650) (October 14): 668–669. doi:10.1038/144668b0.

Espeut, Julien, Amaury Gaussen, Peter Bieling, Violeta Morin, Susana Prieto, Didier Fesquet, Thomas Surrey, and Ariane Abrieu. 2008. “Phosphorylation Relieves Autoinhibition of the Kinetochore Motor Cenp-E..” *Molecular Cell* 29 (5) (March 14): 637–643. doi:10.1016/j.molcel.2008.01.004.

Euteneuer, U, and J R McIntosh. 1981. “Polarity of Some Motility-Related Microtubules.” In.

Evans, L, T Mitchison, and M Kirschner. 1985. “Influence of the Centrosome on the Structure of Nucleated Microtubules..” *The Journal of Cell Biology* 100 (4) (April): 1185–1191.

Ferenz, Nick P, Alyssa Gable, and Pat Wadsworth. 2010. “Mitotic Functions of Kinesin-5.” *Seminars in Cell & Developmental Biology* 21 (3) (May): 255–259. doi:10.1016/j.semcdb.2010.01.019.

Fletcher, D A, and R D Mullins. 2010. “Cell Mechanics and the Cytoskeleton.” *Nature*.

Friel, Claire T, and Jonathon Howard. 2011. “The Kinesin-13 MCAK Has an Unconventional ATPase Cycle Adapted for Microtubule Depolymerization..” *The EMBO Journal* 30 (19) (October 5): 3928–3939. doi:10.1038/emboj.2011.290.

Funabiki, H, and A W Murray. 2000. “The Xenopus Chromokinesin Xkid Is Essential for Metaphase Chromosome Alignment and Must Be Degraded to Allow Anaphase Chromosome Movement..” *Cell* 102 (4) (August 18): 411–424.

Ganguly, Anutosh, Rajat Bhattacharya, and Fernando Cabral. 2008. “Cell Cycle Dependent Degradation of MCAK: Evidence Against a Role in Anaphase Chromosome Movement..” *Cell Cycle (Georgetown, Tex.)* 7 (20) (October): 3187–3193.

Gardner, Melissa K, Marija Zanic, Christopher Gell, Volker Bormuth, and Jonathon Howard. 2011. “Depolymerizing Kinesins Kip3 and MCAK Shape Cellular Microtubule Architecture by Differential Control of Catastrophe..” *Cell* 147 (5) (November 23): 1092–1103. doi:10.1016/j.cell.2011.10.037.

Gascoigne, K E, and S S Taylor. 2008. “Cancer Cells Display Profound Intra-and Interline Variation Following Prolonged Exposure to Antimitotic Drugs.” *Cancer Cell*.

Gibson, Daniel G, Lei Young, Ray-Yuan Chuang, J Craig Venter, Clyde A Hutchison, and Hamilton O Smith. 2009. “Enzymatic Assembly of DNA Molecules Up to

Several Hundred Kilobases.." *Nature Methods* 6 (5) (May): 343–345. doi:10.1038/nmeth.1318.

Gilbert, S P, M R Webb, M Brune, and K A Johnson. 1995. "Pathway of Processive ATP Hydrolysis by Kinesin.." *Nature* 373 (6516) (February 23): 671–676. doi:10.1038/373671a0.

Goshima, G, R Wollman, N Stuurman, and J M Scholey. 2005. "Length Control of the Metaphase Spindle." *Current Biology*.

Goshima, Gohta, and Ronald D Vale. 2003. "The Roles of Microtubule-Based Motor Proteins in Mitosis: Comprehensive RNAi Analysis in the Drosophila S2 Cell Line.." *The Journal of Cell Biology* 162 (6) (September 15): 1003–1016. doi:10.1083/jcb.200303022.

Goshima, Gohta, François Nédélec, and Ronald D Vale. 2005. "Mechanisms for Focusing Mitotic Spindle Poles by Minus End-Directed Motor Proteins.." *The Journal of Cell Biology* 171 (2) (October 24): 229–240. doi:10.1083/jcb.200505107.

Goshima, Gohta, Mirjam Mayer, Nan Zhang, Nico Stuurman, and Ronald D Vale. 2008. "Augmin: a Protein Complex Required for Centrosome-Independent Microtubule Generation Within the Spindle.." *The Journal of Cell Biology* 181 (3) (May 5): 421–429. doi:10.1083/jcb.200711053.

Grishchuk, Ekaterina L, Maxim I Molodtsov, Fazly I Ataullakhanov, and J Richard McIntosh. 2005. "Force Production by Disassembling Microtubules.." *Nature* 438 (7066) (November 17): 384–388. doi:10.1038/nature04132.

Groen, Aaron C, Daniel Needleman, Clifford Brangwynne, Christain Gradinaru, Brandon Fowler, Ralph Mazitschek, and Timothy J Mitchison. 2008. "A Novel Small-

Molecule Inhibitor Reveals a Possible Role of Kinesin-5 in Anastral Spindle-Pole Assembly..” *Journal of Cell Science* 121 (Pt 14) (July 15): 2293–2300. doi:10.1242/jcs.024018.

Gruss, O J, R E Carazo-Salas, C A Schatz, G Guarguaglini, J Kast, M Wilm, N Le Bot, I Vernos, E Karsenti, and I W Mattaj. 2001. “Ran Induces Spindle Assembly by Reversing the Inhibitory Effect of Importin Alpha on TPX2 Activity..” *Cell* 104 (1) (January 12): 83–93.

Hackney, D D, J D Levitt, and J Suhan. 1992. “Kinesin Undergoes a 9 S to 6 S Conformational Transition..” *The Journal of Biological Chemistry* 267 (12) (April 25): 8696–8701.

Hammond, Jennetta W, Dawen Cai, T Lynne Blasius, Zhe Li, Yuyang Jiang, Gloria T Jih, Edgar Meyhofer, and Kristen J Verhey. 2009. “Mammalian Kinesin-3 Motors Are Dimeric in Vivo and Move by Processive Motility Upon Release of Autoinhibition..” *PLoS Biology* 7 (3) (March 31): e72. doi:10.1371/journal.pbio.1000072.

Hayden, J H, S S Bowser, and C L Rieder. 1990. “Kinetochores Capture Astral Microtubules During Chromosome Attachment to the Mitotic Spindle: Direct Visualization in Live Newt Lung Cells..” *The Journal of Cell Biology* 111 (3) (September): 1039–1045.

Helenius, Jonne, Gary Brouhard, Yannis Kalaidzidis, Stefan Diez, and Jonathon Howard. 2006. “The Depolymerizing Kinesin MCAK Uses Lattice Diffusion to Rapidly Target Microtubule Ends..” *Nature* 441 (7089) (May 4): 115–119. doi:10.1038/nature04736.

Hill, T L. 1984. “Introductory Analysis of the GTP-Cap Phase-Change Kinetics at the End of a Microtubule..” *Proceedings of the National Academy of Sciences of the United States of America* 81 (21) (November): 6728–6732.

Holy, T E, and S Leibler. 1994. “Dynamic Instability of Microtubules as an Efficient Way to Search in Space..” *Proceedings of the National Academy of Sciences of the United States of America* 91 (12) (June 7): 5682–5685.

Howard, J. 1996. “The Movement of Kinesin Along Microtubules.” *Annual Review of Physiology*.

Howard, J. 2001. “[Citation][C].”

Howard, Joe, and Anthony A Hyman. 2003. “Dynamics and Mechanics of the Microtubule Plus End..” *Nature* 422 (6933) (April 17): 753–758. doi:10.1038/nature01600.

Howell, B J, B F McEwen, J C Canman, D B Hoffman, E M Farrar, C L Rieder, and E D Salmon. 2001. “Cytoplasmic Dynein/Dynactin Drives Kinetochore Protein Transport to the Spindle Poles and Has a Role in Mitotic Spindle Checkpoint Inactivation..” *The Journal of Cell Biology* 155 (7) (December 24): 1159–1172. doi:10.1083/jcb.200105093.

Hyman, A A. 1991. “Preparation of Marked Microtubules for the Assay of the Polarity of Microtubule-Based Motors by Fluorescence..” *Journal of Cell Science. Supplement* 14: 125–127.

Hyman, A A, and E Karsenti. 1996. “Morphogenetic Properties of Microtubules and Mitotic Spindle Assembly..” *Cell* 84 (3) (February 9): 401–410.

Inoué, S, and E D Salmon. 1995. “Force Generation by Microtubule

Assembly/Disassembly in Mitosis and Related Movements.." *Molecular Biology of the Cell* 6 (12) (December): 1619–1640.

Itabashi, Takeshi, Jun Takagi, Yuta Shimamoto, Hiroaki Onoe, Kenta Kuwana, Isao Shimoyama, Jedidiah Gaetz, Tarun M Kapoor, and Shin'ichi Ishiwata. 2009. "Probing the Mechanical Architecture of the Vertebrate Meiotic Spindle.." *Nature Methods* 6 (2) (February): 167–172. doi:10.1038/nmeth.1297.

Jackson, Jeffrey R, Denis R Patrick, Mohammed M Dar, and Pearl S Huang. 2007. "Targeted Anti-Mitotic Therapies: Can We Improve on Tubulin Agents?." *Nature Reviews. Cancer* 7 (2) (February): 107–117. doi:10.1038/nrc2049.

Jayachandran, D, U Ramkrishna, J Skiles, J Renbarger, and D Ramkrishna. 2014. "Revitalizing Personalized Medicine: Respecting Biomolecular Complexities Beyond Gene Expression." *CPT: Pharmacometrics & Systems Pharmacology* 3 (4) (April 16): e110. doi:10.1038/psp.2014.6.

Jiang, Kai, and Anna Akhmanova. 2011. "Microtubule Tip-Interacting Proteins: a View From Both Ends.." *Current Opinion in Cell Biology* 23 (1) (February): 94–101. doi:10.1016/j.ceb.2010.08.008.

Jones, S F, E R Plummer, and H A Burris. 2006. "Phase I Study of Ispinesib in Combination with Carboplatin in Patients with Advanced Solid Tumors." *Proc Am Soc Clin ….*

Jordan, M A, and L Wilson. 2004. "Microtubules as a Target for Anticancer Drugs." *Nature Reviews. Cancer*.

Kaan, Hung Yi Kristal, David D Hackney, and Frank Kozielski. 2011. "The Structure of the Kinesin-1 Motor-Tail Complex Reveals the Mechanism of Autoinhibition.."

Science (New York, N.Y.) 333 (6044) (August 12): 883–885. doi:10.1126/science.1204824.

Kapitein, Lukas C, Erwin J G Peterman, Benjamin H Kwok, Jeffrey H Kim, Tarun M Kapoor, and Christoph F Schmidt. 2005. “The Bipolar Mitotic Kinesin Eg5 Moves on Both Microtubules That It Crosslinks..” *Nature* 435 (7038) (May 5): 114–118. doi:10.1038/nature03503.

Kapoor, T M, T U Mayer, M L Coughlin, and T J Mitchison. 2000. “Probing Spindle Assembly Mechanisms with Monastrol, a Small Molecule Inhibitor of the Mitotic Kinesin, Eg5..” *The Journal of Cell Biology* 150 (5) (September 4): 975–988.

Kardon, J R, and R D Vale. 2009. “Regulators of the Cytoplasmic Dynein Motor.” *Nature Reviews. Molecular Cell Biology*.

Kelly, R B. 1990. “Microtubules, Membrane Traffic, and Cell Organization..” *Cell* 61 (1) (April 6): 5–7.

Khodjakov, A, and C L Rieder. 1996. “Kinetochores Moving Away From Their Associated Pole Do Not Exert a Significant Pushing Force on the Chromosome..” *The Journal of Cell Biology*.

Khodjakov, A, and C L Rieder. 1999. “The Sudden Recruitment of Γ-Tubulin to the Centrosome at the Onset of Mitosis and Its Dynamic Exchange Throughout the Cell Cycle, Do Not Require Microtubules.” *The Journal of Cell Biology*.

Khodjakov, A, R W Cole, B R Oakley, and C L Rieder. 2000. “Centrosome-Independent Mitotic Spindle Formation in Vertebrates..” *Current Biology : CB* 10 (2) (January 27): 59–67.

Kim, Yumi, Andrew J Holland, Weijie Lan, and Don W Cleveland. 2010. “Aurora Kinases

and Protein Phosphatase 1 Mediate Chromosome Congression Through Regulation of CENP-E.." *Cell* 142 (3) (August 6): 444–455. doi:10.1016/j.cell.2010.06.039.

Kirschner, M. 1986. "Beyond Self-Assembly: From Microtubules to Morphogenesis." *Cell* 45 (3) (May): 329–342. doi:10.1016/0092-8674(86)90318-1.

Klejnot, M, A Falnikar, and V Ulaganathan. 2013. "The Crystal Structure and Biochemical Characterization of Kif15: a Bifunctional Molecular Motor Involved in Bipolar Spindle Formation and Neuronal …." *… Section D: Biological …*.

Kline-Smith, Susan L, Alexey Khodjakov, Polla Hergert, and Claire E Walczak. 2004. "Depletion of Centromeric MCAK Leads to Chromosome Congression and Segregation Defects Due to Improper Kinetochore Attachments.." *Molecular Biology of the Cell* 15 (3) (March): 1146–1159. doi:10.1091/mbc.E03-08-0581.

Komlodi-Pasztor, E, D L Sackett, and A T Fojo. 2012. "Inhibitors Targeting Mitosis: Tales of How Great Drugs Against a Promising Target Were Brought Down by a Flawed Rationale." *Clinical Cancer Research*.

Kops, Geert J P L, Beth A A Weaver, and Don W Cleveland. 2005. "On the Road to Cancer: Aneuploidy and the Mitotic Checkpoint.." *Nature Reviews. Cancer* 5 (10) (October): 773–785. doi:10.1038/nrc1714.

Kops, Geert J P L, Daniel R Foltz, and Don W Cleveland. 2004. "Lethality to Human Cancer Cells Through Massive Chromosome Loss by Inhibition of the Mitotic Checkpoint.." *Proceedings of the National Academy of Sciences of the United States of America* 101 (23) (June 8): 8699–8704. doi:10.1073/pnas.0401142101.

Kotwaliwale, Chitra, and Sue Biggins. 2006. "Microtubule Capture: a Concerted Effort.."

Cell 127 (6) (December 15): 1105–1108. doi:10.1016/j.cell.2006.11.032.

Kull, F J, E P Sablin, R Lau, R J Fletterick, and R D Vale. 1996. “Crystal Structure of the Kinesin Motor Domain Reveals a Structural Similarity to Myosin..” *Nature* 380 (6574) (April 11): 550–555. doi:10.1038/380550a0.

Kuriyama, R, M Kofron, R Essner, T Kato, S Dragas-Granoic, C K Omoto, and A Khodjakov. 1995. “Characterization of a Minus End-Directed Kinesin-Like Motor Protein From Cultured Mammalian Cells..” *The Journal of Cell Biology* 129 (4) (May): 1049–1059.

Kuukasjärvi, T, R Karhu, M Tanner, and M Kähkönen. 1997. “Genetic Heterogeneity and Clonal Evolution Underlying Development of Asynchronous Metastasis in Human Breast Cancer.” *Cancer Research*.

Lampson, Michael A, Kishore Renduchitala, Alexey Khodjakov, and Tarun M Kapoor. 2004. “Correcting Improper Chromosome-Spindle Attachments During Cell Division..” *Nature Cell Biology* 6 (3) (March): 232–237. doi:10.1038/ncb1102.

Lauffenburger, D A, and A F Horwitz. 1996. “Cell Migration: a Physically Integrated Molecular Process..” *Cell* 84 (3) (February 9): 359–369.

Lawo, Steffen, Mikhail Bashkurov, Michael Mullin, Mariana Gomez Ferreria, Ralf Kittler, Bianca Habermann, Andrea Tagliaferro, et al. 2009. “HAUS, the 8-Subunit Human Augmin Complex, Regulates Centrosome and Spindle Integrity..” *Current Biology : CB* 19 (10) (May 26): 816–826. doi:10.1016/j.cub.2009.04.033.

Lecland, Nicolas, and Jens Lüders. 2014. “The Dynamics of Microtubule Minus Ends in the Human Mitotic Spindle..” *Nature Cell Biology* 16 (8) (August): 770–778. doi:10.1038/ncb2996.

Lengauer, C, K W Kinzler, and B Vogelstein. 1997. “Genetic Instability in Colorectal Cancers.” *Nature*.

Lénárt, Péter, Mark Petronczki, Martin Steegmaier, Barbara Di Fiore, Jesse J Lipp, Matthias Hoffmann, Wolfgang J Rettig, Norbert Kraut, and Jan-Michael Peters. 2007. “The Small-Molecule Inhibitor BI 2536 Reveals Novel Insights Into Mitotic Roles of Polo-Like Kinase 1..” *Current Biology : CB* 17 (4) (February 20): 304–315. doi:10.1016/j.cub.2006.12.046.

Loisel, T P, R Boujemaa, D Pantaloni, and M F Carlier. 1999. “Reconstitution of Actin-Based Motility of Listeria and Shigella Using Pure Proteins..” *Nature* 401 (6753) (October 7): 613–616. doi:10.1038/44183.

Longley, D B, and P G Johnston. 2005. “Molecular Mechanisms of Drug Resistance.” *The Journal of Pathology*.

Mack, G J, and D A Compton. 2001. “Analysis of Mitotic Microtubule-Associated Proteins Using Mass Spectrometry Identifies Astrin, a Spindle-Associated Protein.” In.

Mandelkow, E M, E Mandelkow, and R A Milligan. 1991. “Microtubule Dynamics and Microtubule Caps: a Time-Resolved Cryo-Electron Microscopy Study..” *The Journal of Cell Biology* 114 (5) (September): 977–991.

Martin, T A, L Ye, A J Sanders, J Lane, and W G Jiang. 2000. “Cancer Invasion and Metastasis: Molecular and Cellular Perspective.”

Marzo, Isabel, and Javier Naval. 2013. “Antimitotic Drugs in Cancer Chemotherapy: Promises and Pitfalls..” *Biochemical Pharmacology* 86 (6) (September 15): 703–710. doi:10.1016/j.bcp.2013.07.010.

Mayer, T U, T M Kapoor, S J Haggarty, R W King, S L Schreiber, and T J Mitchison. 1999. “Small Molecule Inhibitor of Mitotic Spindle Bipolarity Identified in a Phenotype-Based Screen..” *Science (New York, N.Y.)* 286 (5441) (October 29): 971–974.

Mayr, Monika I, Stefan Hümmer, Jenny Bormann, Tamara Grüner, Sarah Adio, Guenther Woehlke, and Thomas U Mayer. 2007. “The Human Kinesin Kif18A Is a Motile Microtubule Depolymerase Essential for Chromosome Congression..” *Current Biology : CB* 17 (6) (March 20): 488–498. doi:10.1016/j.cub.2007.02.036.

McClelland, S E, R A Burrell, and C Swanton. 2009. “Chromosomal Instability.” *Cell Cycle (Georgetown, Tex.)*.

McDonald, K L, E T O'Toole, and D N Mastronarde. 1992. “Kinetochore Microtubules in PTK Cells..” *The Journal of Cell …*.

McEwen, B F, A B Heagle, and G O Cassels. 1997. “Kinetochore Fiber Maturation in PtK1 Cells and Its Implications for the Mechanisms of Chromosome Congression and Anaphase Onset.” *The Journal of Cell …*.

Megraw, T L, L R Kao, and T C Kaufman. 2001. “Zygotic Development Without Functional Mitotic Centrosomes..” *Current Biology : CB* 11 (2) (January 23): 116–120.

Mendes Pinto, Inês, Boris Rubinstein, and Rong Li. 2013. “Force to Divide: Structural and Mechanical Requirements for Actomyosin Ring Contraction..” *Biophysical Journal* 105 (3) (August 6): 547–554. doi:10.1016/j.bpj.2013.06.033.

Mitchison, T J. 1989. “Polewards Microtubule Flux in the Mitotic Spindle: Evidence From Photoactivation of Fluorescence..” *The Journal of Cell Biology* 109 (2) (August):

637–652.

Mitchison, T J. 1992. “Self-Organization of Polymer-Motor Systems in the Cytoskeleton.” *Philosophical Transactions of the Royal Society B: Biological Sciences* 336 (1276) (April 29): 99–106. doi:10.1098/rstb.1992.0049.

Mitchison, T J, P Maddox, J Gaetz, A Groen, M Shirasu, A Desai, E D Salmon, and T M Kapoor. 2005. “Roles of Polymerization Dynamics, Opposed Motors, and a Tensile Element in Governing the Length of Xenopus Extract Meiotic Spindles..” *Molecular Biology of the Cell* 16 (6) (June): 3064–3076. doi:10.1091/mbc.E05-02-0174.

Mitchison, T, and M Kirschner. 1983. “Microtubule Assembly Nucleated by Isolated Centrosomes..” *Nature*.

Mitchison, T, and M Kirschner. 1984. “Dynamic Instability of Microtubule Growth.” *Nature*.

Mitchison, Timothy J. 2012. “The Proliferation Rate Paradox in Antimitotic Chemotherapy..” *Molecular Biology of the Cell* 23 (1) (January): 1–6. doi:10.1091/mbc.E10-04-0335.

Miyamoto, David T, Zachary E Perlman, Kendra S Burbank, Aaron C Groen, and Timothy J Mitchison. 2004. “The Kinesin Eg5 Drives Poleward Microtubule Flux in Xenopus Laevis Egg Extract Spindles..” *The Journal of Cell Biology* 167 (5) (December 6): 813–818. doi:10.1083/jcb.200407126.

Morii, H, T Takenawa, F Arisaka, and T Shimizu. 1997. “Identification of Kinesin Neck Region as a Stable Alpha-Helical Coiled Coil and Its Thermodynamic Characterization..” *Biochemistry* 36 (7) (February 18): 1933–1942. doi:10.1021/bi962392l.

Mountain, V, C Simerly, L Howard, A Ando, G Schatten, and D A Compton. 1999. “The Kinesin-Related Protein, HSET, Opposes the Activity of Eg5 and Cross-Links Microtubules in the Mammalian Mitotic Spindle..” *The Journal of Cell Biology* 147 (2) (October 18): 351–366.

Nakata, Takao, Shinsuke Niwa, Yasushi Okada, Franck Perez, and Nobutaka Hirokawa. 2011. “Preferential Binding of a Kinesin-1 Motor to GTP-Tubulin-Rich Microtubules Underlies Polarized Vesicle Transport..” *The Journal of Cell Biology* 194 (2) (July 25): 245–255. doi:10.1083/jcb.201104034.

Nicklas, R B. 1983. “Measurements of the Force Produced by the Mitotic Spindle in Anaphase..” *The Journal of Cell Biology* 97 (2) (August): 542–548.

Nicolis, G, and I Prigogine. 1977. “Self-Organization in Nonequilibrium Systems.”

Nogales, E, M Whittaker, R A Milligan, and K H Downing. 1999. “High-Resolution Model of the Microtubule.” *Cell*.

Odde, D J, L Cassimeris, and H M Buettner. 1995. “Kinetics of Microtubule Catastrophe Assessed by Probabilistic Analysis..” *Biophysical Journal* 69 (3) (September): 796–802. doi:10.1016/S0006-3495(95)79953-2.

Ohi, Melanie, Ying Li, Yifan Cheng, and Thomas Walz. 2004. “Negative Staining and Image Classification - Powerful Tools in Modern Electron Microscopy..” *Biological Procedures Online* 6: 23–34. doi:10.1251/bpo70.

Ookata, K, S Hisanaga, and J C Bulinski. 1995. “Cyclin B Interaction with Microtubule-Associated Protein 4 (MAP4) Targets P34cdc2 Kinase to Microtubules and Is a Potential Regulator of M-Phase Microtubule ….” *The Journal of Cell ….*

Oosawa, Fumio, 1922, Sho Asakura, 1927. 1975. “Thermodynamics of the

Polymerization of Protein."

Orth, James D, Rainer H Kohler, Floris Foijer, Peter K Sorger, Ralph Weissleder, and Timothy J Mitchison. 2011. "Analysis of Mitosis and Antimitotic Drug Responses in Tumors by in Vivo Microscopy and Single-Cell Pharmacodynamics.." *Cancer Research* 71 (13) (July 1): 4608–4616. doi:10.1158/0008-5472.CAN-11-0412.

Petry, Sabine, Aaron C Groen, Keisuke Ishihara, Timothy J Mitchison, and Ronald D Vale. 2013. "Branching Microtubule Nucleation in Xenopus Egg Extracts Mediated by Augmin and TPX2.." *Cell* 152 (4) (February 14): 768–777. doi:10.1016/j.cell.2012.12.044.

Piehl, Michelle, U Serdar Tulu, Pat Wadsworth, and Lynne Cassimeris. 2004. "Centrosome Maturation: Measurement of Microtubule Nucleation Throughout the Cell Cycle by Using GFP-Tagged EB1.." *Proceedings of the National Academy of Sciences of the United States of America* 101 (6) (February 10): 1584–1588. doi:10.1073/pnas.0308205100.

Pinsky, B A, and S Biggins. 2005. "The Spindle Checkpoint: Tension Versus Attachment." *Trends in Cell Biology*.

Pollard, T D, and A G Weeds. 1984. "The Rate Constant for ATP Hydrolysis by Polymerized Actin.." *FEBS Letters* 170 (1) (May 7): 94–98.

Pollard, Thomas D, and Gary G Borisy. 2003. "Cellular Motility Driven by Assembly and Disassembly of Actin Filaments.." *Cell* 112 (4) (February 21): 453–465.

Powers, Andrew F, Andrew D Franck, Daniel R Gestaut, Jeremy Cooper, Beth Gracyzk, Ronnie R Wei, Linda Wordeman, Trisha N Davis, and Charles L Asbury. 2009. "The Ndc80 Kinetochore Complex Forms Load-Bearing Attachments to Dynamic

Microtubule Tips via Biased Diffusion.." *Cell* 136 (5) (March 6): 865–875. doi:10.1016/j.cell.2008.12.045.

Purcell, James W, Jefferson Davis, Mamatha Reddy, Shamra Martin, Kimberly Samayoa, Hung Vo, Karen Thomsen, et al. 2010. "Activity of the Kinesin Spindle Protein Inhibitor Ispinesib (SB-715992) in Models of Breast Cancer.." *Clinical Cancer Research : an Official Journal of the American Association for Cancer Research* 16 (2) (January 15): 566–576. doi:10.1158/1078-0432.CCR-09-1498.

Qian, Xiangping, Andrew McDonald, Han-Jie Zhou, Nicholas D Adams, Cynthia A Parrish, Kevin J Duffy, Duke M Fitch, et al. 2010. "Discovery of the First Potent and Selective Inhibitor of Centromere-Associated Protein E: GSK923295.." *ACS Medicinal Chemistry Letters* 1 (1) (April 8): 30–34. doi:10.1021/ml900018m.

Raaijmakers, J A, and RGHP van Heesbeen. 2012. "Nuclear Envelope‐Associated Dynein Drives Prophase Centrosome Separation and Enables Eg5‐Independent Bipolar Spindle Formation." *The EMBO …*.

Rath, O, and F Kozielski. 2012. "Kinesins and Cancer." *Nature Reviews. Cancer*.

Rieder, C L, J G Ault, and U Eichenlaub-Ritter. 1993. "Morphogenesis of the Mitotic and Meiotic Spindle: Conclusions Obtained From One System Are Not Necessarily Applicable to the Other." *Chromosome Segregation …*.

Rieder, Conly L, and E D Salmon. 1998. "The Vertebrate Cell Kinetochore and Its Roles During Mitosis." *Trends in Cell Biology* 8 (8) (August): 310–318. doi:10.1016/S0962-8924(98)01299-9.

Rogers, G C, S L Rogers, and D J Sharp. 2005. "Spindle Microtubules in Flux." *Journal of Cell Science*.

Rosenblatt, Jody, Louise P Cramer, Buzz Baum, and Karen M McGee. 2004. “Myosin II-Dependent Cortical Movement Is Required for Centrosome Separation and Positioning During Mitotic Spindle Assembly..” *Cell* 117 (3) (April 30): 361–372.

Sablin, E P, F J Kull, R Cooke, R D Vale, and R J Fletterick. 1996. “Crystal Structure of the Motor Domain of the Kinesin-Related Motor Ncd..” *Nature* 380 (6574) (April 11): 555–559. doi:10.1038/380555a0.

Salmon, E D, R J Leslie, W M Saxton, M L Karow, and J R McIntosh. 1984. “Spindle Microtubule Dynamics in Sea Urchin Embryos: Analysis Using a Fluorescein-Labeled Tubulin and Measurements of Fluorescence Redistribution After Laser Photobleaching..” *The Journal of Cell Biology* 99 (6) (December): 2165–2174.

Saunders, Adam M, James Powers, Susan Strome, and William M Saxton. 2007. “Kinesin-5 Acts as a Brake in Anaphase Spindle Elongation..” *Current Biology : CB* 17 (12) (June 19): R453–4. doi:10.1016/j.cub.2007.05.001.

Sawin, K E, and J M Scholey. 1991. “Motor Proteins in Cell Division.” *Trends in Cell Biology*.

Sawin, K E, and T J Mitchison. 1991. “Poleward Microtubule Flux Mitotic Spindles Assembled in Vitro..” *The Journal of Cell Biology*.

Saxton, W M, D L Stemple, and R J Leslie. 1984. “Tubulin Dynamics in Cultured Mammalian Cells..” *The Journal of Cell …*.

Schaar, B T, G K Chan, P Maddox, E D Salmon, and T J Yen. 1997. “CENP-E Function at Kinetochores Is Essential for Chromosome Alignment..” *The Journal of Cell Biology* 139 (6) (December 15): 1373–1382.

Schafer-Hales, Katherine, Jon Iaconelli, James P Snyder, Andrew Prussia, James H

Nettles, Adel El-Naggar, Fadlo R Khuri, Paraskevi Giannakakou, and Adam I Marcus. 2007. “Farnesyl Transferase Inhibitors Impair Chromosomal Maintenance in Cell Lines and Human Tumors by Compromising CENP-E and CENP-F Function..” *Molecular Cancer Therapeutics* 6 (4) (April): 1317–1328. doi:10.1158/1535-7163.MCT-06-0703.

Schatz, Christoph A, Rachel Santarella, Andreas Hoenger, Eric Karsenti, Iain W Mattaj, Oliver J Gruss, and Rafael E Carazo-Salas. 2003. “Importin Alpha-Regulated Nucleation of Microtubules by TPX2..” *The EMBO Journal* 22 (9) (May 1): 2060–2070. doi:10.1093/emboj/cdg195.

Schmidt, Mathias, and Holger Bastians. 2007. “Mitotic Drug Targets and the Development of Novel Anti-Mitotic Anticancer Drugs..” *Drug Resistance Updates : Reviews and Commentaries in Antimicrobial and Anticancer Chemotherapy* 10 (4-5) (August): 162–181. doi:10.1016/j.drup.2007.06.003.

Schuck, P. 2000. “Size-Distribution Analysis of Macromolecules by Sedimentation Velocity Ultracentrifugation and Lamm Equation Modeling..” *Biophysical Journal* 78 (3) (March): 1606–1619. doi:10.1016/S0006-3495(00)76713-0.

Segbert, Christoph, Rosemarie Barkus, Jim Powers, Susan Strome, William M Saxton, and Olaf Bossinger. 2003. “KLP-18, a Klp2 Kinesin, Is Required for Assembly of Acentrosomal Meiotic Spindles in Caenorhabditis Elegans..” *Molecular Biology of the Cell* 14 (11) (November): 4458–4469. doi:10.1091/mbc.E03-05-0283.

Seiler, S, J Kirchner, C Horn, A Kallipolitou, G Woehlke, and M Schliwa. 2000. “Cargo Binding and Regulatory Sites in the Tail of Fungal Conventional Kinesin..” *Nature Cell Biology* 2 (6) (June): 333–338. doi:10.1038/35014022.

Sharp, D J, G C Rogers, and J M Scholey. 2000. “Microtubule Motors in Mitosis.” *Nature*.

Shin, Y, J H Davis, R R Brau, A Martin, J A Kenniston, T A Baker, R T Sauer, and M J Lang. 2009. “Single-Molecule Denaturation and Degradation of Proteins by the AAA+ ClpXP Protease.” *Proceedings of the National Academy of Sciences* 106 (46) (November 17): 19340–19345. doi:10.1073/pnas.0910484106.

Silk, A D, L M Zasadil, and A J Holland. 2013. “Chromosome Missegregation Rate Predicts Whether Aneuploidy Will Promote or Suppress Tumors.” In.

Silkworth, William T, Isaac K Nardi, Raja Paul, Alex Mogilner, and Daniela Cimini. 2012. “Timing of Centrosome Separation Is Important for Accurate Chromosome Segregation..” *Molecular Biology of the Cell* 23 (3) (February): 401–411. doi:10.1091/mbc.E11-02-0095.

Silljé, HHW, S Nagel, R Körner, and E A Nigg. 2006. “HURP Is a Ran-Importin B-Regulated Protein That Stabilizes Kinetochore Microtubules in the Vicinity of Chromosomes.” *Current Biology*.

Steitz, Thomas A. 2008. “A Structural Understanding of the Dynamic Ribosome Machine..” *Nature Reviews. Molecular Cell Biology* 9 (3) (March): 242–253. doi:10.1038/nrm2352.

Stelling, J, U Sauer, Z Szallasi, F J Doyle III, and J Doyle. 2004. “Robustness of Cellular Functions.” *Cell*.

Stumpff, Jason, Yaqing Du, Chauca A English, Zoltan Maliga, Michael Wagenbach, Charles L Asbury, Linda Wordeman, and Ryoma Ohi. 2011. “A Tethering Mechanism Controls the Processivity and Kinetochore-Microtubule Plus-End

Enrichment of the Kinesin-8 Kif18A..” *Molecular Cell* 43 (5) (September 2): 764–775. doi:10.1016/j.molcel.2011.07.022.

Su, X, R Ohi, and D Pellman. 2012. “Move in for the Kill: Motile Microtubule Regulators.” *Trends in Cell Biology*.

Su, X, W Qiu, M L Gupta Jr, and J B Pereira-Leal. 2011. “Mechanisms Underlying the Dual-Mode Regulation of Microtubule Dynamics by Kip3/Kinesin-8.” *Molecular Cell*.

Su, Xiaolei, Hugo Arellano-Santoyo, Didier Portran, Jeremie Gaillard, Marylin Vantard, Manuel Thery, and David Pellman. 2013. “Microtubule-Sliding Activity of a Kinesin-8 Promotes Spindle Assembly and Spindle-Length Control..” *Nature Cell Biology* 15 (8) (August): 948–957. doi:10.1038/ncb2801.

Subramanian, Radhika, Elizabeth M Wilson-Kubalek, Christopher P Arthur, Matthew J Bick, Elizabeth A Campbell, Seth A Darst, Ronald A Milligan, and Tarun M Kapoor. 2010. “Insights Into Antiparallel Microtubule Crosslinking by PRC1, a Conserved Nonmotor Microtubule Binding Protein..” *Cell* 142 (3) (August 6): 433–443. doi:10.1016/j.cell.2010.07.012.

Svoboda, K, and S M Block. 1994. “Force and Velocity Measured for Single Kinesin Molecules..” *Cell* 77 (5) (June 3): 773–784.

Tanenbaum, M E, L Macůrek, and N Galjart. 2008. “Dynein, Lis1 and CLIP‐170 Counteract Eg5‐Dependent Centrosome Separation During Bipolar Spindle Assembly.” *… EMBO Journal*.

Tanenbaum, Marvin E, and René H Medema. 2010. “Mechanisms of Centrosome Separation and Bipolar Spindle Assembly..” *Developmental Cell* 19 (6) (December

14): 797–806. doi:10.1016/j.devcel.2010.11.011.

Tanenbaum, Marvin E, Libor Macůrek, Aniek Janssen, Erica F Geers, Mónica Alvarez-Fernández, and René H Medema. 2009. “Kif15 Cooperates with Eg5 to Promote Bipolar Spindle Assembly..” *Current Biology : CB* 19 (20) (November 3): 1703–1711. doi:10.1016/j.cub.2009.08.027.

Tikhonenko, Irina, Dilip K Nag, Nora Martin, and Michael P Koonce. 2008. “Kinesin-5 Is Not Essential for Mitotic Spindle Elongation in Dictyostelium.” *Cell Motility and the Cytoskeleton* 65 (11) (November): 853–862. doi:10.1002/cm.20307.

Tokai, N, A Fujimoto-Nishiyama, Y Toyoshima, S Yonemura, S Tsukita, J Inoue, and T Yamamota. 1996. “Kid, a Novel Kinesin-Like DNA Binding Protein, Is Localized to Chromosomes and the Mitotic Spindle..” *The EMBO Journal* 15 (3) (February 1): 457–467.

Toso, Alberto, Jennifer R Winter, Ainslie J Garrod, Ana C Amaro, Patrick Meraldi, and Andrew D. McAinsh. 2009. “Kinetochore-Generated Pushing Forces Separate Centrosomes During Bipolar Spindle Assembly..” *The Journal of Cell Biology* 184 (3) (February 9): 365–372. doi:10.1083/jcb.200809055.

Tripet, B, R D Vale, and R S Hodges. 1997. “Demonstration of Coiled-Coil Interactions Within the Kinesin Neck Region Using Synthetic Peptides. Implications for Motor Activity..” *The Journal of Biological Chemistry* 272 (14) (April 4): 8946–8956.

Tucker, J B. 1984. “Spatial Organization of Microtubule-Organizing Centers and Microtubules..” *The Journal of Cell Biology* 99 (1 Pt 2) (July): 55s–62s.

Tulu, U Serdar, Carey Fagerstrom, Nick P Ferenz, and Patricia Wadsworth. 2006. “Molecular Requirements for Kinetochore-Associated Microtubule Formation in

Mammalian Cells.." *Current Biology : CB* 16 (5) (March 7): 536–541. doi:10.1016/j.cub.2006.01.060.

Uehara, Ryota, Ryu-suke Nozawa, Akiko Tomioka, Sabine Petry, Ronald D Vale, Chikashi Obuse, and Gohta Goshima. 2009. "The Augmin Complex Plays a Critical Role in Spindle Microtubule Generation for Mitotic Progression and Cytokinesis in Human Cells.." *Proceedings of the National Academy of Sciences* 106 (17) (April 28): 6998–7003. doi:10.1073/pnas.0901587106.

Vale, R D, and R J Fletterick. 1997. "The Design Plan of Kinesin Motors.." *Annual Review of Cell and Developmental Biology* 13: 745–777. doi:10.1146/annurev.cellbio.13.1.745.

Vale, R D, R Case, E Sablin, C Hart, and R Fletterick. 2000. "Searching for Kinesin's Mechanical Amplifier.." *Philosophical Transactions of the Royal Society of London. Series B, Biological Sciences* 355 (1396) (April 29): 449–457. doi:10.1098/rstb.2000.0586.

Vale, R D, T S Reese, and M P Sheetz. 1985. "Identification of a Novel Force-Generating Protein, Kinesin, Involved in Microtubule-Based Motility.." *Cell* 42 (1) (August): 39–50.

Vale, Ronald D. 2003. "The Molecular Motor Toolbox for Intracellular Transport.." *Cell* 112 (4) (February 21): 467–480.

van der Vaart, Babet, Wilhelmina E van Riel, Harinath Doodhi, Josta T Kevenaar, Eugene A Katrukha, Laura Gumy, Benjamin P Bouchet, et al. 2013. "CFEOM1-Associated Kinesin KIF21A Is a Cortical Microtubule Growth Inhibitor." *Developmental Cell* 27 (2) (October): 145–160. doi:10.1016/j.devcel.2013.09.010.

VanBuren, Vincent, David J Odde, and Lynne Cassimeris. 2002. “Estimates of Lateral and Longitudinal Bond Energies Within the Microtubule Lattice..” *Proceedings of the National Academy of Sciences of the United States of America* 99 (9) (April 30): 6035–6040. doi:10.1073/pnas.092504999.

Vanneste, David, Masatoshi Takagi, Naoko Imamoto, and Isabelle Vernos. 2009. “The Role of Hklp2 in the Stabilization and Maintenance of Spindle Bipolarity..” *Current Biology : CB* 19 (20) (November 3): 1712–1717. doi:10.1016/j.cub.2009.09.019.

Vasquez, R J, D L Gard, and L Cassimeris. 1994. “XMAP From Xenopus Eggs Promotes Rapid Plus End Assembly of Microtubules and Rapid Microtubule Polymer Turnover..” *The Journal of Cell Biology* 127 (4) (November): 985–993.

Vassilev, Lyubomir T, Christian Tovar, Shaoqing Chen, Dejan Knezevic, Xiaolan Zhao, Hongmao Sun, David C Heimbrook, and Li Chen. 2006. “Selective Small-Molecule Inhibitor Reveals Critical Mitotic Functions of Human CDK1..” *Proceedings of the National Academy of Sciences of the United States of America* 103 (28) (July 11): 10660–10665. doi:10.1073/pnas.0600447103.

Verde, F, M Dogterom, E Stelzer, and E Karsenti. 1992. “Control of Microtubule Dynamics and Length by Cyclin a-and Cyclin B-Dependent Kinases in Xenopus Egg Extracts..” *The Journal of Cell ….*

Verhey, K J, and J W Hammond. 2009. “Traffic Control: Regulation of Kinesin Motors.” *Nature Reviews. Molecular Cell Biology*.

Vladimirou, Elina, Nunu McHedlishvili, Ivana Gasic, Jonathan W Armond, Catarina P Samora, Patrick Meraldi, and Andrew D. McAinsh. 2013. “Nonautonomous Movement of Chromosomes in Mitosis..” *Developmental Cell* 27 (1) (October 14):

60–71. doi:10.1016/j.devcel.2013.08.004.

Voges, D, P Zwickl, and W Baumeister. 1999. “The 26S Proteasome: a Molecular Machine Designed for Controlled Proteolysis..” *Annual Review of Biochemistry* 68: 1015–1068. doi:10.1146/annurev.biochem.68.1.1015.

Voter, W A, and H P Erickson. 1984. “The Kinetics of Microtubule Assembly. Evidence for a Two-Stage Nucleation Mechanism..” *The Journal of Biological Chemistry* 259 (16) (August 25): 10430–10438.

Walczak, C E, and R Heald. 2008. “Mechanisms of Mitotic Spindle Assembly and Function.” *International Review of Cytology*.

Walczak, C E, T J Mitchison, and A Desai. 1996. “XKCM1: a Xenopus Kinesin-Related Protein That Regulates Microtubule Dynamics During Mitotic Spindle Assembly..” *Cell* 84 (1) (January 12): 37–47.

Walczak, Claire E, Sophia Gayek, and Ryoma Ohi. 2013. “Microtubule-Depolymerizing Kinesins.” *Annual Review of Cell and Developmental Biology* 29 (1) (October 6): 417–441. doi:10.1146/annurev-cellbio-101512-122345.

Walker, R A, E T O'Brien, N K Pryer, M F Soboeiro, W A Voter, H P Erickson, and E D Salmon. 1988. “Dynamic Instability of Individual Microtubules Analyzed by Video Light Microscopy: Rate Constants and Transition Frequencies..” *The Journal of Cell Biology* 107 (4) (October): 1437–1448.

Wall, M E. 1998. “Camptothecin and Taxol: Discovery to Clinic..” *Medicinal Research Reviews* 18 (5) (September): 299–314.

Weaver, A M. 2006. “Invadopodia: Specialized Cell Structures for Cancer Invasion.” *Clinical & Experimental Metastasis*.

Weaver, Lesley N, Stephanie C Ems-McClung, Jane R Stout, Chantal LeBlanc, Sidney L Shaw, Melissa K Gardner, and Claire E Walczak. 2011. “Kif18A Uses a Microtubule Binding Site in the Tail for Plus-End Localization and Spindle Length Regulation..” *Current Biology : CB* 21 (17) (September 13): 1500–1506. doi:10.1016/j.cub.2011.08.005.

Weil, D, L Garçon, M Harper, D Duménil, F Dautry, and M Kress. 2002. “Targeting the Kinesin Eg5 to Monitor siRNA Transfection in Mammalian Cells..” *BioTechniques* 33 (6) (December): 1244–1248.

Weisenberg, R C, W J Deery, and P J Dickinson. 1976. “Tubulin-Nucleotide Interactions During the Polymerization and Depolymerization of Microtubules..” *Biochemistry* 15 (19) (September 21): 4248–4254.

Welburn, Julie P I. 2013. “The Molecular Basis for Kinesin Functional Specificity During Mitosis..” *Cytoskeleton (Hoboken, N.J.)* 70 (9) (September): 476–493. doi:10.1002/cm.21135.

Wignall, Sarah M, and Anne M Villeneuve. 2009. “Lateral Microtubule Bundles Promote Chromosome Alignment During Acentrosomal Oocyte Meiosis..” *Nature Cell Biology* 11 (7) (July): 839–844. doi:10.1038/ncb1891.

Wittmann, T, A Hyman, and A Desai. 2001. “The Spindle: a Dynamic Assembly of Microtubules and Motors.” *Nature Cell Biology*.

Wittmann, T, H Boleti, C Antony, E Karsenti, and I Vernos. 1998. “Localization of the Kinesin-Like Protein Xklp2 to Spindle Poles Requires a Leucine Zipper, a Microtubule-Associated Protein, and Dynein..” *The Journal of Cell Biology* 143 (3) (November 2): 673–685.

Wittmann, T, M Wilm, E Karsenti, and I Vernos. 2000. “TPX2, a Novel Xenopus MAP Involved in Spindle Pole Organization..” *The Journal of Cell Biology* 149 (7) (June 26): 1405–1418.

Wong, Jim, and Guowei Fang. 2006. “HURP Controls Spindle Dynamics to Promote Proper Interkinetochore Tension and Efficient Kinetochore Capture..” *The Journal of Cell Biology* 173 (6) (June 19): 879–891. doi:10.1083/jcb.200511132.

Wood, K W, L Lad, L Luo, and X Qian. 2010. “Antitumor Activity of an Allosteric Inhibitor of Centromere-Associated Protein-E.” In.

Wood, K W, R Sakowicz, LSB Goldstein, and D W Cleveland. 1997. “CENP-E Is a Plus End–Directed Kinetochore Motor Required for Metaphase Chromosome Alignment.” *Cell*.

Wood, K W, W D Cornwell, and J R Jackson. 2001. “Past and Future of the Mitotic Spindle as an Oncology Target..” *Current Opinion in Pharmacology* 1 (4) (August): 370–377.

Wordeman, L, and T J Mitchison. 1995. “Identification and Partial Characterization of Mitotic Centromere-Associated Kinesin, a Kinesin-Related Protein That Associates with Centromeres During Mitosis..” *The Journal of Cell Biology* 128 (1-2) (January): 95–104.

Wühr, Martin, Yao Chen, Sophie Dumont, Aaron C Groen, Daniel J Needleman, Adrian Salic, and Timothy J Mitchison. 2008. “Evidence for an Upper Limit to Mitotic Spindle Length..” *Current Biology : CB* 18 (16) (August 26): 1256–1261. doi:10.1016/j.cub.2008.07.092.

Yajima, Junichiro, Masaki Edamatsu, Junko Watai-Nishii, Noriko Tokai-Nishizumi,

Tadashi Yamamoto, and Yoko Y Toyoshima. 2003. “The Human Chromokinesin Kid Is a Plus End-Directed Microtubule-Based Motor.” *The EMBO Journal* 22 (5) (March 3): 1067–1074. doi:10.1093/emboj/cdg102.

Yan, Youwei, Vinod Sardana, Bei Xu, Carl Homnick, Wasyl Halczenko, Carolyn A Buser, Michael Schaber, George D Hartman, Hans E Huber, and Lawrence C Kuo. 2004. “Inhibition of a Mitotic Motor Protein: Where, How, and Conformational Consequences.” *Journal of Molecular Biology* 335 (2) (January): 547–554. doi:10.1016/j.jmb.2003.10.074.

Yang, J T, R A Laymon, and L S Goldstein. 1989. “A Three-Domain Structure of Kinesin Heavy Chain Revealed by DNA Sequence and Microtubule Binding Analyses..” *Cell* 56 (5) (March 10): 879–889.

Yildiz, Ahmet, Michio Tomishige, Ronald D Vale, and Paul R Selvin. 2004. “Kinesin Walks Hand-Over-Hand..” *Science (New York, N.Y.)* 303 (5658) (January 30): 676–678. doi:10.1126/science.1093753.

Zasadil, Lauren M, Kristen A Andersen, Dabin Yeum, Gabrielle B Rocque, Lee G Wilke, Amye J Tevaarwerk, Ronald T Raines, Mark E Burkard, and Beth A Weaver. 2014. “Cytotoxicity of Paclitaxel in Breast Cancer Is Due to Chromosome Missegregation on Multipolar Spindles..” *Science Translational Medicine* 6 (229) (March 26): 229ra43. doi:10.1126/scitranslmed.3007965.

Zhai, Y, P J Kronebusch, and G G Borisy. 1995. “Kinetochore Microtubule Dynamics and the Metaphase-Anaphase Transition..” *The Journal of Cell Biology* 131 (3) (November): 721–734.

Zhang, H, and R K Dawe. 2011. “Mechanisms of Plant Spindle Formation.”

Chromosome Research.

Zhang, Shuguang. 2002. “Emerging Biological Materials Through Molecular Self-Assembly.” *Biotechnology Advances* 20 (5-6) (December): 321–339. doi:10.1016/S0734-9750(02)00026-5.